March 2015

Bicontinuous Materials from Telechelic Macromonomers Using Thiol-ene Chemistry

Catherine Nancy Walker
University of Massachusetts - Amherst

Bicontinuous Materials from Telechelic Macromonomers Using Thiol-ene Chemistry

A Dissertation Presented

by

CATHERINE N. WALKER

Submitted to the Graduate School of the
University of Massachusetts Amherst in partial fulfillment
of the requirements for the degree of

DOCTOR OF PHILOSOPHY

February 2015

Polymer Science and Engineering

Bicontinuous Materials from Telechelic Macromonomers Using Thiol-ene Chemistry

A Dissertation Presented

by

CATHERINE N. WALKER

Approved as to style and content by:

Gregory N. Tew, Chair

Ryan C. Hayward, Member

Mark Tuominen, Member

David Hoagland, Department Head
Polymer Science and Engineering

DEDICATION

To those who come after me.

ACKNOWLEDGMENTS

This thesis contains work modified from articles published in ACS Macro Letters, reprinted with permission. Work from 10.1021/mz300090m appears in Chapter 3, work from and 10.1021/mz5001288 appears in Chapters 2 and 5.

Greg:

Thank you for your energy, for your frustration with red tape, for emphasizing stories and for teaching me how to promote my science.

Ryan:

Thank you so much for your patience, I could tell you were putting a lot of time and effort into reading my paper. I enjoyed working with you, your students and I hope the collaboration in this area continues.

Mark:

Thank you for your help with the ion conductivity. I enjoyed working with you and your students. I think the way you work things through at the blackboard was actually quite fun.

To my collaborators Craig, Kyle, Scott and Ramesh:

Thank you all for adding dimensions and techniques to my work that I wouldn't have been able to do on my own.

To the Tew Group:

One of the first events I went to as a new Tew group member was the 6th floor pot-luck. All the Tew group members participated in bringing food and were the last ones to leave the party. Someone told me, "We all like eating." This made me feel like I had joined a good group, because I also enjoy eating. It did work out, I did join a good group, but not just for the food. We've always worked on very different projects but everyone generally seemed happy to help, or talk, or whatever they could do. Thank you Trouble, I don't think the group would function without you. I can't take responsibility for this metaphor but are like the string to Greg's kite.

Thank you for keeping track of him It's also very fun to walk down the hallway and say, "I'm looking for Trouble," and have that be a perfectly normal statement. I especially miss Ke, he fixed my prospectus and I knew I was in trouble when he said, "that's a weird, hard problem." I'm generally surprised I made it this last year without Melissa sharing my lab or office. Mike, as always, thank you for the conversation. I had so many people to look up to when I started out, Semra, Raj, Jun, Yongping, Hitesh, Ozgul, Jing, Ahbi, and Yan. Karen, I didn't get to work with you for very long, but I want to thank you for talking a bit about your personal life in your seminar and encouraging young women that they can have a family and still pursue their career, I hope you keep doing that. Fede I will miss you, thank you for teaching me how to make tiramisu. Bob, thank you for being genuine and not caring what others think and for teaching us "real" chemistry. Katie, thank you for being the lab ninja and my conference buddy. Brittany, you've been such a good friend, thank you for feeling that you can bring your problems to me. Madhura, thank you for being a good officemate and teaching me about Indian food and culture.

To the PSE Staff:

Thank you to all of the PSE staff especially Jack, Lou, Alex and Sekar for maintaining and helping us with the instruments Thank you to all of the office staff that keep Conte running. Thank you to Lisa for not only setting up everything for my defense, but reassuring me several times that everything was or would be taken care of and should go relax and focus on my work.

To the Lesser Group:

I spent a lot of time in the 3rd floor thermal lab. During that time, I talked with most of the Lesser group students about one issue or another. I owe several people thanks for training me on instruments, and for discussing sample prep, test parameters or data. Mostly, I am very grateful that it was not my responsibility to keep the thermal lab up and running. Thank you to Andrew, Naveen, Henry, Polina, Angela, Brian and Connor for maintaining and repairing those instruments.

To my classmates:

I want to thank my classmates for being relatively drama-free. We were a small group but I couldn't have asked for better classmates. Not only were we there for each other during all of the PSE hurdles, we did a lot of growing up together too.

Also, thanks to the 3rd floor lunch group. I was always glad to see a few different faces and it was good to know I was always welcome.

To the PSE Wives Club:

I want to thank a very special group of friends called the "PSE Wives Club." As a member of the PSE department, I am ineligible to be part of this exclusive group as it consists of spouses, partners loved ones etc., of PSE students. However, I do know that the group's motto is "Putting up with tomorrow's innovators today." To all of these friends, Neith, Itza, Vera, Garn, Engin, Adam, CJ, Orf and others, thank you for putting up with not only your own significant other, but all of us. I'm glad to count you among my friends.

To the softball teams:

I know a lot of the international students comment on how they were just learning the sport and how much they improved. I never thought I would but I improved quite a bit too. I want to thank all of the teams for making it fun.

To GWIS/Mentoring:

The timing of both of these groups starting couldn't have been more perfect. I was initially skeptical about joining a peer mentoring group, but it's probably been one of the biggest assets in combating grad school blues. Both Jesses, Whitney, Elizabeth, Dana, Szuchia and Andra: it was great to hear outside perspective and have a group of people to turn to with problems small and large. I don't know how our group managed to work so well. Thank you for all of your help, and I will continue to rely on you in the future.

I'm so glad we started and outward facing group as well. I thought in grad school I would have to give up extracurriculars, but GWIS reminded me how important it is to have something to care about and to meet with other people who care about the same things. The women I met through these groups are as close to Wells Women and I very much appreciate knowing all of them.

To the Pioneer Valley Symphony Orchestra and Chorus:

Thank you to all of the friends and musicians I met through the PVS choir and orchestra. Jonathan, thank you for your endless patience as you led a group with such diverse skill and experience. Paul, thank you for making our final rehearsals leading up to our concerts enjoyable instead of stressful. Thank you to Kathleen for checking in on me and to Carol for being so reliable. Thank you Heather, Evie and Nancy for goofing off in the back row with me, since everyone knows you can't goof off up front. Alan Dann, you were so sweet and had the best stories, you will be missed.

To Wells:

I want to thank a number of the Wells faculty for giving me my start. Professor Godert, I don't know if I would have applied to grad school if you didn't ask me about it every other time you saw me fall semester of my senior year. I'm fortunate to have been able to keep in touch with several people through trustees and alumni functions. Professor Bailey, thank you for inviting me/accepting my volunteering to give Science Colloquium. To the Wells community in general, thank you for making women in STEM not a big deal. Where else can you have twin sisters TA for your gen chem. and intro physics classes?

Thank you to the friends I've made through the trustees and alumni association, especially Renee. Thank you for being part of the letter writing brigade and for talking me through some tough times. I apologize that you found out about my job offer through Facebook. That wasn't right, I owe you for that. Fran and Randy, thank you for taking Travis and I under

your wings. I never did plan on talking about beam bending after my 1st year classes, thanks for surprising me. Flory, it was so great to meet you at reunion and hear your talk. This thanks may be coming a bit in advance, but I'm excited to spend more time with you and the other D.C. area alums. Nancy, I'm so glad I've stayed in touch with you. I know I have several mentors and friends within academia who have gone through this Ph.D. process, but it's so refreshing to have an outside perspective as well.

To my Wells classmates and friends, I did not have the time to appreciate the liberal arts perspective we share and the fact that most of us don't share the same or similar fields of study. At times, I so badly needed this outside perspective. Thank you all for reminding me that science can be fun and exciting and I should appreciate and enjoy my opportunities to be in the lab. Also thank you to Kate, Ryan, John and Dave for not being upset that I published a hazily remembered and heavily edited story about "man weekend." The impact it had on my me and my gratitude to you are certainly genuine. To Erin, Jess, Tess, Rachel, Janine, Laura, Beth and Kat, thank you for preventing me from working on my dissertation at Erin's bachelorette weekend. Even though it was less than a month before my defense, the lessons I learned from all of you were far more valuable than any bit of writing or editing I might have squeezed in that weekend. Thank you for all helping me to reflect on what I was doing, for reminding me of its significance and for being proud of my accomplishments. Otherwise, I would have been in danger of "just checking this off the list," and would have regretted not taking the time to spend with all of you.

To Ms. Bentley:

It's kind of a lot to go all the way back to high school, but I had to make one exception. Ms. Bentley, thank you for teaching calculus. I didn't like math until I took your AP class my senior year. You started quite the domino effect. I remember sitting on the couch and looking at college brochures that fall and considering taking more math and wondering what I could do with

it. I thought to myself, “I could be an engineer.” After working with GWIS, I realize how rare it is that a 17 year old girl says that to herself and it needs to happen more often.

To The Grandmas:

Thank you to my grandparents and to Travis’s grandma Judy. I know you all supported me in your own way. Thank you for trying to understand my work, or for just being proud of me anyway. Thank you for checking on me and making sure I was staying healthy, cooking some good food and eating my vegetables.

To Travis’s family Ann, Carl, Hollie, Jon, Renee, Josiah, Bethany and anyone else who came and went in the Niles household:

I don’t know how you did it but thank you for always finding room for just one more.

To my brother:

I want to thank my brother for the interesting role he played in my job search. Dan served in the Navy for six years and we heard lots of stories over that time. When I told Greg I was applying to NRL, he said that military labs were weird, without much further clarification. I went on applying to other things and put the comment in the back of my mind. I went to NRL for my interview and reminded myself to look for things that might be weird. It was only after getting an offer did I finally go ask Greg why he thought military labs were weird. I don’t remember exactly what he said, I just remember thinking, “Greg’s stories aren’t nearly as weird as Dan’s stories. I think I’ll be ok.” Thank you Dan, for your weird stories.

To my parents:

Thank you for listening to all the troubles and frustrations and all of the times I wanted to quit. I’m sorry you had to wait until the end to see the experiments and explanations that were deemed well done and exciting.

To Travis:

Thank you for being more excited for me and proud of me than I have ever been for myself.

ABSTRACT

BICONTINUOUS MATERIALS FROM TELECHELIC MACROMONOMERS USING THIOL-ENE CHEMISTRY

FEBRUARY 2015

CATHERINE N. WALKER, B.A., WELLS COLLEGE

M.S., UNIVERSITY OF MASSACHUSETTS AMHERST

Ph.D., UNIVERSITY OF MASSACHUSETTS AMHERST

Directed by: Professor Gregory N. Tew

Bicontinuous structures are beneficial to many applications from health and medicine to energy and the environment. Although these materials can be used for many applications, current strategies yield bicontinuous structures only under highly specific processing conditions. Development of a versatile platform to reliably obtain bicontinuous morphologies will be broadly beneficial. This work presents two platforms that can be used to produce bicontinuous morphologies using a simple Mitsunobu/thiol-ene strategy. This platform allows for the incorporation of a variety of polymer chemistries to yield well-defined polymer networks or multiblock copolymers (MBCs). It also allows for the systematic investigation of factors affecting the morphology such as the molecular weight between cross-links and the volume fraction of the network components. The ease at which these variables can be systematically investigated allows for rigorous fundamental studies of these composite systems.

In the first co-network system, the platform's ability to tailor mechanical properties while maintaining good ion conductivity was demonstrated by comparing PEG-PDMS co-networks to PEG networks using EIS and DMA. Also, the effect of salt loading on thermal properties was explored using DSC. The second system, PEG-PS co-networks, demonstrated that varying the molecular weight of the precursor polymers results in control over d-spacing that fits well to de Gennes's prediction ($d \sim M_n^{0.5}$). Despite the variation in d-spacing, 22 - 55 nm, the ion

conductivity and mechanical properties remained relatively consistent, demonstrating versatility in this system. Critical percolation thresholds were investigated by using ion conductivity and storage modulus to probe the continuity of the PEG and PS phases, respectively. Percolation theory suggests this system has a wide bicontinuous compositional window from ϕ_{PEG} = 0.225 - 0.675. A preliminary phase diagram was generated by combining results from the molecular weight and volume fraction series. Finally, a simple synthesis for (MBCs) is demonstrated using the same Mitsunobu/thiol-ene platform. MBCs with ~4 blocks and two or three types of macromonomers were synthesized. Disordered phase separation was shown by SAXS and AFM. The versatile Mitsunobu/thiol-ene platform is easily able to synthesize different architectures using a range of polymer chemistries for various morphology and property studies.

TABLE OF CONTENTS

Page

LIST OF TABLES

Page

LIST OF FIGURES

Page

CHAPTER 1

INTRODUCTION

1.1 Bicontinuous Morphology

Within the realm of soft materials, the bicontinuous morphology which enables percolation of at least two different phases, and their respective properties, throughout the material is highly sought after.[1] These bicontinuous morphologies could be especially advantageous when two fundamentally different properties are required from the same material. A good example is in the area of polymer electrolyte membranes which require efficient transport and simultaneously robust mechanical properties. Despite its potential, this type of morphology is fundamentally difficult to obtain because it requires variable curvature, high packing frustration, and large interfacial area.[2,3] Overcoming these morphological challenges will be advantageous for a variety of fields such as ion,[4,5,6] charge,[7] and oxygen transport, as well as water purification,[6] and mechanical reinforcement of membranes.[8,9] A system with bicontinuous phases would provide uninterrupted ion-conducting pathways, for example, while maintaining favorable mechanical properties, bypassing the geometric limitation demonstrated previously in solid electrolyte materials.[8,9]

1.1.1 Previous Approaches

Given the interest in bicontinuous morphology, several researchers have tried different techniques in order to study how best to obtain it. The next section focuses on several polymeric approaches to materials with bicontinuous morphology. Strategies to access bicontinuous morphologies have predominantly fallen into two broad categories: those that take advantage of equilibrium self assembly and those that prevent demixing by kinetically trapping phase-

separated structures. Additionally, the two strategies used in this thesis are specifically addressed.

1.1.1.1 Equilibrium Structures

Traditional diblock copolymer equilibrium self assembly is widely studied; however, it is only able to produce bicontinuous structures under rigorously controlled conditions.[2,10,11] Bicontinuous morphologies, such as the gyroid phase, occupy only a narrow composition range of the phase diagram,[12] shown in Figure 1.1, and obtaining them requires precise control of the processing conditions.[2,13] The bicontinuous gyroid geometry is characterized by varied curvature and high packing frustration that requires the block copolymer chains to stretch to fill space;[14] however, block copolymer melts prefer the constant curvature and low packing frustration found in less complex lamellar and cylindrical phases.[10] These physical challenges limit the combinations of polymer chemistries, molecular weights, and temperatures that are able to form this desirable bicontinuous morphology.

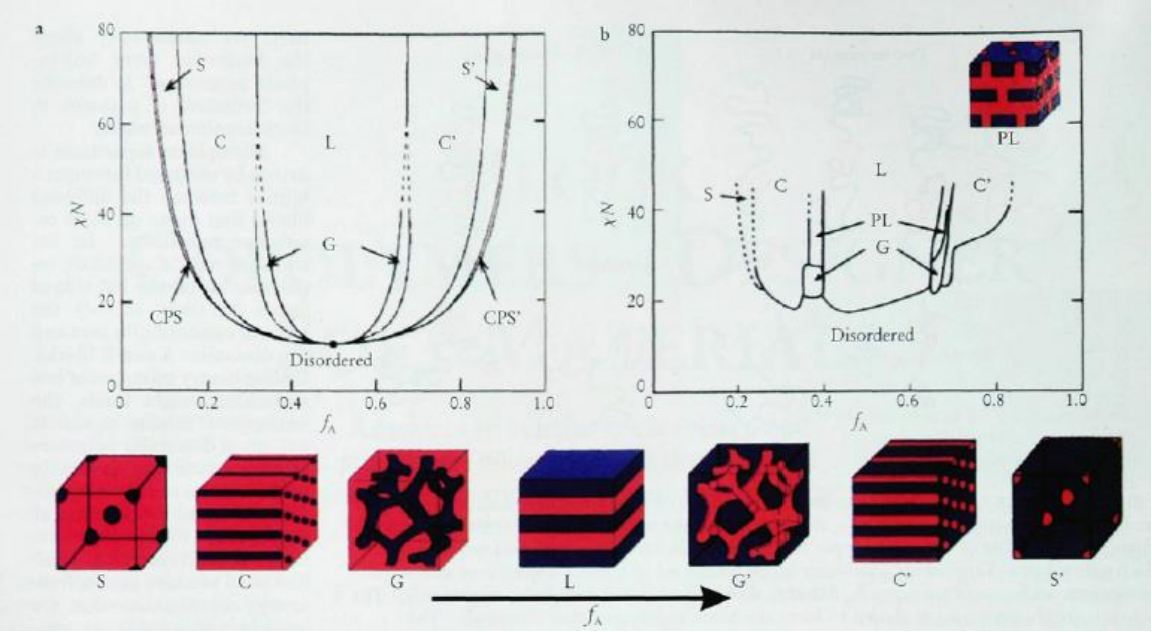

Figure 1.1 a) Predicted and b) observed morphologies of polystyrene-polyisoprene block copolymers, from reference [12].

In order to increase the likelihood of obtaining bicontinuous morphologies, some variations on traditional diblock copolymers have been investigated. A polydisperse mid-block in ABA triblock copolymers was shown to yield bicontinuous morphology over a slightly wider compositional range, as shown in Figure 1.2.[15,16,17,18] The polydisperse mid-block allows for variation in size and shape of the polydisperse domains, decreasing packing frustration. However, the lamellar morphology occupies a much larger compositional range than the bicontinuous morphology. This system also lacks a mechanism to control the domain sizes as the d-spacing is only weakly dependent on the total molecular weight of the block copolymer.[15,16]

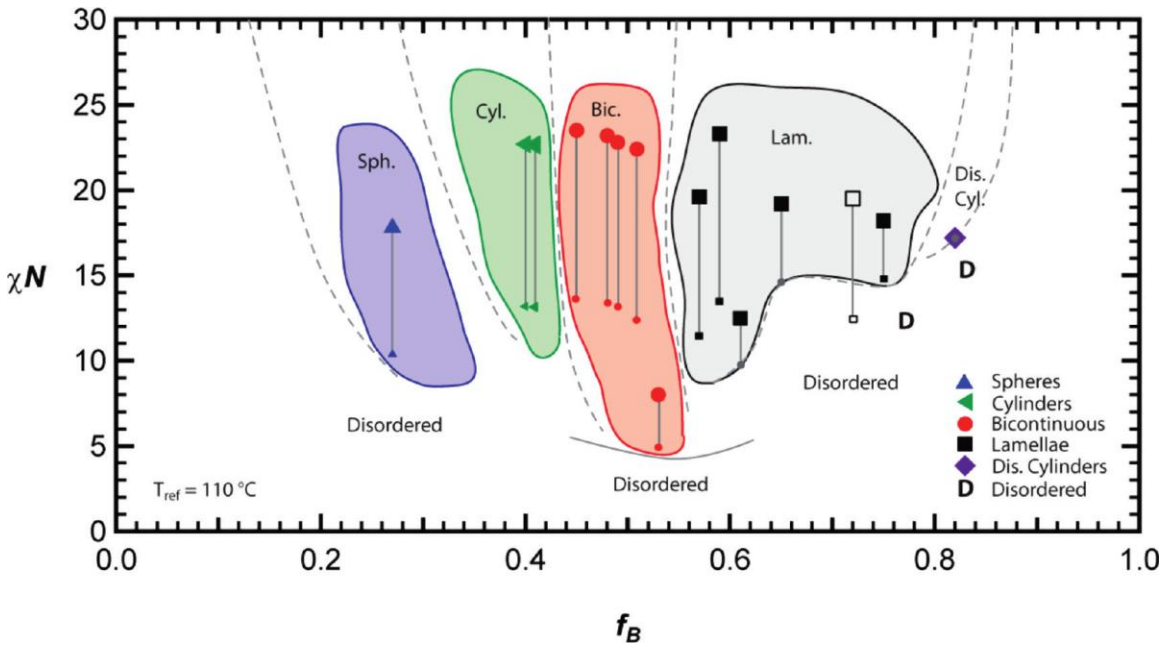

Figure 1.2 Phase diagram of polydisperse triblock copolymers, from reference [15].

Reactive blending decreases interfacial tension in polymer blends.[19] It can also be used to induce randomness and polydispersity which increases the thermodynamic stability of the bicontinuous morphology.[20] In a study by Liebler and co-workers,[20] random graft copolymers were synthesized from two precursor polymers carrying complementary reactive groups. The backbone polymers have functional groups randomly distributed in the main chain, while the graft polymers are semi-telechelic. The products of the reactive blending were polydisperse graft co-polymers with a highly variable graft density. Bicontinuous morphologies were observed by TEM in three perpendicular planes of a single sample.[20]

Tapered block copolymers include a gradient copolymer block, in which monomer compositions gradually fade from A to B, with blocks of A and B on either side. This increases the mixing of A and B reduces the sharpness of the interface between phases. Simulations using self-consistent field theory and random phase approximation show that this increase mixing can slightly broaden the composition window of the gyroid phase,[14] as shown in Figure 1.3.

Experimentally, gradient copolymers have demonstrated sponge-like or disordered phases; however these occur concurrently with lamellar phases or only at narrow composition ranges.[21,22]

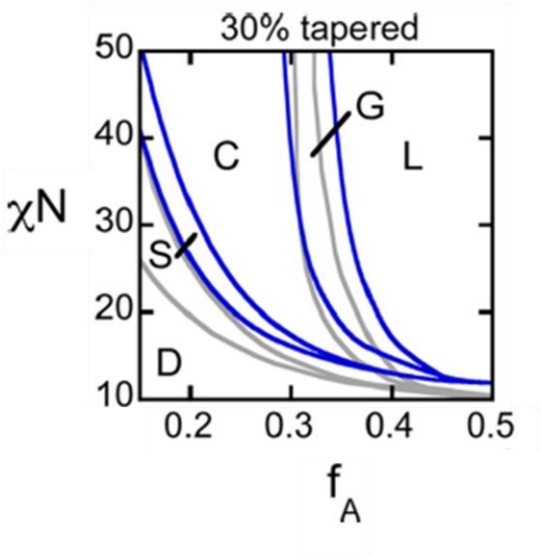

Figure 1.3 Phase diagram for (blue) tapered block copolymer with a tapered block 30% of the total length and (grey) traditional diblock copolymers.[14]

1.1.1.2 Non-equilibrium Structures

In contrast to equilibrium structures, several groups have investigated methods to trap non-equilibrium bicontinuous morphologies created by spinodal decomposition.[23,24,25,26] Demixing is typically induced through solvent,[27] temperature,[28] or polymerization[29,30] induced phase separation, and coarsening of the bicontinuous morphology is then kinetically arrested using several routes including vitrification,[24] chemical cross-linking,[31] or jamming/gelation of nanoparticles.[32] Some of these strategies have been used to generate nano-porous materials[33] as well as ion-conducting membranes with high modulus and bicontinuous morphology.[29,30] However, due to the delicate interplay between the kinetics of demixing and structural arrest, obtaining bicontinuous structures typically requires rigorously controlled processing conditions that are highly specific to a given chemical system.

Polymerization induced phase separation (PIPS) uses growing molecular weight to drive phase separation of a block copolymer.[34] Cross-links can be added to this type of system to prevent the bicontinuous morphology from coarsening and to allow control over the domain size. This technique has been used to generate nano-porous materials[33] as well as ion-conducting membranes with high a modulus.[29,30] It offers several ways to independently control different properties. PIPS, like other routes to kinetically trapped phase-separated structures, requires stringent control of a variety of experimental parameters.[29,30,33,35]

Recently, the morphology and ion conductivity of a block copolymer material was compared before and after annealing.[36] Prior to annealing, the sample showed small grain size and therefore many grain boundaries and high ion conductivity. However, after thermal annealing, the grain size increased and the ion conductivity decreased irreversibly.[36]

1.1.1.3 Cross-linked Co-networks

Here, a third approach is considered that has received far less attention, namely, cross-linking of a homogenous solution or blend of two or more polymers in order to control the equilibrium phase separation. The cross-linked, co-network physically restricts the phase separation making highly ordered phases unfavorable.[37,38] This leads to systems with disordered microphase separation and domain spacing (d) that can be tuned by the molecular weight between cross-links (M_c) according to the prediction[39] $d \sim M_c^{0.5}$, which was confirmed by neutron scattering.[40] However, in these early studies, the exact morphology was not determined, thus the possibility of bicontinuous phases was not discussed, despite this promising approach.[40]

More recent studies use a telechelic polymer to randomly cross-link a co-monomer leading to uncontrolled network architectures.[37,38,41,42,43] Furthermore, bicontinuity has most commonly been established through measurements of the swelling ratios in water and non-polar

solvents, which can be complicated to interpret due to the possibility for solvent-induced structural rearrangements.[37,38,41,42] Other networks use block copolymers of various lengths to achieve a more defined architecture, yet these studies still rely heavily on swelling or AFM for their morphology characterization.[44,45,46] Several strategies for amphiphilic co-network synthesis have been reviewed by Erdodi and Kennedy in 2006.[43] Broadly, these strategies are random copolymerization or cross-linking of monomers with telechelic macromonomers, sequential living polymerization and cross-linking, and cross-linking precursor polymer chain segments. Examples of amphiphilic co-network studies since this review are listed in Table 1.1 Chemistries of co-networks.Table 1.1 and classified according to the same scheme. Interpenetrating or semi-interpenetrating networks were excluded as this survey focused on co-networks where two or more types of chains are directly, chemically connected.

Table 1.1 Chemistries of co-networks.

Monomer 1	Monomer 2	Strategy	Reference
Vinyl imidazole	Poly(THF) dimethacrylate	Free radical copolymerizatoin	42
Tetrahydrophranyl methacrylate, methacrylic acid	2-butyl-1-octyl methacrylate	Sequential GTP: polymerization then end-linking	45
TMS protected methacrylaic acid	Polyisobutylene dimethacrylate	Free radical copolymerizatoin	41
Styrene-co-β-pinene	di-alkynyl PEG	Sequential RAFT polymerization then click end-linking	47
Methyl methacrylate	di-methacrylate poly caprolactone	Free radical co-polymerization	48
Hydroxyethyl methacrylate 2-(acryloxyethoxy) trimethylsilane	Alpha omega methacryloxymethyl-polydimethylsiloxane	Free radical co-polymerization	49
N,N-dimethylamino-2-ethyl methacrylate co (2-azidoethoxy)ethyl methacrylate	Alpha omega alkyne polycaprolactone	Linking polymer segments	50
2-Hydroxyethyl acrylate	Di methacrylamide Poly(2-ethyl-1,3-oxazoline)	Free radical co-polymerization	51
2-(Dimethylamino)ethyl methacrylate	Methyl methacrylate	Sequential ATRP: polymerizations then end - inking	46

While these initial approaches have generated a number of important insights and material systems, a simpler, more versatile route that is widely tolerant to variations in temperature, degree of polymerization, χ, and processing conditions will have broader applications and is expected to provide excellent model systems for fundamental investigations.

1.1.1.4 Multiblock Copolymers

Also presented later, multiblock copolymers have demonstrated an increased likelihood of obtaining the bicontinuous phase[52,53] because the additional blocks increase the polymer chain's kinetic and thermodynamic barriers to rearrangement.[54,55] By reacting precursor polymers of various molecular weights, materials with disordered, bicontinuous-like morphologies were obtained and characterized by SAXS and TEM. The SAXS curves showed broad peaks, generally without higher order reflections. TEM, some examples are shown in Figure 1.4 confirmed this was due to a disordered structure. While the d-spacings ranged from ~14-30 nm, the volume fraction of one phase (PS) was probed over only a relatively narrow range, 0.60 to 0.85. In addition to showing bicontinuous morphology, MBCs would offer a rout to materials that are thermoplastic. Unlike cross-linked networks which are thermosets, MBC bicontinuous materials have the potential to be melted and remolded.

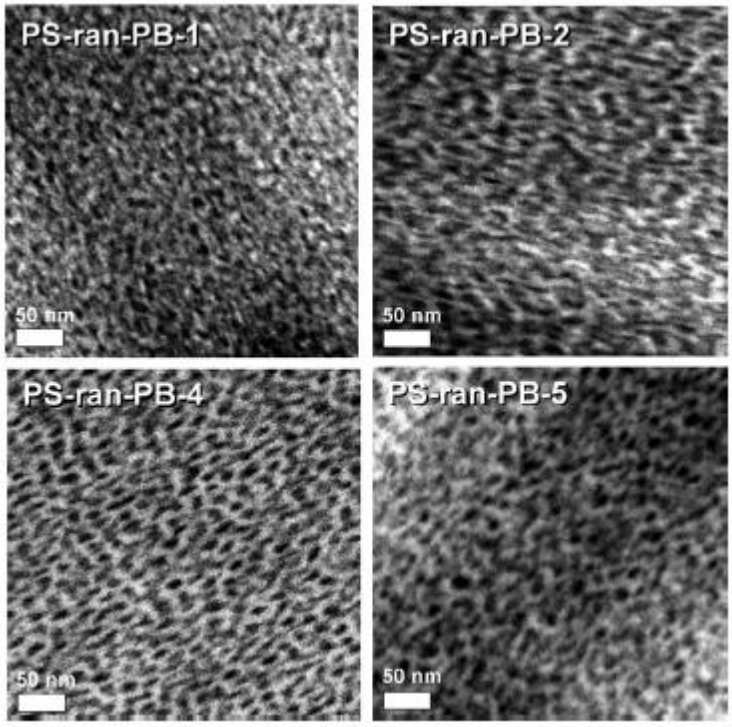

Figure 1.4 TEM images of select MBC materials from reference [56].

1.1.2 Percolation Theory

In this work, percolation theory is used to determine the critical volume fraction of a phase based on property measurements. Percolation theory was originally developed to describe the vulcanization of rubber and has since been applied to many other areas such as electronic composites, forest fires and oil fields. The basic assumptions of percolation theory can be applied to various types of lattices, such as bond or site, with different geometries and degree of connections. To build the model, for site percolation a configuration of empty sites is chosen. Then, the sites are randomly filled in. The fraction of filled sites is defined as p. It is assumed that the interactions between filled or unfilled sites are neutral. In order to find the critical percolation threshold (p_c) filled sites are added until neighboring filled sites span the entire

diagram. The first example is a 1 x 6 matrix of squares, shown in Figure 1.5 part a). In order to consider this system percolated, filled squares need to stretch across the width of the system, or a row of six. Next squares in the lattice are randomly filled in with purple. Parts b) and c) show two possible configurations below p_c. Finally in d) $p = p_c = 1$, the filled sites percolate across the entire lattice. This oversimplified one-dimensional example may seem obvious or silly; however it has been used to describe the size of clusters, or groups of filled squares that do not percolate. This description also matches the Carouther's prediction for the polydispersity of step growth polymers.

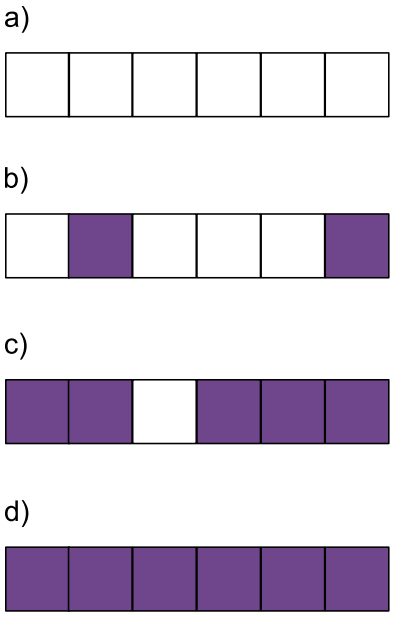

Figure 1.5 One dimensional percolation a) empty lattice p = 0 b) p = 0.33, c) p = 0.83 and d) $p = p_c = 1$.

Expanding this same example to two dimensions becomes more useful. This time a lattice of 6 x 6 squares will be used. Again percolation will be defined as the point at which a path of filled squares stretches from the left side to the right side of the diagram. As shown in

Figure 1.6 a, the lattice starts empty. As the first few scattered sites are filled, they are not close enough to create any clusters larger than one site. A cluster is defined a group of sites that are connected through shared borders. These are called "nearest neighbors." The two filled sites that are diagonal from each other in the lower right corner of

Figure 1.6 b are not considered nearest neighbors. Parts c) and d) show that as p grows to 0.33 and 0.5, respectively, some clusters start to form; however none are large enough to stretch through the entire sample area. Finally at $p = 0.55$ an "infinite" cluster can be seen in the top two rows of

Figure 1.6 e). In this cluster, nearest neighbor sites are filled that span the width of the diagram. As shown in part f) continuing to add filled sites adds to the size of the percolating cluster. For this type of two dimensional lattice, $p_c \sim= 0.5$, which is reasonably well demonstrated by this test case.[57]

From this simple lattice model, a general scaling model of percolation theory was developed, as given in equation 1.1, where E is the extent of the percolation, and β is the critical exponent. Depending on the specific conditions or system that this equation is used with, various values or symbols of the exponent are expected. However, this general form applies to many diverse problems and geometries.

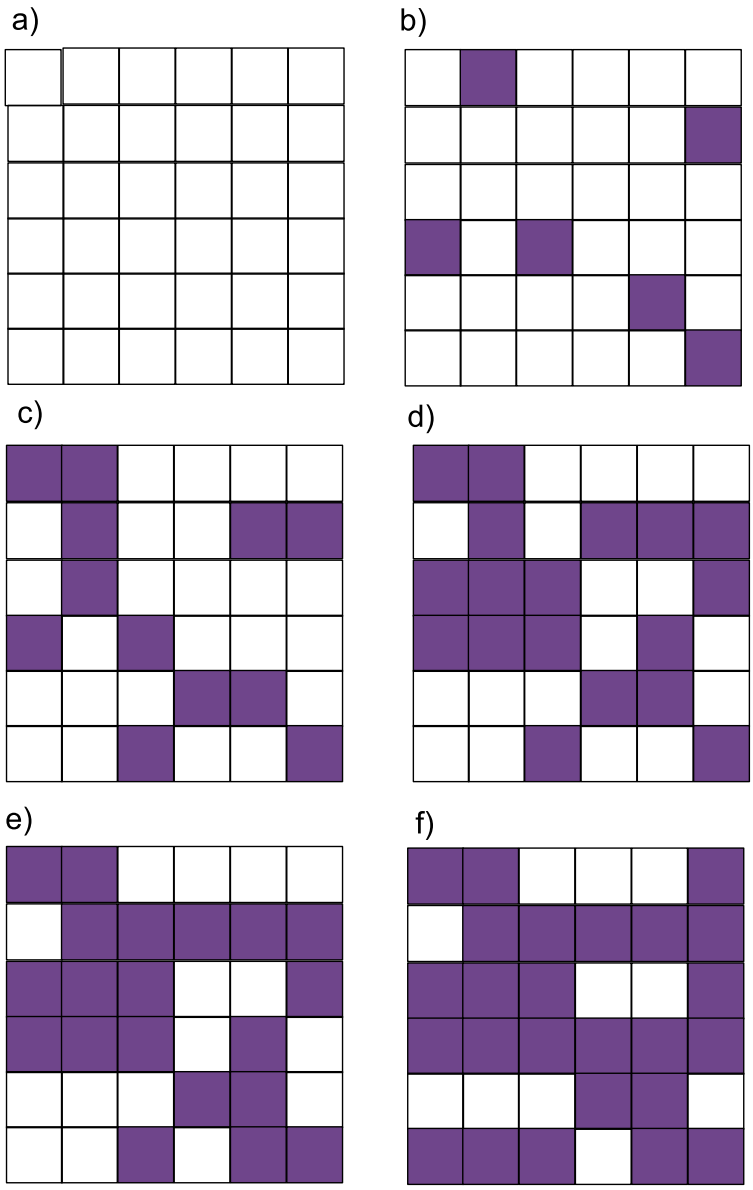

Figure 1.6 Site percolation example in two dimensions a) empty lattice, b) p = 0.17, c) p = 0.33, d) p = 0.5, e) p = 0.56 first percolated cluster formed, f) p = 0.69.

$$E \sim (p - p_C)^{\beta} \qquad (1.1)$$

For transport phenomenon in composites, such as ion conductivity the paths not only need to exist, the mobile species must move through them. This type of event is modeled after an

"ant in a labyrinth."[57] Referring to Figure 1.6, an ant may only walk on a purple site and the ant may only proceed to the next purple site if the sites are nearest neighbors. In other words, the ant can only move around within a single cluster. If the clusters are small and do not percolate the length scale of diffusion is limited. However, at $p >> p_c$, where there are large, percolating clusters, random walk-type motion is recovered.[57] For the exact solution of conductivity on a Bethe lattice, the critical exponent is 3. However, from Monte Carlo simulations, the value is approximately 2.0 in three dimensions.[58] This difference comes from presence of many dead ends in the network, especially near p_c. While the dead ends contribute to the fraction of percolated material, they do not contribute to the conductivity. This was confirmed by experiments on graphene sheets with randomly punched holes. The measured conductivity was much less than expected, given the amount of percolated material.[59]

Recently, percolation theory has been heavily applied in the area of electrical polymer composites. These materials generally use carbon nanotubes carbon black, or graphene as the conducting phase.[60] There are far fewer examples of percolation applied to solid lithium ion conducting polymers. A few recent reports use percolation theory to evaluate ion conductivity in swollen polymer membranes, such as those used for ion exchange.[61] They found good agreement with percolation and determined that the percolation threshold was dependent on the processing methods.[61] Hoarfrost and Selegman combined percolation theory with the Vogel-Tamman-Fulcher (VTF) equation to create a universal scaling relationship for the conductivity of block copolymers where one phase is swollen in ionic liquid.[62] Their equation was a good fit for two different types of polymers swollen with various ionic liquids. Both percolation theory and the VTF equation are necessary to accurately describe this system because changing the amount of ionic liquid changes both the T_g and volume fraction of the conducting phase.[62]

1.2 Ion Conductivity in PEG

One of the many areas that will benefit from facile synthesis of bicontinuous morphologies is the ability to improve and tailor the mechanical properties of solid electrolytes. Access to affordable, clean energy is a well-recognized scientific and technical challenge for this century.[63] Although many different opportunities are being investigated, every solution involves better batteries, as they represent the main energy storage device.[64] Despite wide-spread use, current batteries are far from their theoretical storage potential and significant improvements can be made (up to 95% of theoretical values) by eliminating components such as the separator.[65] Among commercially available batteries, lithium ion batteries are attractive because they have the highest energy density.[66,67] One important area of research focuses on replacing the current liquid or gel electrolyte of these batteries with a solid material. This is expected to double the energy density and eliminate the volatile organic solvents, which pose a fire hazard.[66,68] For a solid material to replace liquid and gel electrolytes, it should have a minimum ion conductivity of 10^{-3} Scm^{-1} throughout the expected range of operating temperatures.[64,66] At the same time, solid electrolytes should have enough mechanical integrity to replace separators currently used in the liquid electrolyte design. While many material systems have been examined,[5,66,67,68] few exhibit the necessary conductivity or mechanical properties; simultaneously improving both remains a challenge. Soft materials enable rapid chain-relaxation and thus higher conductivity, while stiffer materials, which yield more appropriate mechanical properties, generally have lower conductivity.[69] Notable exceptions to this trade-off are the equilibrium phase-separated, PEG-PS block copolymer materials such as those studied by Balsara and coworkers.[4,70,71,72] These materials had a shear modulus of approximately 100 MPa, demonstrating that the mechanical properties are dictated by the polystyrene phase.[70] The major drawback to this strategy is that ion conductivity is limited by grain orientation; any lamellar grains aligned perpendicular to the

applied voltage act as barriers to the ion conductivity. A bicontinuous morphology would overcome this drawback by insuring that pathways for conductivity are uninterrupted in all directions.[4]

1.2.1 Approaches

In addition to morphology investigations, several studies with the goal of understanding and improving the ion conductivity in solid materials are underway. According to *ab initio* calculations, Li+ is coordinated to approximately four or five ether oxygens at any one time.[73] As the chains relax, Li+ is passed along a single chain or from one chain to the next as shown in Figure 1.7 a. This mechanism yields ion conductivity with a temperature dependence that can be well described by Williams-Landel-Ferry (WLF) or Vogel-Tammen-Fulcher (VTF) equation. Contrary to the WLF behavior, is the Arrhenius mechanism in which the ion hops from one coordination site to the next, shown in Figure 1.7 b. Arrhenius conductivity is identified by a linear relationship between the log of conductivity and the inverse temperature, which is not often seen in PEG-based materials.

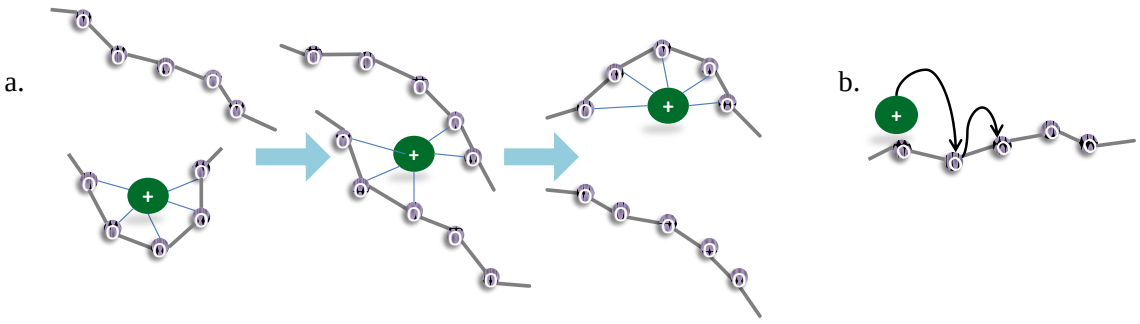

Figure 1.7 Transport mechanisms of lithium ions in PEG-based materials. (a.) Chain relaxation mechanism (b.) Arrhenius "hopping" mechanism. Below each figure is the equation to fit temperature dependence of conductivity. In the WLF equation: σ is the conductivity in Scm^{-1}, T is the temperature in K, A is a parameter related to the number of charge characters, B is a parameter related to the activation energy and T_0 is a parameter which gives the temperature at which molecular motion stops, usually about 50K below T_g. In the Arrhenius equation: σ_0 is a parameter related to the number of charge carriers, E_a is the activation energy in and k_B is the Boltzmann constant.

Since Wright discovered the ion conducting properties of PEG,[74] this material has been extensively studied as the main component of solid electrolytes, and remains one of the best lithium ion conductors known. However, PEG is known for being highly crystalline and the chain-relaxation mechanism only takes place in the amorphous phase. Efforts to improve conductivity by reducing PEG crystallinity include using branched polymer architectures and using lithium salts with an optimized counter ion. Hawker and coworkers synthesized a hyperbranched PEG-based polymer based on an AB_2 monomer, shown in Figure 1.8, which did not exhibit a melting peak when probed with DSC. However, the conductivity of this system was still low, 7×10^{-5} Scm^{-1} at 30 °C. This could be due to the increased T_g of the hyperbranched polymers, -5 °C compared to -67 °C recorded for linear PEG, or the salt choice of $LiClO_4$.[75] Angell and coworkers compared a series of lithium salts including: lithium tetrafluoroborate ($LiBF_4$), lithium perchlorate ($LiClO_4$), lithium trifluoromethanesulfonate (LiOTf), lithium bis(trifluoromethanesulfonyl imide) (LiTFSI) and lithium bis(oxoloato) borate (LiBOB) (Figure 1.9). They found that samples loaded with $LiBF_4$, $LiClO_4$ and $LiSO_3CF_3$ had a sharp decrease in ion conductivity at low temperatures due to PEG crystallization. LiTFSI- and LiBOB-containing

samples did not show this decrease in conductivity. Also, differential thermal analysis showed that samples loaded with LiTFSI or LiBOB did not crystallize.[76] The bulk and irregular shape and LiTFSI and LiBOB allow them to disrupt PEG crystallinity.[77]

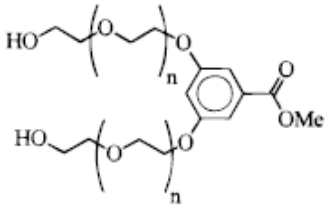

Figure 1.8 Structure of an AB_2 monomer used in Hawker *et al.*'s hyper-branched polymer studies, from reference [75].

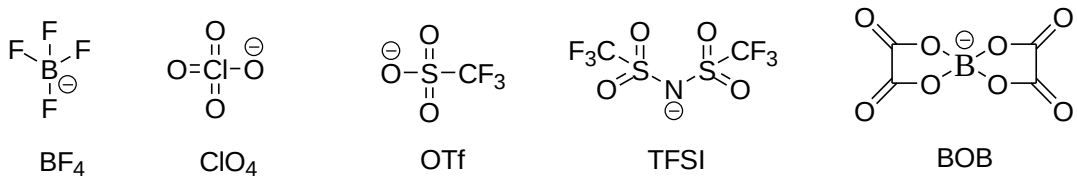

Figure 1.9 Structure of the counter ions studied by Angell and coworkers. Large, bulky anions are able to disrupt crystallinity in PEG which improves conductivity.

It has also been shown that materials with low T_g generally have better ion conductivity.[78,79,80] This inspired the study of PDMS-based materials including comb-like polymers consisting of a polymethylhydrosiloxane (PMHS) backbone with oligo(ethylene glycol) side chains, shown in Figure 1.10. These polymers alone did not have sufficient mechanical properties to yield free-standing films so they were entrapped in a network of PEG-dimethacrylate. The resulting semi-interpenetrating networks were free-standing and exhibited ion conductivity of approximately 10^{-4} Scm^{-1} at 37 °C.[78] This group did not measure the T_g of their material; however, their conductivity was improved compared to a branched polymer with a polyphosphazine backbone with a T_g of -84 °C.[81]

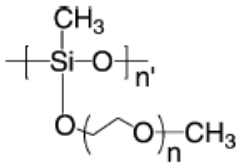

Figure 1.10 Structure of the poly(siloxane-g-ethylene oxide) used in interpenetrating network studies in reference [78].

1.3 Mechanical Properties

1.3.1 Battery Separator Requirements

The separator is a critical component of any battery. Its role is to prevent a short circuit by keeping the anode and cathode from coming into electrical contact.[82] While mechanical stability is essential to fulfill this role and to enable large scale processing,[66] the specific mechanical property requirements of the solid electrolyte/separator have not been well defined. This could be partially due to the wide range of separator requirements among different types of lithium ion batteries.

Current lithium ion batteries use intercalation electrode materials, meaning lithium ions diffuse in and out of lattice sites in the electrode material.[64,83] These materials include lithiated graphite (LiC_6) and lithium vanadium disulfide ($LiVS_2$) for anodes and lithium manganese oxide ($LiMn_2O_4$) and lithium cobalt oxide ($LiCoO_2$) for cathodes.[64,84] As a result of the lithium ions intercalating and deintercalating, these materials exhibit noticeable volume changes upon cycling.[85] These volume changes can cause up to 50% compressive strain in the separator material. Current separators, porous polyethylene or polypropylene membranes, cannot

withstand this amount of strain as demonstrated by the mechanical fatigue seen after repeated cycling. As a result, the pores close preventing lithium ion passage, which reduces the storage potential of the battery.[85] New anode and cathode materials are being developed to accommodate these large volume changes. Silicon-based anodes can accommodate volume changes up to 300% when fully charged.[64,84,86,87] Solid electrolytes for devices with intercalation electrodes will need to keep pace and withstand these high strains without fracturing or losing ion conducting capability in order to ensure long-term and safe operation of the battery.

Replacing the intercalating anode material with lithium metal has several advantages. Lithium is the most electropositive and the lightest of all metals which would allow for a device with high energy density. Using the lithium metal would increase the supply of lithium ions thus increasing the life of the battery compared to intercalation electrodes.[67] However, lithium metal anodes suffer from dendrite formation. As the battery goes through several charge and discharge cycles, the lithium deposited on the anode surface forms needle-like crystals called dendrites, shown in Figure 1.11. These crystals can grow through the separator, eventually bridging the anode and cathode causing a short circuit.[82] Mathematical simulations have shown that increasing the modulus of the electrolyte material to the order of 1 GPa will prevent surface roughening of the anode, thus preventing dendrite formation.[88] Solid electrolytes for devices with a lithium metal electrode should have a very high modulus to ensure safe operation of the battery. Several prospective electrode systems currently under exploration contain a lithium metal anode. Examples of these include lithium/air,[89,90] lithium/sulfur[91] and lithium seawater[92] A chemical platform for creating solid electrolyte materials with tunable properties will allow electrolyte materials to keep pace with the demands of new electrode materials as they are developed.

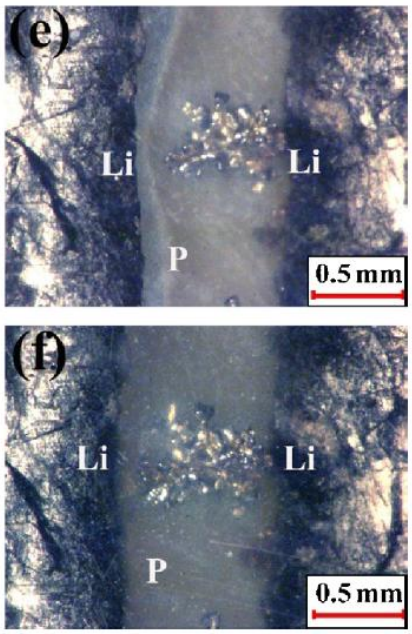

Figure 1.11 Dendrite growth on lithium electrodes from reference [82].

1.3.2 Approaches

Cross-linking often increases mechanical stability of many polymeric materials.[2] However, the cross-linking must be efficient since loops, dangling ends or other defects compromise the mechanical properties.[67] Several examples of cross-linked, PEG-based solid electrolytes have elastic moduli on the order of $10^4 – 10^6$ Pa and ion conductivity on the order of 10^{-5} Scm^{-1} at 25 °C.[93,94,95]

A majority of the time, PEG is used as the ion-conducting phase while a second component imparts mechanical strength or other desired properties. Introducing a rigid component with a high T_g such as polystyrene is one strategy to improve mechanical properties. Balsara and coworkers developed a system based on PEG-PS block co-polymers which demonstrates the ability to decouple the mechanical properties from the ion conductivity. Focusing on the lamella morphology, they reported materials with a shear modulus of 10 to 100

MPa and ion conductivity on the order of 10^{-4} Scm^{-1} at 90 °C which improves with increasing molecular weight of the block copolymers.[70,96] While this is an excellent proof of concept, measurements were only taken at high temperatures so that PEG crystallinity did not affect any of the data. These samples also contained small amounts of lithium salt compared to other systems. Most of Balsara's samples contain 50 ether oxygen atoms for each lithium ion or, EO:Li = 50. [3,4] Often, PEG based materials exhibit maximum conductivity at EO:Li = 16.[97] It is likely that the ambient temperature ion conductivity is poor due to this low salt loading and crystallinity in the PEG domains.

1.4 Composite Models

When two or more components are used in a material, it is often useful to predict the properties of the resulting composite. Composite properties are affected by the characteristics and ratio of the components as well as the morphology or arrangement of the phases. One of the simplest models for mechanical properties are the Voigt and Reuss bounds. As shown in Figure 1.12, these two models are based on an assumption that the components of the composite are arranged either parallel or perpendicular to the strain, as shown by the arrows. This assumption gives either a maximum (Voigt, equation 1.2) or minimum (Reuss, equation 1.3) prediction of the composite property E_C, where E_1 and E_2 are the properties of the components and ϕ_1 and ϕ_2 are the volume fraction of the components. While these equations were originally developed to predict the Young's modulus, they apply to several areas such as toughness, mass density, and thermal and electrical conductivity.

$$E_C = E_1\phi_1 + E_2\phi_2 \qquad (1.2)$$

$$E_C = \frac{1}{\frac{\phi_1}{E_1} + \frac{\phi_2}{E_2}} \qquad (1.3)$$

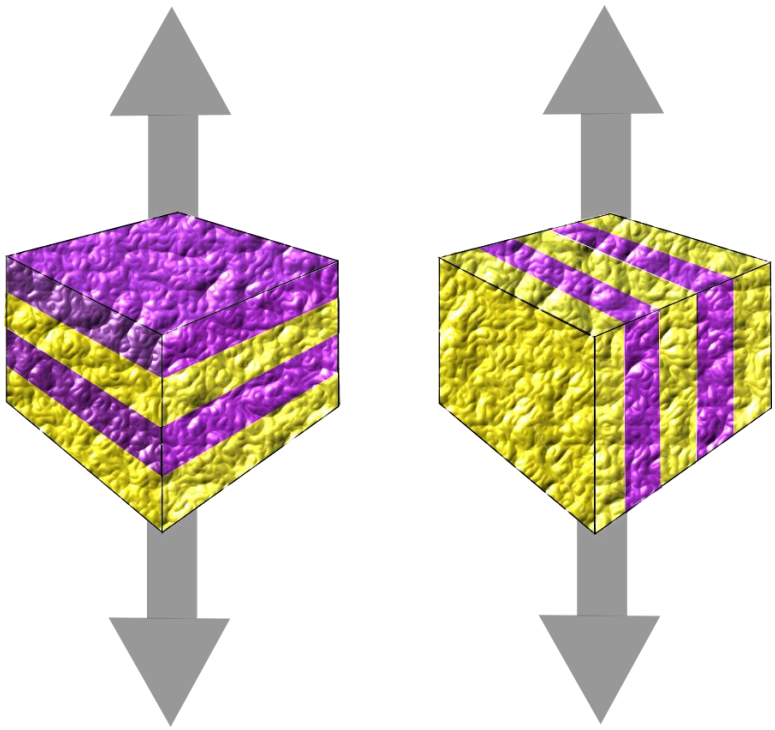

Figure 1.12 Reuss (left) and Voigt (right) models where the arrows show the direction of property measurement.

1.5 Outline

This thesis is presented in eight chapters. Chapter two discusses the chemical platform used for materials synthesis, the Mitsunobu and thiol-ene reactions. It also offers a comparison between the synthesis of the co-networks and multiblock copolymers. These two types of materials present unique challenges despite using a similar chemical design. Chapter three discusses the properties of PEG and PEG-PDMS salt-loaded networks, focusing on the relationship between thermal properties and ion conductivity. Chapters four and five are dedicated to the PEG-PS network system. Chapter four describes the relationship between the molecular weight between cross-links and the morphology, as well as the relatively molecular weight independent properties of ion conductivity and mechanics. In Chapter five, ion conductivity and mechanical properties are used as probes to demonstrate cocontinuity of the

PEG and PS phases, respectively. Also fitting this data to various percolation models gives a definition of the breadth of the bicontinuous phase composition window. Chapter six discusses the preliminary work on the properties of the multiblock copolymers. Chapter seven gives some perspectives and an outlook to the future. Finally the experimental methods are given in Chapter eight.

CHAPTER 2

CHEMISTRY

2.1 Introduction

This thesis describes end-linked materials made via a two step process. The starting materials are various commercially available α,ω-dihydroxy end-functionalized polymers, norbornene acid, and di- or tetra-functional thiols. Norbornene is added to the alcohol end-groups *via* a Mitsunobu reaction. These precursor polymers are then end-linked together using a tetrafunctional thiol to make co-networks or a difunctional thiol to make multiblock copolymers (MBCs). This chapter describes the reactions used, their outcomes, compares the two systems and offers some suggestions on how to improve conversion in the thiol-ene platform.

2.1.1 Mitsunobu Chemistry

The Mitsunobu reaction is widely used to couple alcohol and acid functionalities to form ester bonds.[98] This reaction uses coupling reagents such diisopropylazodicarboxylate (1) and triphenylphosphine (2) to accomplish this reaction with high conversion. In this work, it was used to attach norbornene acid (3) to a variety of α,ω-dihydorxyl polymers. Figure 2.1 shows the mechanism for a generic polymer with one alcohol end group (4). The reaction begins when (2) attacks the azo group of (1) creating a zwitterionic intermediate (ZI) that can then deprotonate the norbornene acid. This leaves a positive charge on DIAD-PPh_3 intermediate, which the alcohol group on the polymer attacks. This generates the first side product, diisopropyl carbamate and creates a good leaving group, triphenyl phosphine oxide ($POPh_s$), on the end of the polymer chain. The deprotonated (3) can then react with the terminal CH_2 group of the polymer causing $POPh_3$ to leave *via* an SN_2-type reaction.

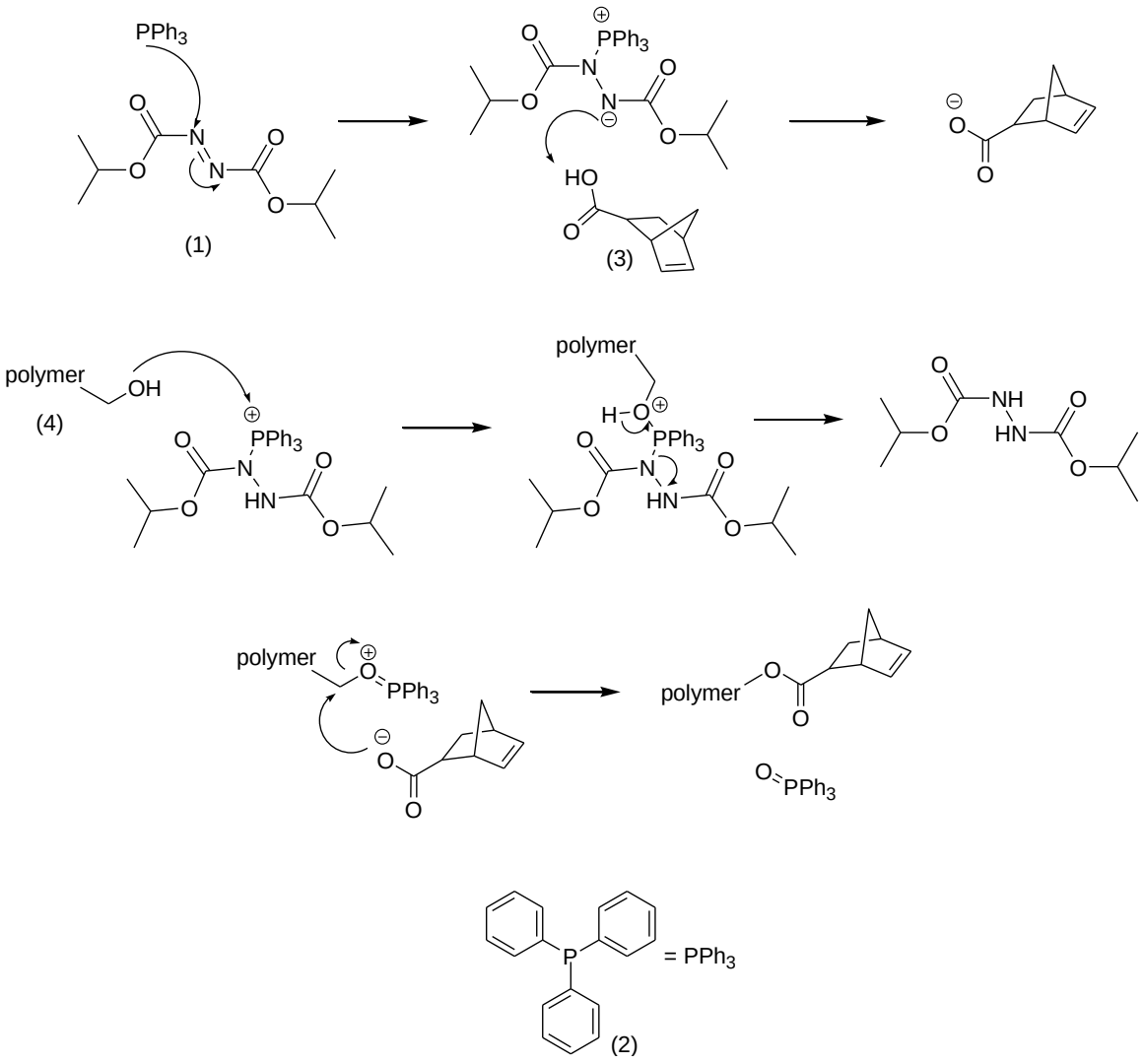

Figure 2.1 General mechanism for end-functionalizing polymers with norbornene via Mitsunobu chemistry.

2.1.2 Thiol-ene Chemistry

The general mechanism of thiol-ene chemistry, in which thiol and alkene groups are coupled into a thioether *via* a radical reaction, is shown in Figure 2.2. In this study radicals were

generated using photoinitiation; however, other methods of generating radicals such as heat[99] or red-ox[100] are useful. After the radical is generated from the photonitiator (PI) it abstracts a proton from a thiol creating a thiyl radical. This attacks the alkene group creating a secondary radical. The reaction propagates by attacking another thiol regenerating the thiyl radical. This cycle proceeds until all radicals are consumed.

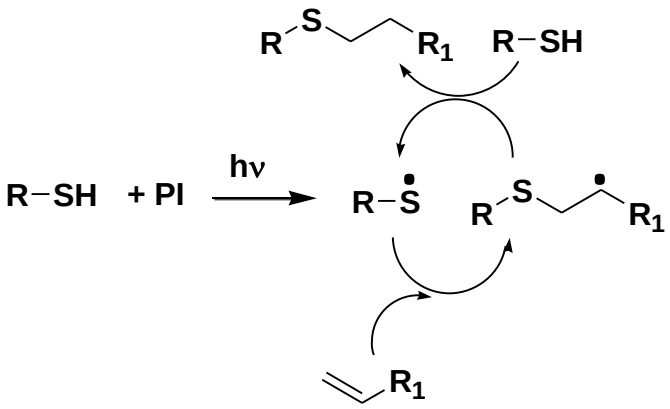

Figure 2.2 General mechanism of thiol-ene chemistry.

Click reactions have gained recognition for their ability to react efficiently and selectively. Radical thiol-ene chemistry has many advantages such as high tolerance to functional groups, water, and oxygen, is metal free, and a variety of radical initiators offer spatial and temporal control of the reaction.[63,101] This has been demonstrated as thiol-ene chemistry is often used in polymer functionalization,[102] cyclization[103] and for synthesizing end-linked polymer networks.[63,104,105,106,107,108,109,110] However, this technique has thus far proved to be unsuccessful in polymer-polymer conjugation, or end-linking reactions. Koo *et al.*, attempted the photo-initiated conjugation of thiol-terminated PS and vinyl-terminated poly(vinyl acetate). By GPC and IR, the conjugation appeared successful; however, qualitative data from ^{1}H-NMR and elemental reviled this technique produced only a 25% yield of the desired diblock largely due to side reactions, as shown Figure 2.3.[111] Further theoretical work by Derboven *et al.*, shows that these side reactions

play a large role in photoinitiated polymer-polymer conjugation using thiol and vinyl ether functional groups.[112]

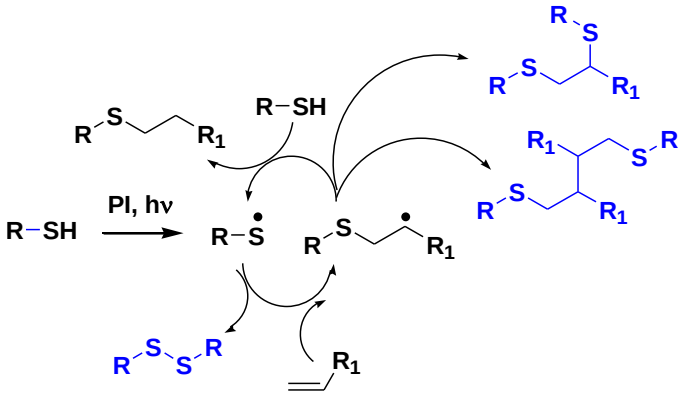

Figure 2.3 General scheme for thiol-ene chemistry where R_1 and R_2 stand for polymers or small molecules. Examples of side products from radical coupling are highlighted in blue.

The thiol-ene reaction rate can vary greatly depending on the structure of the thiol and ene reactants. Several studies cite that norbornene is the most reactive ene due to the release of ring strain,[113,114,115] and absence of abstractable protons,[116] which contributes to its wide use in polymer networks.[104,105,107] Recently, computational studies by Northrop and Coffey[117] corroborate this trend showing that norbornene shows the largest negative $\Delta H°_{rxn}$ and $\Delta G°_{rxn}$ of several enes when reacted with methane thiol. Also, norbornene gives the highest computationally predicted reaction rate and reaches the most complete conversion of the twelve ene structures tested. Norbornene also gives the added advantage of reacting only though a step-growth mechanism rather than the combined step- and chain-growth mechanism of radical initiated thiol-acrylate reactions.[118]

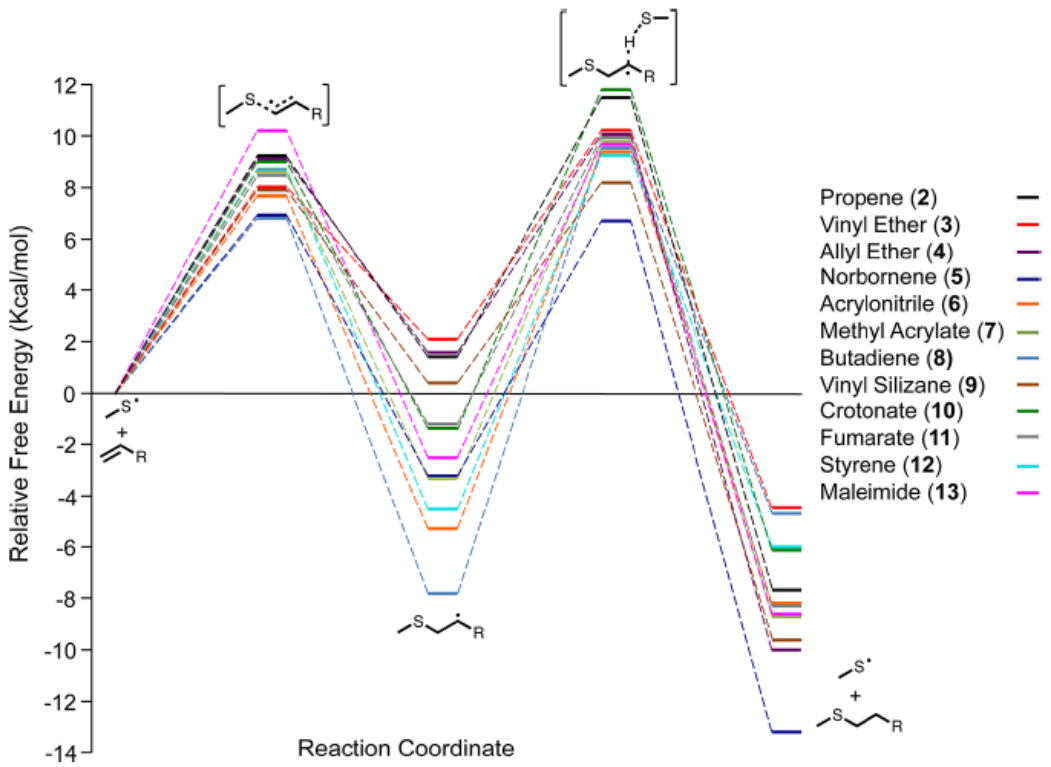

Figure 2.4 Relative free energies for various "enes" during the thiol-ene reaction.[117]

Far fewer investigations have been conducted on the structure of the thiol. The most often cited study compares three thiol structures: an alkane thiol, a mercaptioacetate and a mercaptopropionate.[119] The Mercaptopropionate is the most reactive of the three, showing nearly six times the activity of the alkane thiol. Morgan *et al.*, suggest this is because the mercaptopropionate can form a six membered ring through hydrogen bonding which weakens the S-H bond making it more reactive as shown in Figure 2.5.[119] Other studies have investigated the effect of steric hindrance on the thiol group. Wutticharoenwong and Soucek[120] studied the reactivity of three dithiols against three different alkenes. Of the three thiols studied, *trans*-1,4-bis(mercptomethyl)cyclohexane (CHDMT) was consistently the less reactive than 1,8-octanedithiol (ODT) *trans*-1,4 bis(mercaptomethyl)benzne (BDMT). CHDMT is much more

sterically hindered than either the linear ODT or the planar BDMT molecule which contributes to its slow reactivity despite the fact that the α carbon is primary. There are only a few examples of radical thiol-ene reactions using tertiary thiols. One such examples is from an investigation of a new photonitiator,[100] $Ru(bpy)_3^{2+}$. The effectiveness of this catalyst was investigated on seven different thiols reacting with styrene. All of products were obtained in yields of greater than 86%; however the lowest yielding product was made from *tert*-butylmercaptan and this reaction took the longest, 20 hrs. The next longest reaction was with cyclohexylmercaptan (a secondary thiol) which had a yield of 98% in 8 hrs. The primary thiols tested both gave yields of over 95% in 2 hrs or less.[100] These studies demonstrate the both the advantage of using primary thiols and the need for comprehensive evaluation of thiol structure on reactivity using model compounds that accurately represent the system of interest.

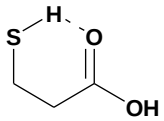

Figure 2.5 Six membered ring giving stabilization to hydrogen abstraction.

2.1.3 Polymer Networks

Polymer networks make up several classes of polymeric materials. Depending on the cross-link density, they can be classified as thermosets or elastomers and they can be swollen in solvent to create gels.[121] These classes have widely variable properties, making polymer networks broadly applicable. Their wide-spread use makes polymer networks interesting materials for fundamental investigation.

2.1.4 Multiblock Copolymers

Utilizing different block chemistries, block lengths, and number of blocks, nearly endless combinations of multiblock copolymers (MBCs) can be generated. However, covering this vast territory of combinations cannot be efficiently accomplished with traditional block copolymerization techniques.[122] Few combinations of monomers can be alternatingly polymerized as their propagating centers need to have nearly equivalent reactivities to initiate subsequent blocks.[122] Furthermore, block copolymer synthesis often requires the stringent conditions of living polymerizations.[122,123,124,125,126] While living polymerizations have been used to generate sequence controlled MBCs with up to 20 blocks, these techniques remain highly specialized.[55,123,124] The coupling of individual blocks through telechelic functional groups is an alternative MBC synthesis technique. This simplified synthetic approach allows for broader ranges of block chemistries, milder polymerization techniques, and the incorporation of commercially available starting blocks.

Generally, linear MBCs fall into three categories: alternating (ABABAB); random (AABBAB); and sequence-specific (ABCDEF). Lee and Bates synthesized random and alternating MBCs from α,ω-dihydroxy functionalized polystyrene (PS), polybutadiene (PB), and polylactide (PLLA), an example of which is shown in Figure 2.6.[52,53] Random MBCs were formed by linking these macromonomers with a diisocyanate to form urethane bonds. Alternating MBCs were formed by first end-capping PS with the diisocyanate, purifying this macromonomer, then adding the alcohol-terminated PB.[52,53] While polyurethane chemistry is a reasonable approach, it has significant limitations, including sensitivity to moisture, and side reactions resulting in biurets and allophanates that lead to branching. Other examples of this general route to MBCs include disulfide linked poly(n-butyl acrylate)/poly(methyl methacrylate) systems in which ABA triblocks with α,ω-dithiols were synthesized by RAFT and subsequently reduced to

form MBCs,[127] and poly(arylene ether sulfone)-based MBCs synthesized by step growth.[128,129] Expanding MBC chemistry will require the development of high-yielding conjugation reactions.

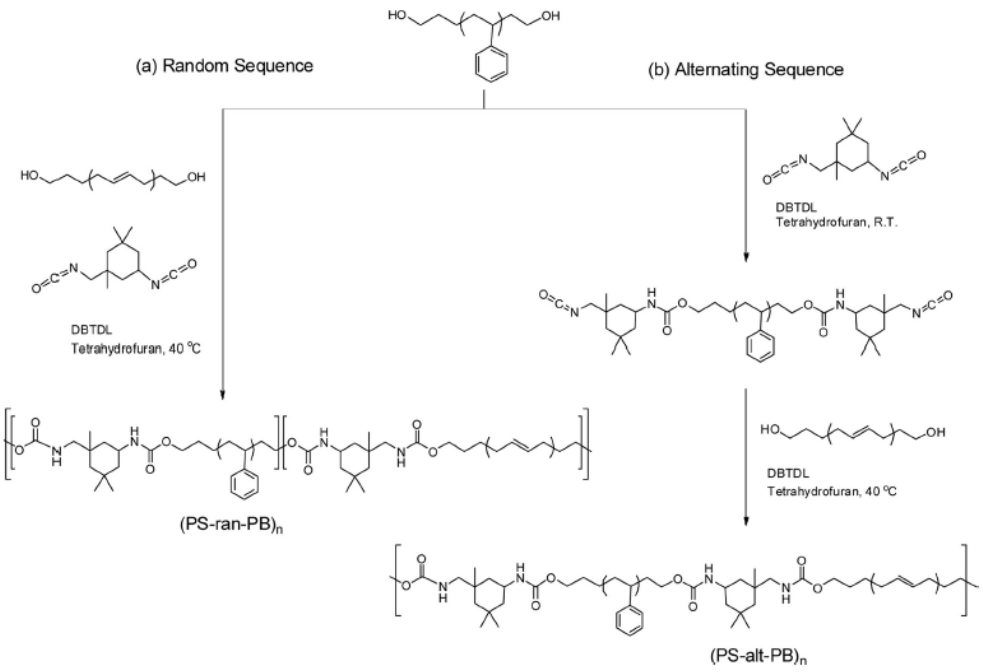

Figure 2.6 Random and alternating multiblock synthesis from reference [56]

2.1.5 Carouther's Prediction vs. Percolation Theory

High conversion efficiency is paramount for synthesizing multiblock copolymers by coupling end-functionalized precursor polymers. This strategy closely mimics the condensation polymerization of AA+BB type monomers. As described by Carouthers in Figure 2.7, the degree of polymerization (d) is inversely dependent on the extent of reaction (p) according to the equation $d = 1/(1-p)$.[130] In order to obtain a high number of blocks (i.e. n=20), a near-quantitative coupling reaction (p = 95%) must be achieved. N = 20 is significant target as random phase approximation calculations show that this number of blocks is a good approximation for the micro-phase separation behavior for an infinite number of blocks.[55] However, improvements the

mechanical properties such as toughness and the appearance of a brittle-ductile transition can be realized with as few as five blocks.[131,132]

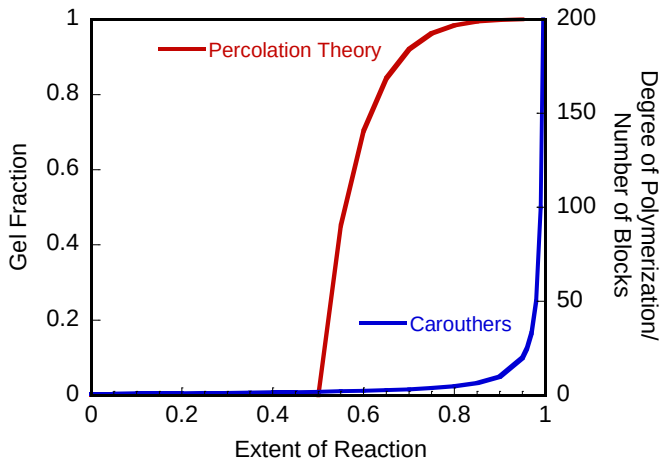

Figure 2.7 Comparison between gelation (left axis, red line) and step growth (right axis, blue line) as the reaction proceeds.

In contrast, percolation theory predicts that a high gel fraction can be reached at a more modest extent of reaction. In Figure 2.7, the percolation theory prediction is given for a network with junction functionalities of f = 3. The networks described here use equimolar amounts of difunctional and tetra functional reagents, therefore f=3 is reasonable, albeit simplified prediction. The first feature of this curve (red) is that below the critical extent of reaction, p_c, the gel fraction is 0. This is because an infinitely percolating network has not been formed. p_c is given by the relationship 1/f-1; therefore in this trifunctional example, $p_c = 0.5$. Once p_c is reached, new connections contribute to the gel fraction rapidly, causing the gel fraction reach nearly 1 at approximately $2p_c$, explained in Chapter 1. Applying critical percolation to the Carouther's equation (blue) it follows that infinite percolation is only achieved a $p_c = 1$. Our multiblock synthesis links precursor polymers together two at a time, therefore f = 2 and 1/f-1 =1.

2.2 Results

2.2.1 Precursor Functionalization

The general strategy for norbornene end-functionalization is given in Figure 2.8. Several polymers of various molecular weights were successfully functionalized; however, this reaction possesses some limitations.

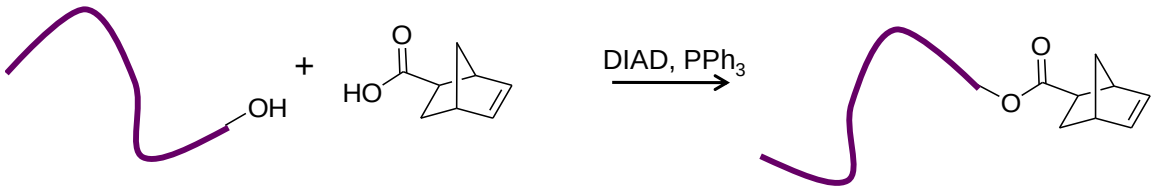

Figure 2.8 Mitsunobu end-functionalization strategy.

2.2.1.1 Polymers Used for Networks and MBCs

Representative ^{1}H-NMR spectra are given in the following figures. Norbornene end-functionalization conversion was determined by comparing the signal from the terminal –CH_2- group (3.7 – 4.3 ppm, depending on the polymer backbone) to the signal from the double bond protons in the norbornene group (~6.1 ppm) and is summarized in Table 2.1. For all polymers used in networks, a high conversion was achieved, over approximately 90%. This is due to the excess of coupling reagents and norbornene acid used during functionalization.

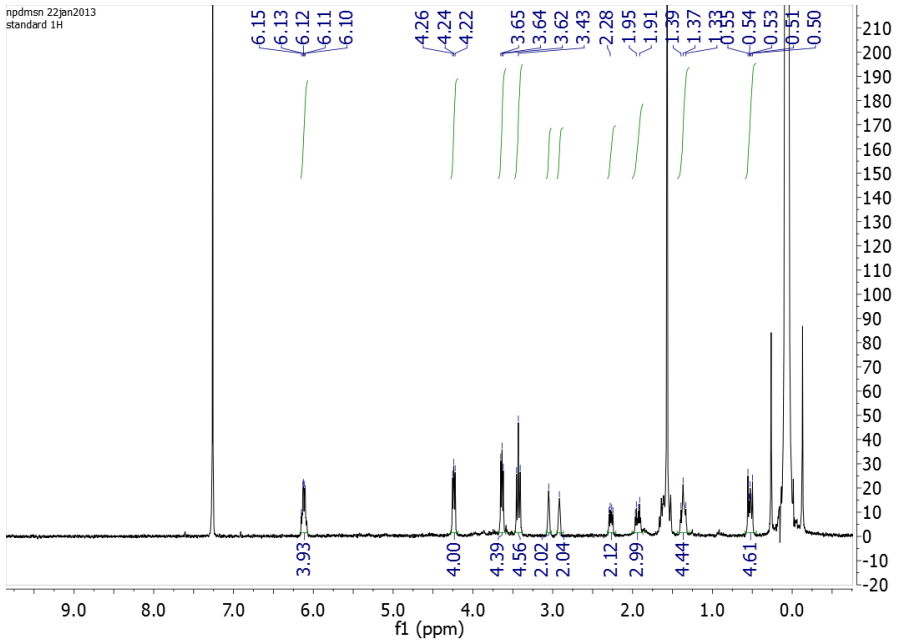

Figure 2.9 ^{1}H NMR of PDMS 4.5 kg/mol functionalized with norbornene in $CDCl_3$.

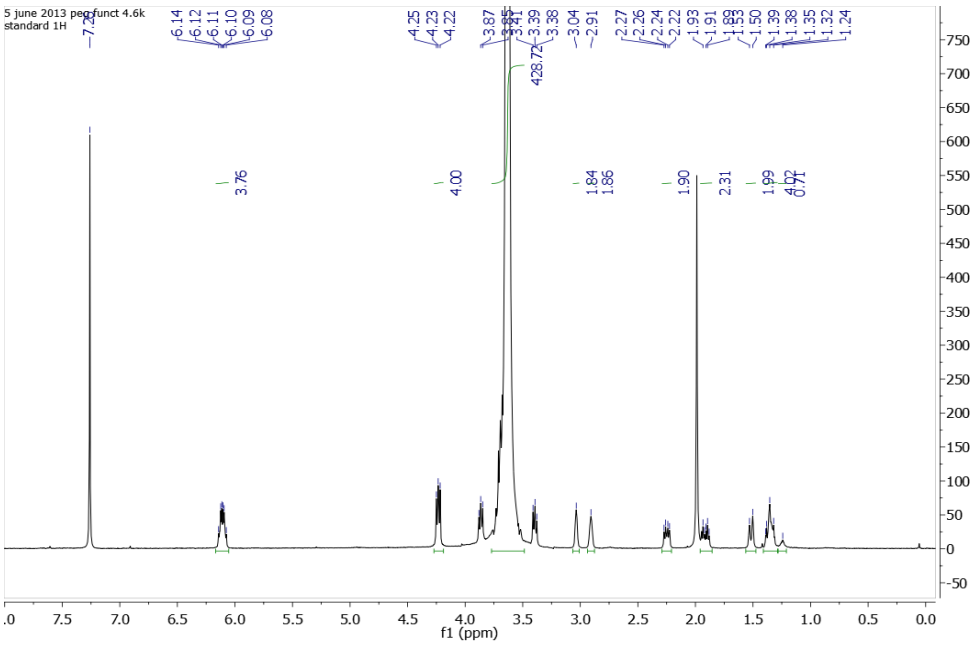

Figure 2.10 ^{1}H NMR of PEG 4.6 kg/mol functionalized with norbornene in $CDCl_3$.

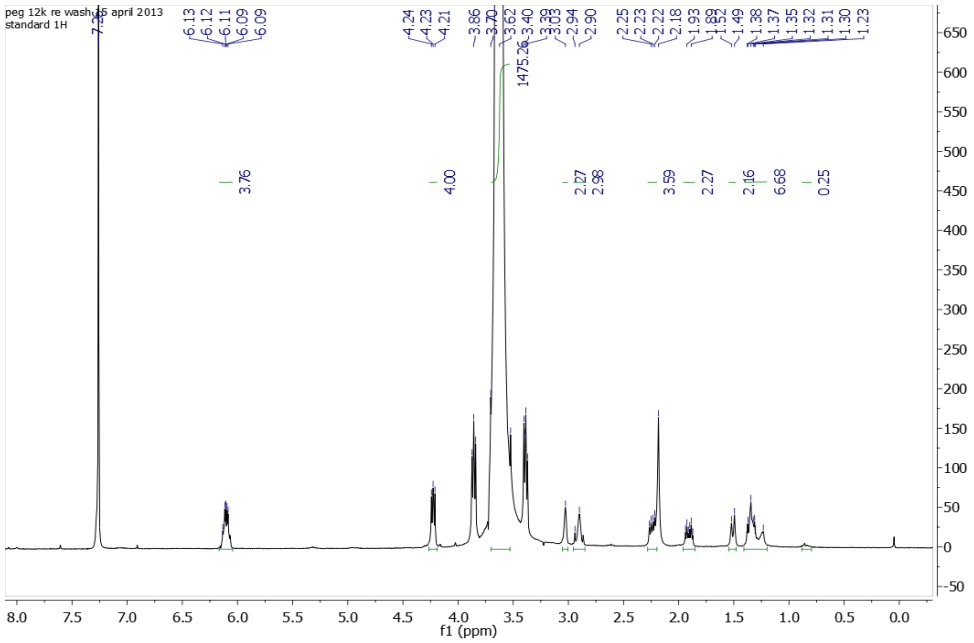

Figure 2.11 ^{1}H NMR PEG 12 kg/mol end-functionalized with norbornene in $CDCl_3$.

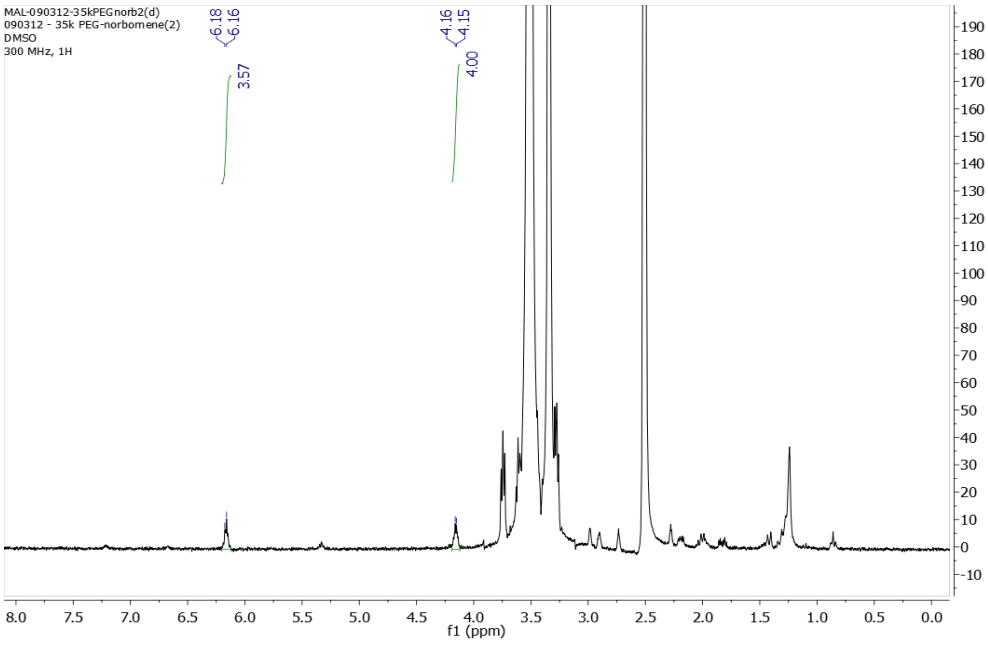

Figure 2.12 ^{1}H NMR in DMSO-(d_6) of PEG (35 kg/mol) functionalized with norbornene end groups.

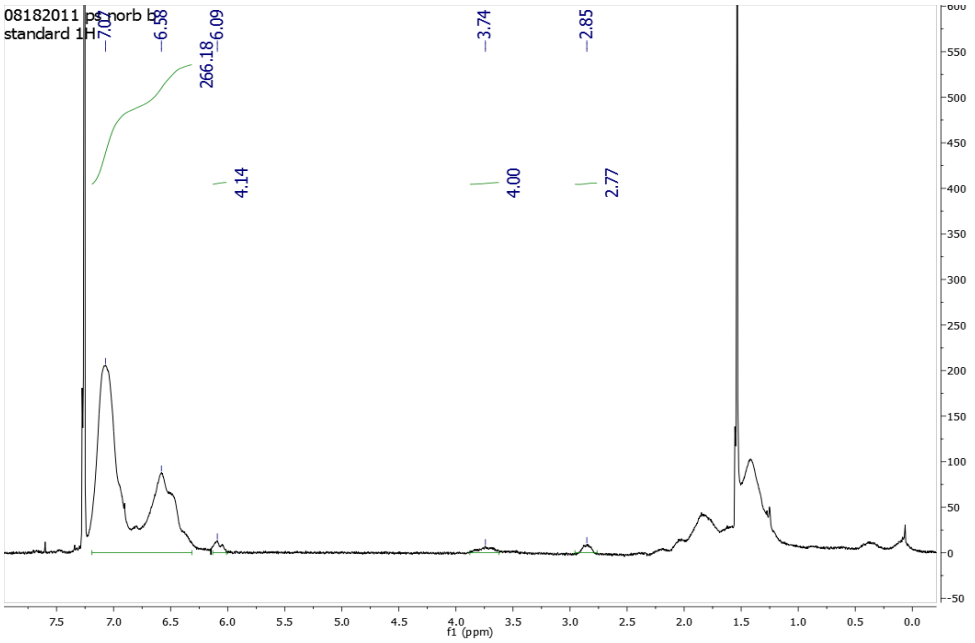

Figure 2.13 ^{1}H NMR in $CDCl_3$ of PS (4.8 kg/mol) functionalized with norbornene end groups.

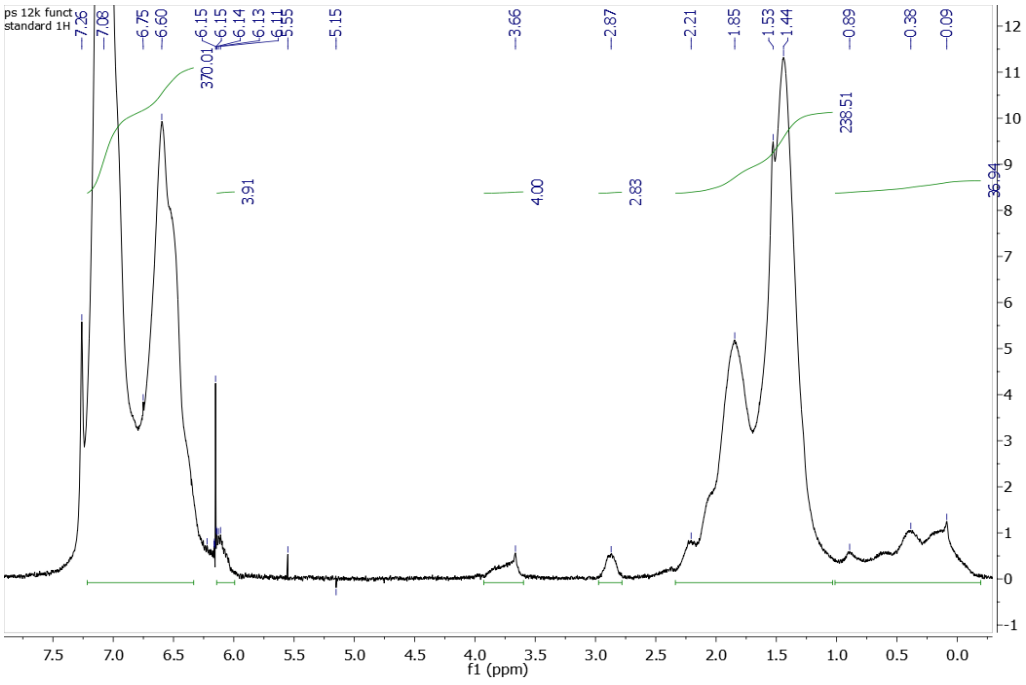

Figure 2.14^{1}H NMR in $CDCl_3$ of PS (12 kg/mol) functionalized with norbornene end groups.

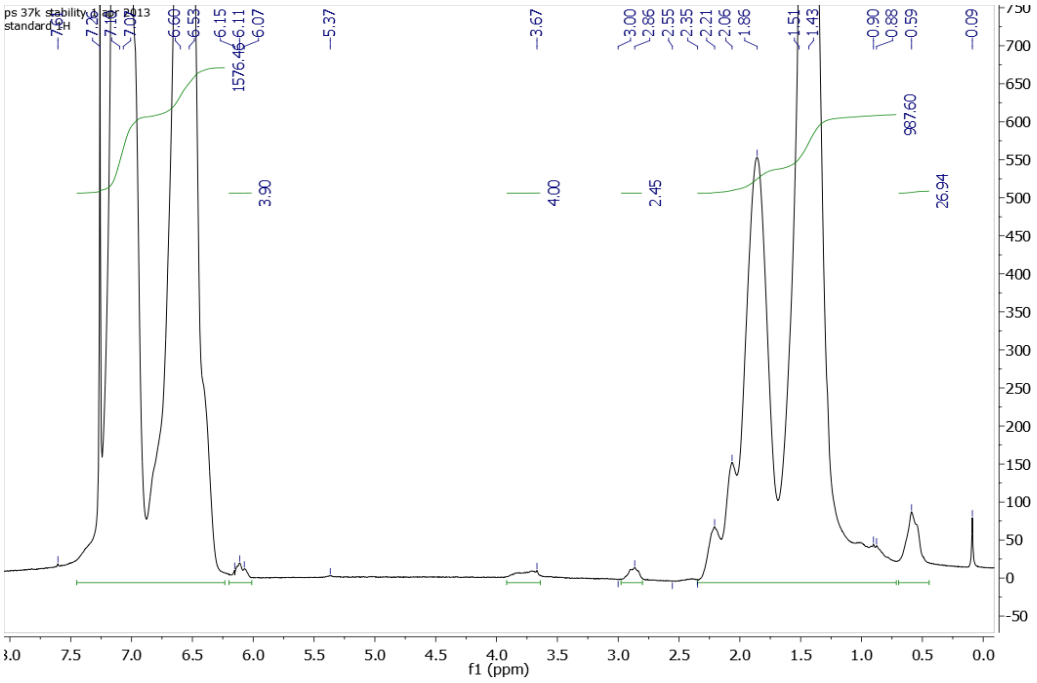

Figure 2.15 ^{1}H NMR in $CDCl_3$ of PS (35 kg/mol) functionalized with norbornene end groups.*

Table 2.1 Conversion of end-groups from representative NMR of norbornene end-functionalized polymers.

Polymer	Conversion (%)
PDMS 4.5 kg/mol	98
PEG 4.6 kg/mol	94
PEG 12 kg/mol	94
PEG 35 kg/mol	89
PS 4.8 kg/mol	< 99
PS 12 kg/mol	98
PS 37 kg/mol	98

2.2.1.2 Other Polymers Functionalized by Mitsunobu

3.0 kg/mol α,ω-dihydroxy terminated polybutadiene (PB) was end-functionalized with norbornene acid in order to demonstrate the high reactivity of the norbornene double bond

* Courtesy of Dr. Melissa Lackey.

compared the linear enes. Functionalization proceeded to approximately complete conversion as shown in Figure 2.16. Also, this PB is made of approximately 37% 1,2-monomers and 63% 1,4-monomers. This was determined by comparing the peak at 5.0 ppm (end of 1,2) with the peak at 2.0 ppm (alkyl of 1,4). Reactivity of the various double bonds with thiols will be discussed later.

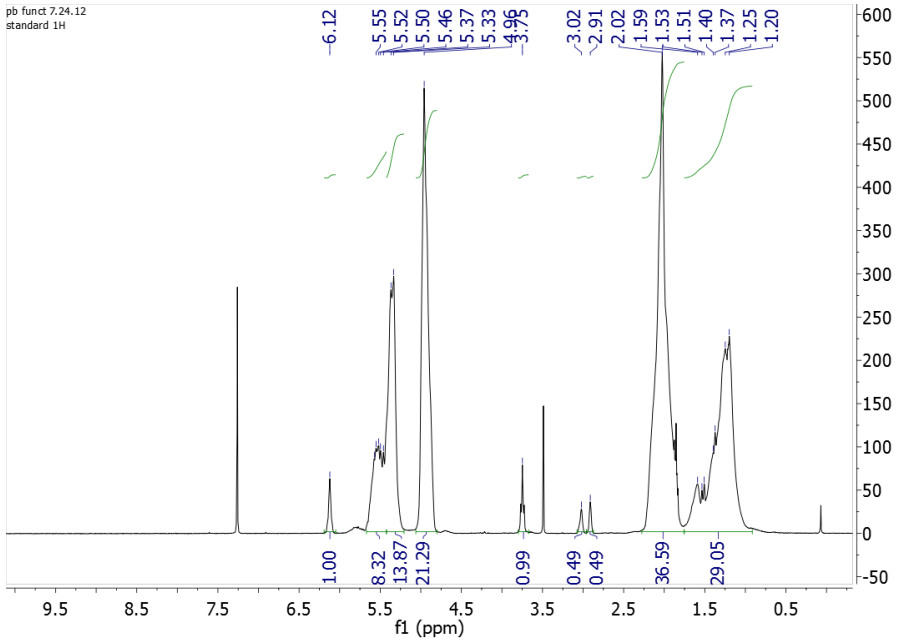

Figure 2.16 ^{1}H-NMR of norbornene end-functionalized polybutadiene in $CDCl_3$.

Finally, a commercial perfluoropolyether (PFPE), Fomblin®, was reacted with norbornene acid. PFPEs are known for their insolubility in many common solvents; therefore, this reaction was carried out in 1,1,2-trichloro-1,2,2-trifluoroethane (Freon®). As this polymer had no protons in its backbone, end-functionalization, or lack thereof, was determined using ^{19}F-NMR. The alcohol end-functionalized polymer, as received is shown in Figure 2.17. The signals at -82.8 and -84.8 ppm correspond to the terminal $–CF_2$-OH groups. After functionalization, these signals should move, for example to -77.5 and -79.5 ppm for an ester linkage.[133] However, the terminal -CF_2- signal remains at -82.7 and 85.2 ppm, post functionalization, as shown in Figure 2.18. This change is not significant enough to support end-functionalization. Likely this

reaction does not proceed because the electron withdrawing florenes make it difficult for the alkoxide to attack the DIAD-PPH_3 intermediate and some of the Mitsuonbu reagents have poor solubility in Freon®. In order to further pursue using PFPE with this chemical platform, a different coupling strategy should be used. PFPE has been end functionalized using an isocyannate linkage.[134] Had this reaction been successful, cross-linking into a co-network would have been difficult because the PFPE is not soluble in many common solvents.

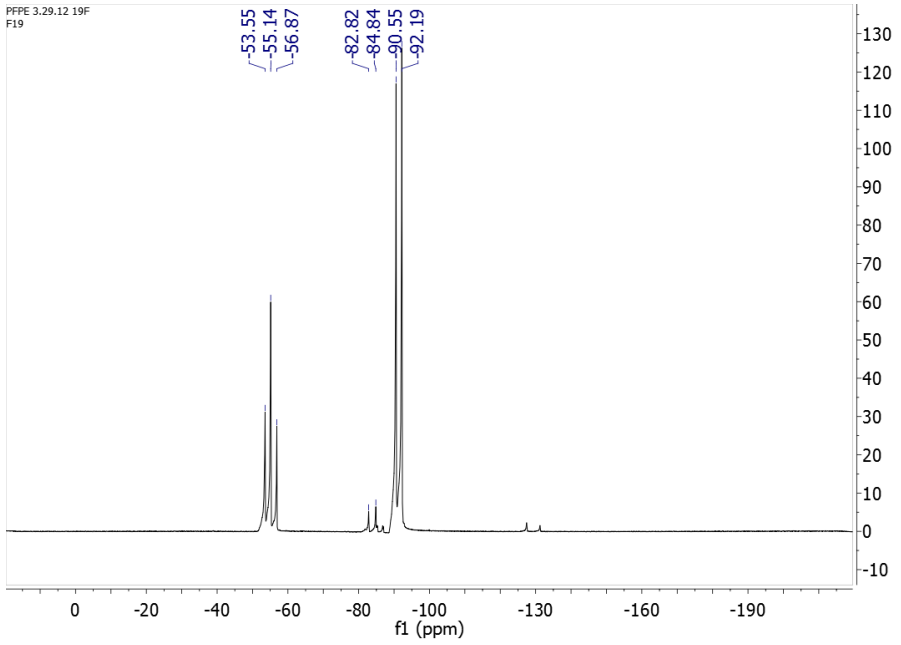

Figure 2.17 ^{19}F-NMR of alcohol end-functionalized PFPE, neat. The -CF_2- backbone peak at 55.14 was used as reference.

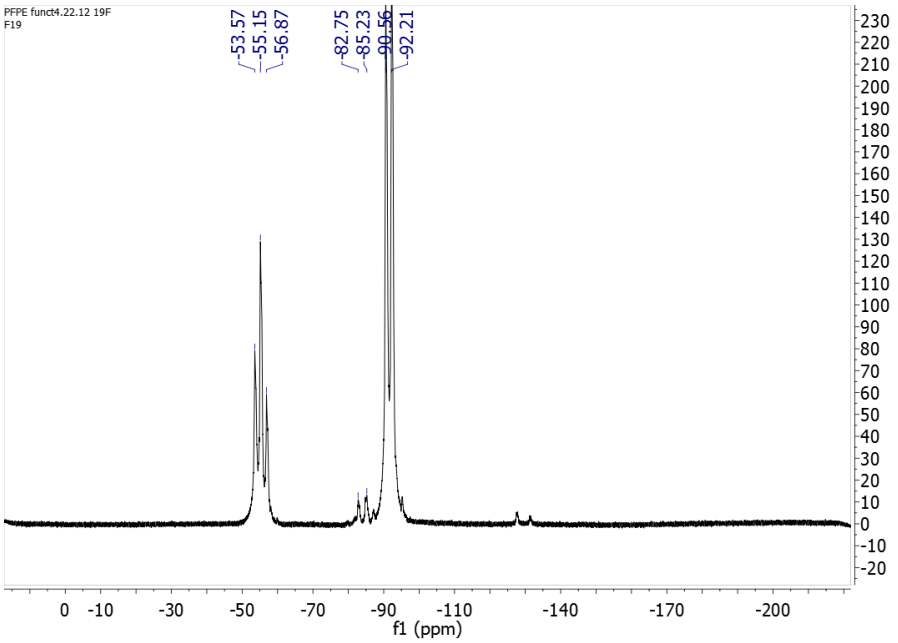

Figure 2.18 ^{19}F-NMR of PFPE after attempted functionalization with norbornene, neat. The -CF_2- backbone peak at 55.14 was used as reference.

2.2.2 Thiol-ene Cross-linking

The overall strategy for network synthesis is given in Figure 2.19. Networks can be synthesized using only one type of precursor polymer for a single phase network or a mixture of polymers, as shown in the figure, to yield a co-network. Generally, networks used for the various property studies were synthesized at high gel fraction, approximately 0.95, as shown in Table 2.1. The notable exception to this is the PEG-PS 37 kg/mol network, which has a typical gel fraction of approximately 0.78. This is consistent with other studies on 35 kg/mol PEG networks[135] and the fact that the thiol-ene reaction gives lower gel fraction with increasing molecular weight of the precursor polymers.[136] It has been suggested that this is due to the decrease in end-group concentration with increasing precursor polymer molecular weight and a sub-optimal ratio of photoinitiator to reactive end groups.[112] This high gel fraction allows us to assume that the

composition of the curing solution is a good representation of the composition of the final network, aside from solvent removal.

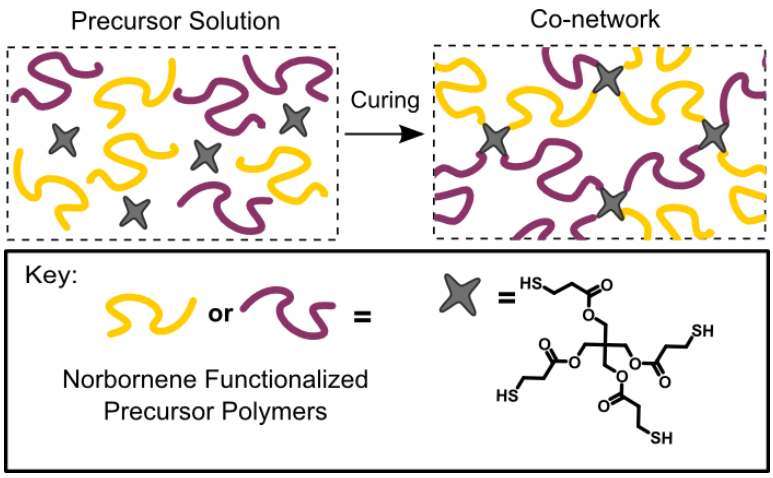

Figure 2.19 General strategy for co-network synthesis.

Table 2.2 Typical Gel Fractions for networks used in property studies. The gel type is given by the polymer(s) used in the gel and their precursor molecular weights in kg/mol. The PEG-PS 12 gel fraction is representative of the full volume fraction series. The gel fraction was not greatly affected by the presence of salt in the curing solution.

Gel Type	Typical Gel Fraction
PEG 12	0.96
PEG 12 – PDMS 4.5	0.93
PEG 4.6 – PS 4.8	0.97
PEG 12 – PS 12	0.95
PEG 35 – PS 37	0.78

For PB networks, not used in further property studies, the gel fraction of networks made with norbornene functionalized polymers was compared to alcohol functionalized polymers. The gels made using the norbornene-functionalized precursors had an average gel fraction of 0.70, which is rather low. However this system was not optimized with respect to variables such as polymer or photoinitiator concentration in the curing solution. For the alcohol-functionalized precursor polymers, the gel fraction of those synthesized with using molar equivalents of thiol

and polymer chain ends (same ratio used for norbornene-functionalized precursors) made only a viscous solution with a gel fraction of approximately 0. After increasing the ratio of thiol groups to 20 relative to the polymer chain ends, a gel fraction of 0.85 was observed. However, this demonstrates that norbornene is necessary for network formation. High quality (high gel fraction) networks are not obtained from the non-cyclic double bonds present in the PB backbone unless a large excess of thiol is used.

2.2.3 Thiol-ene Model Compounds

In order to explore more deeply the role of the thiol structure, several small-molecule thiols were added to telechelic PEG-norbornene polymer using the same conditions as the multiblock synthesis, as shown in

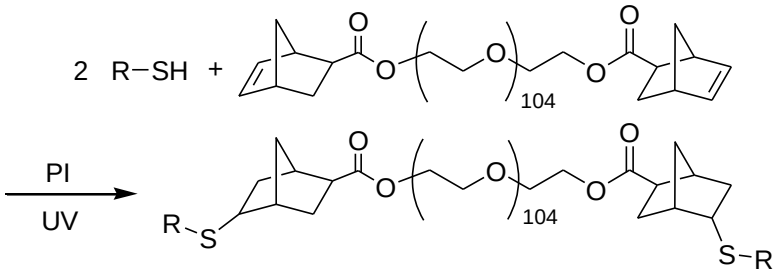

Alkyl Series

R =

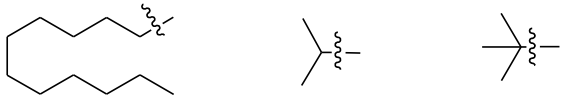

(1) 99+ % **(2)** 99+ % **(3)** 42 %

Electronic Series

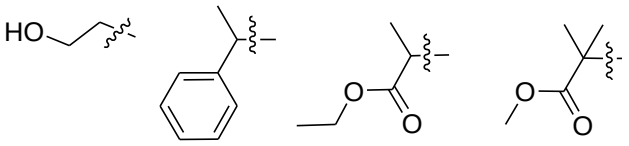

(4) 97 % **(5)** 82 % **(6)** 96 % **(7)** 87 %

Figure 2.20. The first series of alkane thiols asses only the contribution of sterics as only the geometry of the α carbon changes. The percent yield was determined by ^{1}H-NMR as the disappearance of the double bond peaks of norbornene at 6.1 ppm compared to the signal from the terminal -CH_2- group adjacent to the ester bond at 3.8 ppm. As shown in

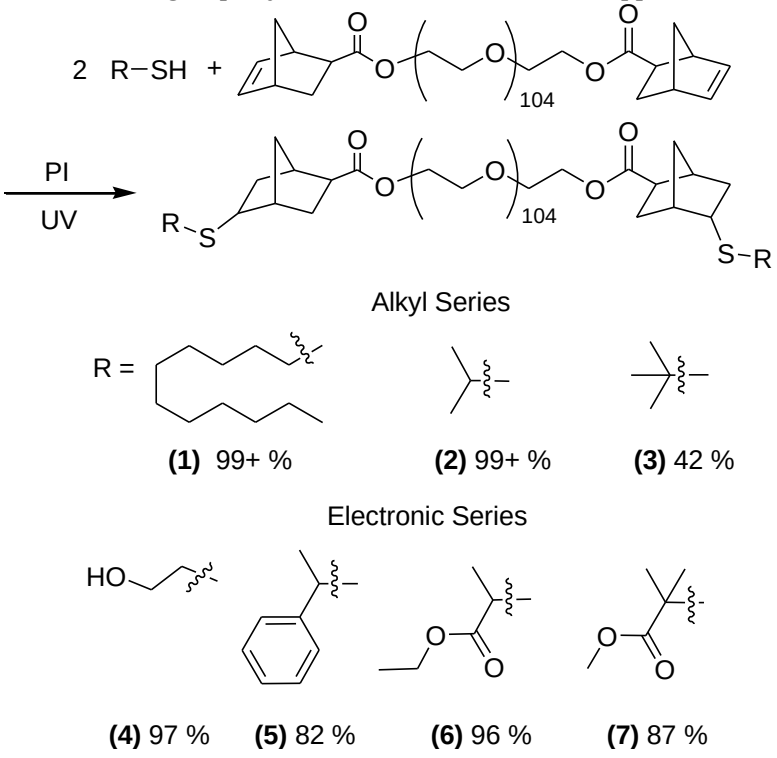

Figure 2.20 the reactivity suffers greatly from steric hindrance. Primary and secondary thiols showed near-quantitative results while the reaction with the tertiary thiol was less than half as productive. Resin curing studies by Li *et al.,* corroborate this data as they found that a primary mercaptopropionate ester and secondary mercaptobutylate ester showed similar reactivity with a variety of enes.[137]

A second series of small molecule thiols was chosen to mimic the geometry and electronic structure of common or easily synthesized thiol-terminated polymers. Mercaptoethanol (4) is similar to the last monomer of a thiol-terminated PEG. 1-Phenyl ethane thiol (5) corresponds to polystyrene while Ethyl 2-mercaptopropinoate (6) and 2-mercapto-2-methyl-propionic acid methyl ester (7) correspond to poly(methyl acrylate) poly(methyl methacrylate). While the conversions of 5 and 7 do not appear vastly lower than 4 and 6, these same conversions

would cause the number of blocks to drop from approximately 25 (for p = 96%) to approximately 7 (for p = 86%) according to the widely accepted Carouthers equation.

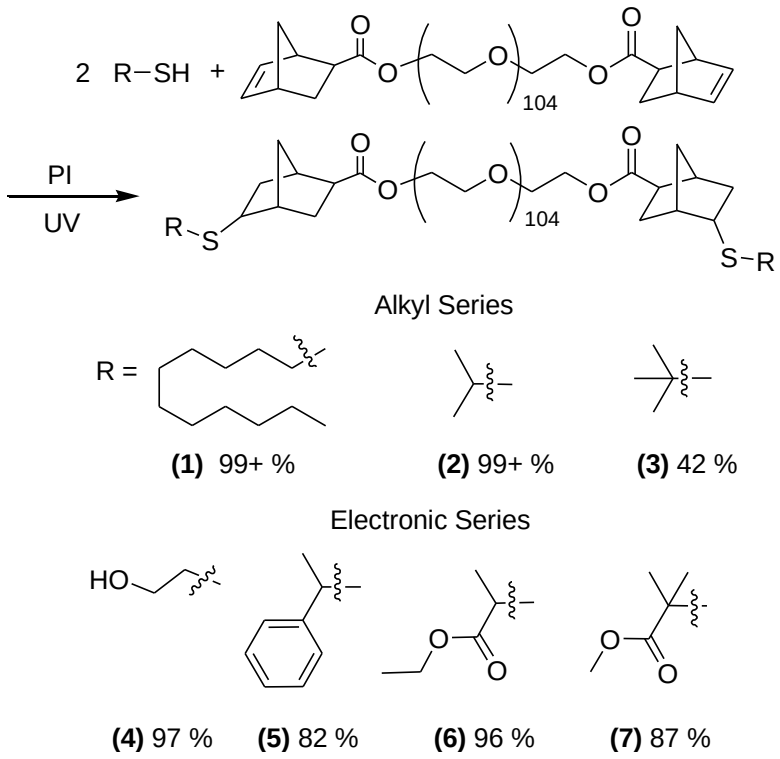

Figure 2.20 Reactivity of small-molecule thiols with norbornene-terminated PEG. % conversion of norbornene double bonds as determined by ^{1}H-NMR for each thiol is given with the structures.

2.2.4 Thiol-ene Multiblocks

Given the broad success of the Mitsunobu/Thiol-ene platform in synthesizing end-linked polymer networks,[104,105,106,138] the same strategy was applied to synthesize multiblock copolymers. As depicted in Figure 2.21, we describe a chemically simple, commercially accessible multiblock copolymer synthetic approach, capable of yielding both random and alternating multiblocks. To access the random multiblock architecture, commercially available α,ω-dihydroxyl- PEO, PS and

PDMS were further end functionalized via Mitsunobu coupling with norbornene carboxylic acid. The resulting macromonomers were used in conjunction with a small molecule di-thiol linker and photoinitiator (PI) to produce random multiblock copolymers, as shown in Figure 2.22. Alternating multiblocks involved similar procedure, but instead of using a small molecule di-thiol to join blocks together, commercially available α,ω-dithiol PEO was used alongside the di-norbornene PS mentioned above.

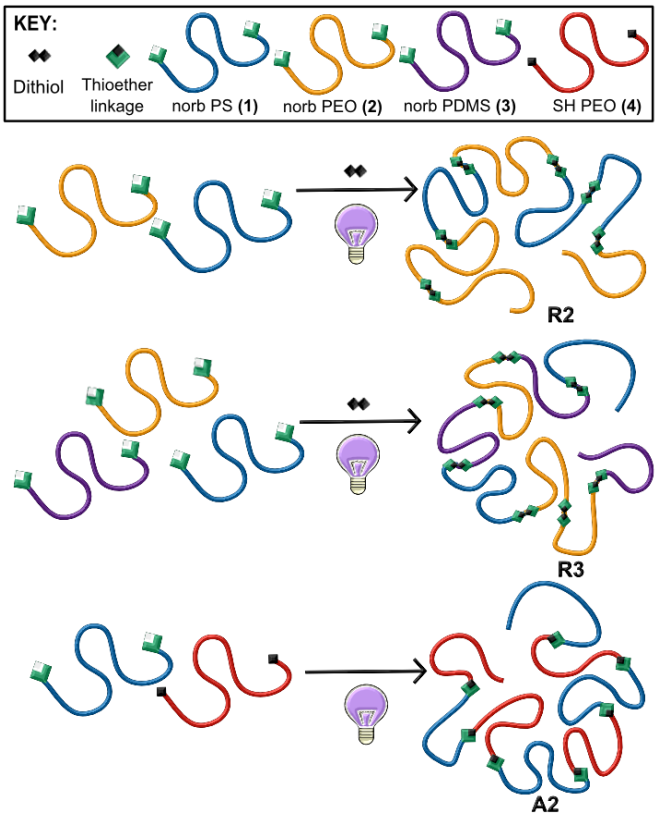

Figure 2.21 Illustration of synthetic approach to random and alternating multiblock copolymers.[†]

[†] Ms. Vanessa Kung and Ms. Ashely Hall assisted with synthesizing and characterizing the random MBCs while Mr. Joel Sarapas worked on the alternating MBCs.

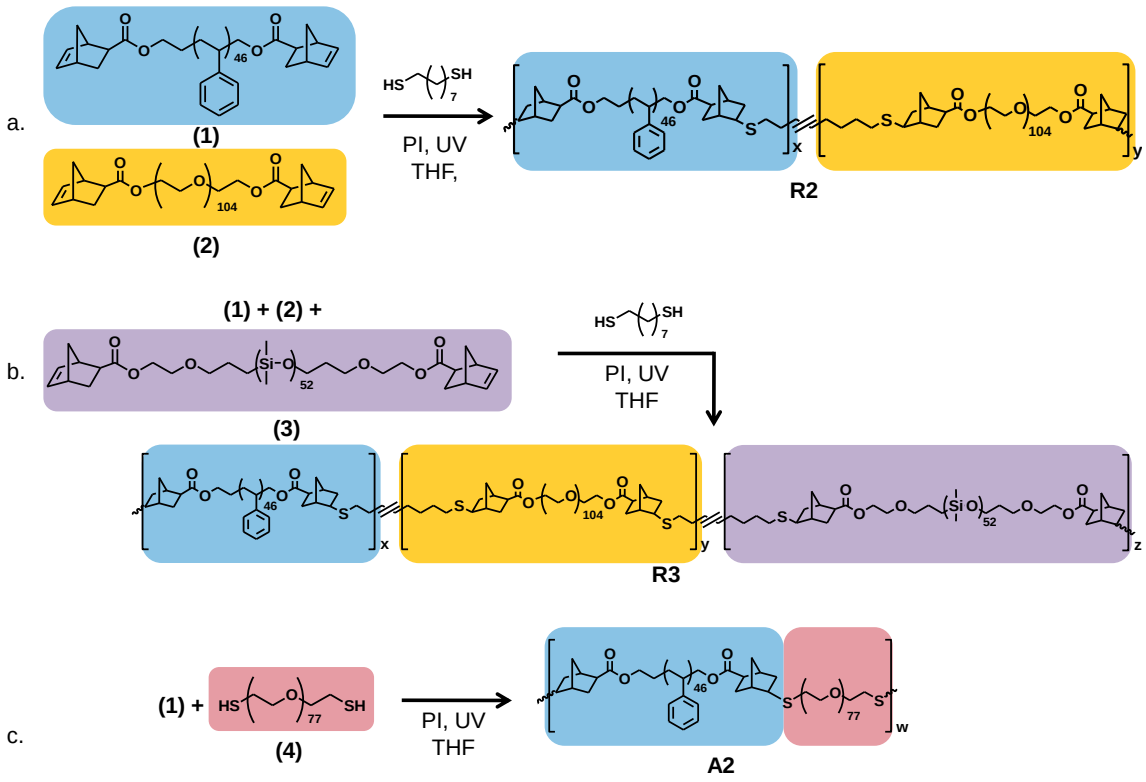

Figure 2.22 Synthetic scheme for the synthesis of (a) **R2**, (b) **R3** and (c) **A2**. The random binary MBC (**R2**) was synthesized from norbornene(norb)-terminated PS, and –PEO, and a dithiol linker. The random ternary MBC (**R3**) was synthesized using norb-PS, -PEO, and –PDMS and a dithiol linker. The alternating MBC was synthesized using norb-PS, thiol-terminated PEO and did not require a linker.

GPC chromatograms (Figure 2.23) confirmed the presence of a higher molecular weight species and a sharp decline in the lower molecular weight macromonomers. GPC results are summarized in Table 2.3. Briefly, both random systems had an average of roughly 4 blocks (based on multiblock M_n), with the alternating copolymers having a slightly higher number. Additionally, all three systems had M_n values very near 30 kg/mol, compared to the 5-9 kg/mol of the macromonomers. These average block numbers and molecular weights could be a result of decreasing functional group concentration as double bonds and thiols are consumed. The MBCs

may also reach a critical size which, greatly inhibits diffusion and decreases the functional group collision rate, limiting molecular weight.

It is also worth noting that the lower molecular weight polymer remaining in the two random multiblocks is lower than that of any macromonomers used in those reactions. This is likely due to the presence of a small molecule di-thiol in these two reactions, which would allow for single macromonomer cyclization.[130] Such cyclizations would decrease both the hydrodynamic radius and the molecular weight by GPC of the molecule.[139,140] Whether or not cyclization is present in the larger multiblocks is still unknown and requires further characterization. Cyclization also likely limits the size of a multiblock copolymer by consuming functional groups which could also explain the observed M_ns.

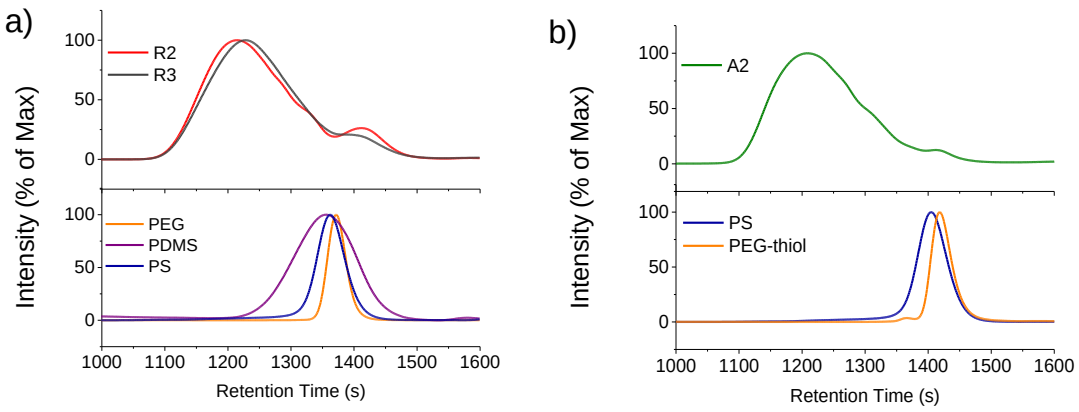

Figure 2.23 GPC traces of the a-top) random and b-top) alternating multiblock copolymers compared with a-bottom) and b-bottom) the precursor homopolymers.

Table 2.3 GPC values from Macromonomers and MBCs.

	Sample	M_n (g/mol)	Đ	n (avg number of blocks)
Macromonomers	PEO	6,800	1.03	n/a
	PS	8,600	1.14	n/a
	PDMS	8,900	1.24	n/a
	PEO-thiol	4500	1.04	n/a

	R2	29,700	1.7	3.7
MBCs	R3	31,800	1.4	3.9
	A2	29,300	1.6	4.5

Multi-angle laser light scattering (MALLS) GPC confirms the presence of high molecular weight species in **R2** and **R3** samples. **R2** has an M_n 16,000 g/mol and an M_w of 18,000 g/mol while **R3** has an M_n of 35,000 g/mol and an M_w of 41,000 g/mol. This technique gives absolute molecular weights as opposed to relative molecular weights. The change in refractive index with concentration (dn/dc) was calculated for each sample.

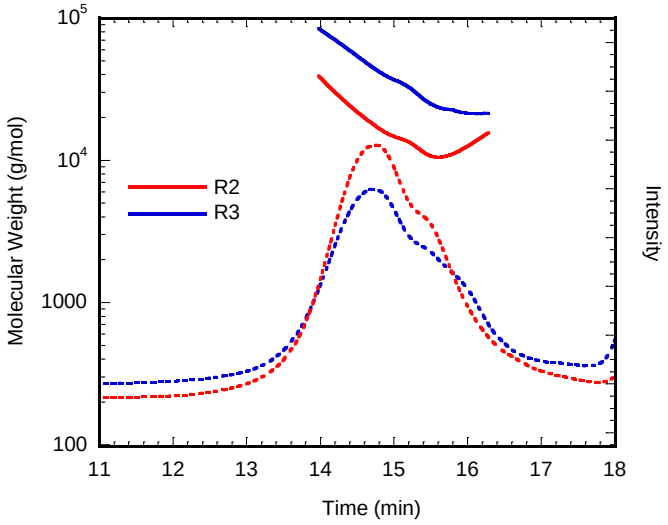

Figure 2.24 MALLS GPC of **R2** (red) and **R3** (blue). The dashed lines give the intensity of the refractive index detector while the solid lines give absolute molecular weight based on dn/dc calculated for each sample.

The expected stoichiometric block ratios for all three multiblock copolymers were observed by ^{1}H NMR, as summarized in Table 2.4 as well as the absence of the characteristic norbornene peak at ~6 ppm shown in Figure 2.25 - Figure 2.27. The absence of the norbornene

peak and the presence of molecular weight species slightly lower than the precursor polymer molecular weight is consistent with the formation of cyclic multiblock copolymers.

Table 2.4 Molar composition of MBCs calculated ^{1}H-NMR integration.

Sample	PS	PEO	PDMS
R2	52%	48%	N/A
R3	35%	31%	34%
A2	61%	39%	N/A

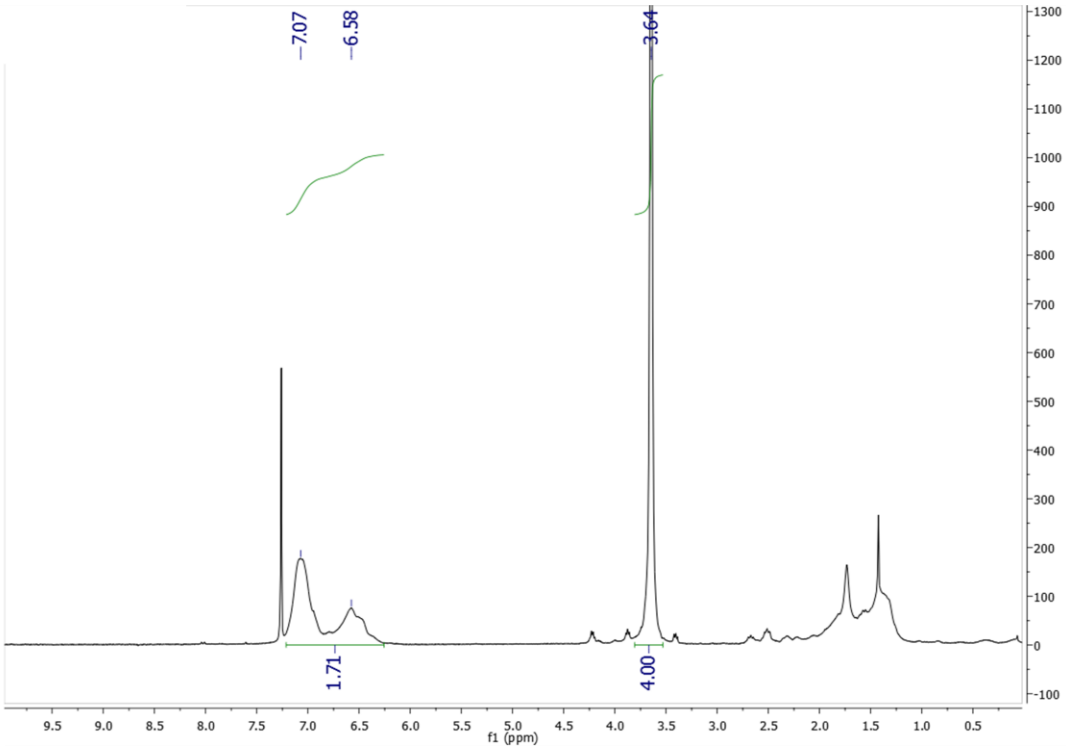

Figure 2.25 ^{1}H NMR of multiblock copolymer R2 showing approximately equal incorporation of both homopolymers (55 wt% PEO, 45 wt % PS) and full conversion of norbornene end groups by the absence of the peak at 6.0 ppm.

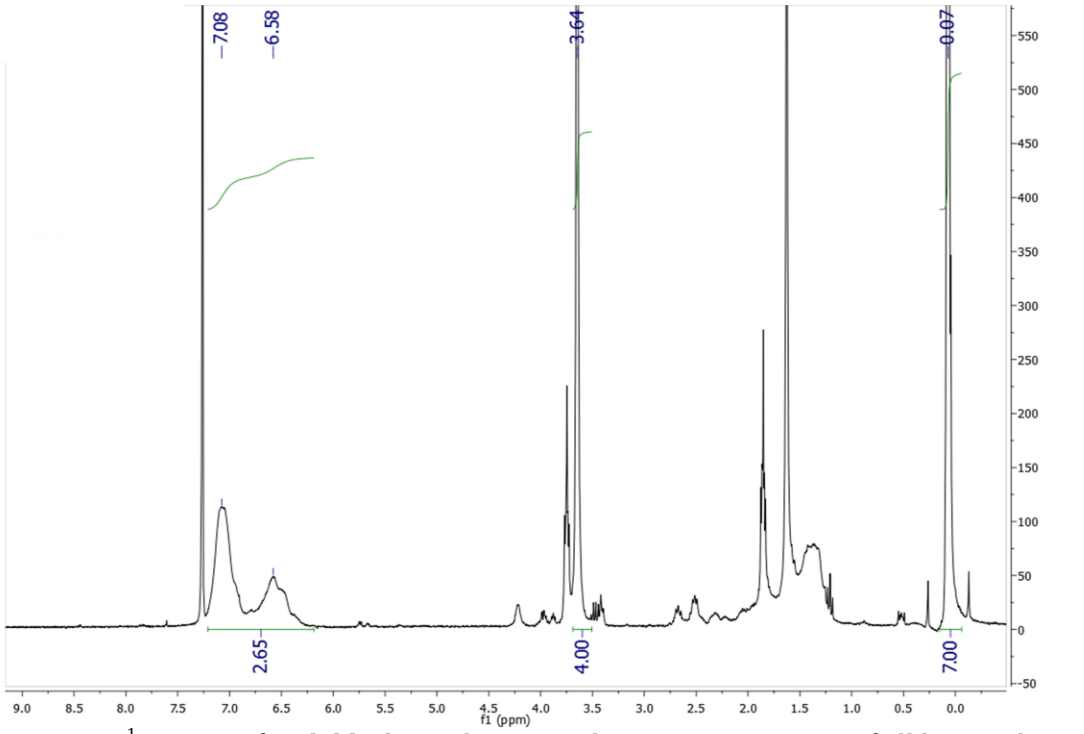

Figure 2.26 ^{1}H-NMR of multiblock copolymer R3 showing incorporation of all homopolymer blocks (24 wt% PEO, 29 wt% PS and 47 wt% PDMS) and full conversion of norbornene end groups by the absence of a peak at 6.0 ppm.

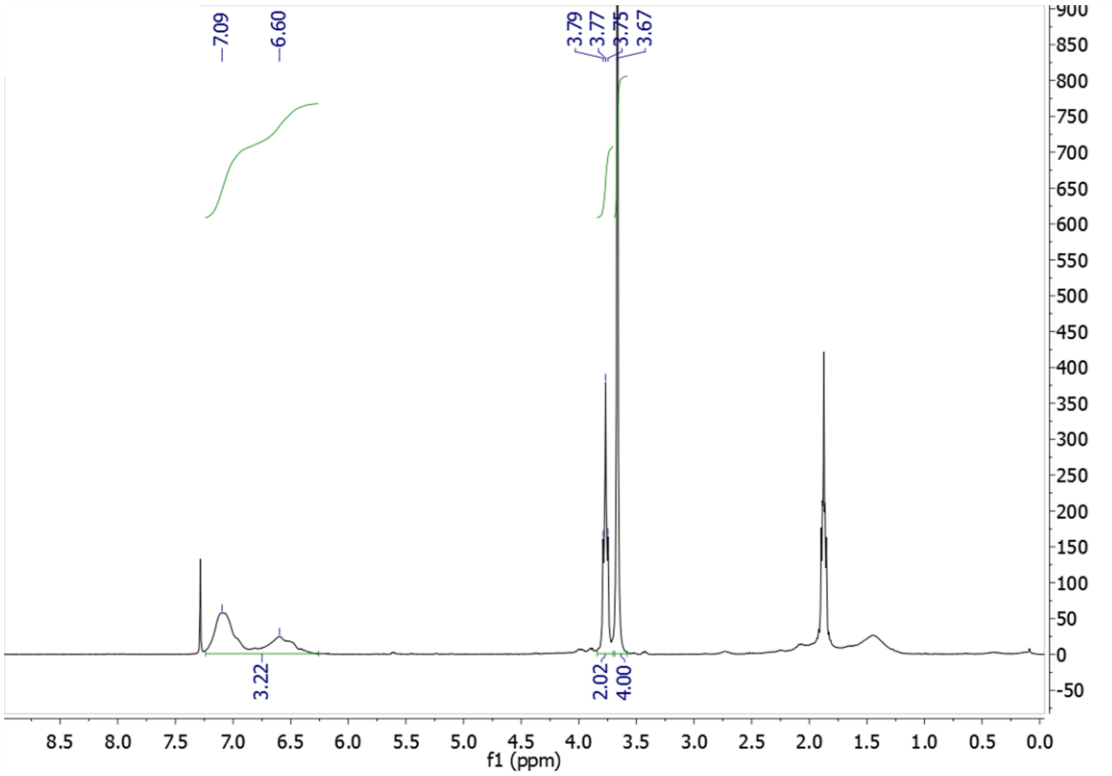

Figure 2.27 ^{1}H NMR of multiblock copolymer A2 showing incorporation of both homopolymer blocks (40 wt% PEO and 60 wt% PS) and full conversion of norbornene end groups by the absence of a peak at 6.0 ppm.

2.3 Conclusions

The Mitsunobu/thiol-ene end-linking platform has been shown to be a versatile system. It gives the ability to synthesize end-linked polymer networks with a variety of compositions and a variety of precursor molecular weight polymers. The gel fractions in the network synthesis are generally high, though they fall with increasing precursor polymer molecular weight. This could be remedied by optimizing the ratio of photoinitiator to functional group ratios. MBCs can be synthesized using either small-molecule or polymeric dithiol linkers. While these first attempts at MBC synthesis seem to yield only a small number of blocks, it may be sufficient for improved properties. This difference was not unexpected given the different predictions of percolation theory for networks and the Carouther's equation for MBCs. Also using Carouther's prediction, a

modest increase in end group conversion (from 80% to 90%) would double the number of blocks from an average of 5 to an average of 10. This could be accomplished by insuring the alcohol and norbornene functionality of the starting materials and macromonomers respectively is complete. As we learn more about the Mitsunobu and thiol-ene reactions, this modest improvement in conversion seems easily achievable.

CHAPTER 3

PEG-PDMS NETWORKS

3.1 Introduction

Silicones, such as polydimethylsiloxane (PDMS), are highly useful due to their chemical and thermal stability.[141] PDMS has a low T_g (around -125 °C) due to the flexible nature of the –Si-O- backbone. For this reason, it has been previously used in solid electrolyte materials to reduce the T_g of the material and thus improve ion mobility.[94] The Si-O bond also has some slight ionic character.[141] Despite being hydrophobic, this could lead to PDMS interacting with charge carriers. PEG-PDMS hydrogels have also been synthesized and their mechanical properties have been well characterized by our lab.[104,105,106] For these reasons, PEG-PDMS networks were chosen for initial ion conductivity studies.

3.1.1 Salt-in-Polymer vs. Polymer-in-Salt Regimes

Generally, PEG-based polymer electrolytes exhibit a maximum conductivity at fairly low salt loadings such as a molar ratio of ether oxygens to lithium ions (EO:Li) of 16. This trend is due to the lithium ions acting as additional physical cross-links between polymer chains, increasing the T_g, thus reducing the molecular mobility.[70,97,142] At significantly higher salt loading, the polymer T_g decreases, causing conductivity to increase. This regime has been dubbed 'polymer-in-salt' as opposed to the conventional 'salt-in-polymer' sample described above.[97] It has been suggested that this T_g decrease is due to saturation of the salt loaded network or that the salt form its own set of percolating pathways.[143] Provided the molecular weight of the linear, non-cross-linked polymer is high ($>8 \times 10^6$ $gmol^{-1}$), it takes as little as 10 wt% to give the material rubbery properties (shear modulus of 10^4 Pa) despite the high salt content.[144] Because

networks have an infinite molecular weight, they should also be able to exhibit rubbery properties at high salt loading, for example EO:Li = 1.

3.2 Salt Loading

Synthesis of PEG and PEG-PDMS networks are described in Chapter 2. To vary the EO:Li, networks were swollen in different concentrations of LiTFSI in THF, as shown in Table 3.1. After thorough drying, the samples were weighed to determine the amount of salt inside the network. From this weight change the EO:Li ratio was calculated using equation 3.1 for PEG networks and equation 3.2 for PEG-PDMS networks where M_1 is the dry mass of the network before salt loading, M_2 is the dry mass of the network after salt loading, $M_{w,\,EO}$ is the molecular weight of the PEO repeat unit, $M_{w,\,LiTFSI}$ is the molecular weight of the salt and φ_{PEO} is the weight fraction of PEG in the PEG-PDMS network. Increasing the concentration of LiTFSI leads to higher salt loading (lower EO:Li) in both PEG and PEG-PDMS networks.

$$\left(\frac{M_1}{M_{w,EO}}\right) / \left(\frac{M_2 - M_1}{M_{w,LiTFSI}}\right) \qquad (3.1)$$

$$\left(\frac{M_1 \varphi_{PEO}}{M_{w,EO}}\right) / \left(\frac{M_2 - M_1}{M_{w,LiTFSI}}\right) \qquad (3.2)$$

Table 3.1 Salt loading from different concentrations of salt (M LiTFSI) in THF.

PEG Networks		PEG-PDMS Networks	
M LiTFSI	EO:Li	M LiTFSI	EO:Li
0.043	15.8	0.027	16.1
0.115	10.0	0.077	9.94
0.247	4.66	0.178	5.11
0.465	2.52	0.309	2.83
0.387	2.11	0.465	2.06
0.600	1.27	1.25	1.07

3.3 Ion Conductivity

The ion conductivity of PEG and PEG-PDMS networks obtained from impedance spectroscopy is shown in Figure 3.1. Loading either network with lithium salt increases the ion conductivity by at least two orders of magnitude when compared to the control networks which contain no added salt. The PEG and PEG-PDMS networks show ion conductivity ($8.6x10^{-5}$ to $6.7x10^{-4}$ and $1.3x10^{-5}$ to $4.2x10^{-4}$ Scm^{-1}, at 30 °C respectively) similar to other materials in the field, ($1x10^{-5}$ to $6x10^{-4}$ Scm^{-1}).[78,79,80,93,94,95,145] The conductivity as a function of temperature shows non-Arrhenius behavior with decreasing slope at lower temperatures. The control networks show a different behavior, which includes a sharp decrease in conductivity at approximately 55 °C due to the crystallization of the PEG chains. In both networks, the highest salt loadings, EO:Li = 1:1 and 2:1, show a slight increase in conduction over conventional salt loadings, EO:Li = 10:1 and 16:1. As expected, ion conductivity in the PEG-PDMS networks is slightly lower than that of the PEG-networks due to the reduced volume fraction of PEG.

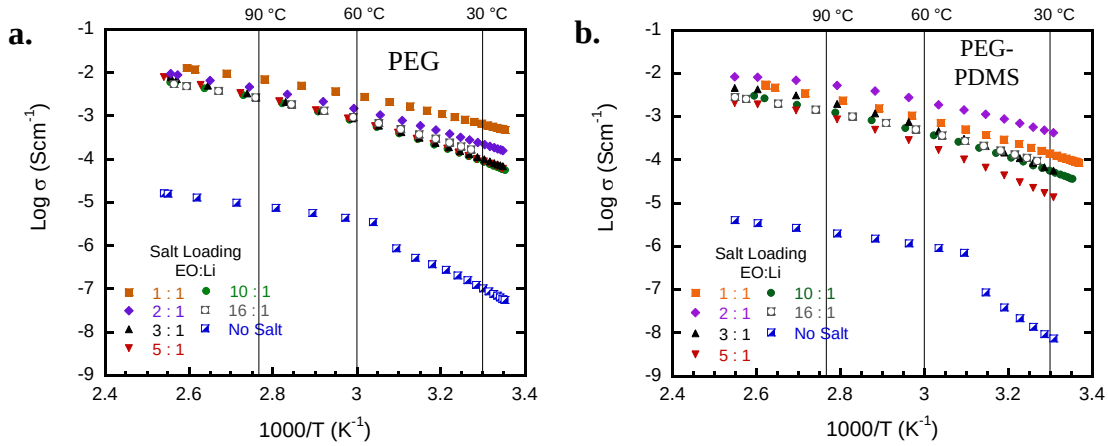

Figure 3.1 Ion conductivity of (a) PEG networks and (b) PEG-PDMS networks in Arrhenius plots. Approximate temperatures in °C are given as a reference at the top of the plot. The salt loadings, EO:Li are given in the legend.

The values reported in Figure 3.1 are taken from a cooling curve after holding the samples at 120°C under vacuum for several hours. It is well known that PEG and LiTFSI are hygroscopic. This "baking" process allows for the removal of any residual solvents or moisture from the salt loaded networks. The ion conductivity during this baking process shows that all networks reach a stable state before the samples are cooled, as seen in Figure 3.2 where the ion conductivity is plotted against time. It has been demonstrated that the effect of moisture on conductivity is largely reversible once the water is removed with heat.[146] It is logical that the effects of any other plasticizing solvent are also largely reversible. Based on this assumption, THF was chosen as the solvent for salt loading because it is easy to remove on heating.

In order to reduce the effect residual solvent and moisture on conductivity, the salt-loaded networks were held at approximately 120 °C under vacuum for several hours. During this time, the ion conductivity was recorded to confirm that the conductivity had reached a stable value in all samples. The cooling portion of this curve corresponds to the data reported in Figure 3.1.

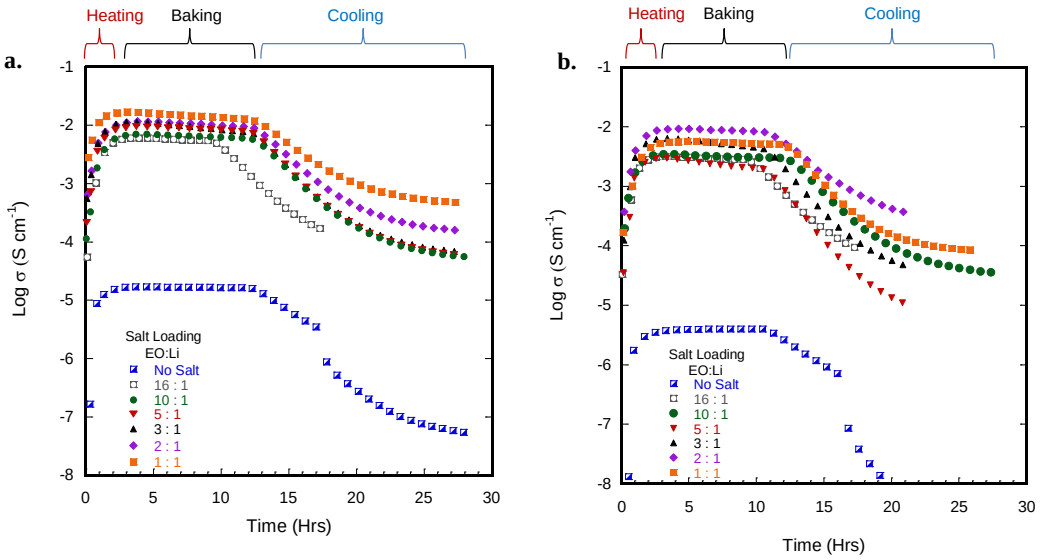

Figure 3.2 Ion Conductivity of (a.) PEG and (b.) PEG-PDMS networks as a function of time. In the first two hours, the sample is quickly heated, then held at approximately 120 °C for several hours to ensure removal of moisture and any residual solvent. The sample then cools to room temperature.

3.3.1 Model Comparison

Ion conductivity in polymer electrolytes is often described by two different models, the Arrhenius equation for hopping motion and the Vogel-Tammen-Fulcher or Williams-Landel-Ferry equations for chain relaxation. These models are described more in depth in Chapter 1. Figure 3.4 shows the Arrhenius fit which describes an exponential temperature dependence. While the R^2 values for the fits are high, > 0.96, it can be seen that the temperature dependence is more complex than this simple exponential relationship. Generally, the Arrhenius fit overestimates ion conductivity at the extremes of the temperature range investigated, while underestimating ion conductivity at intermediate temperatures.

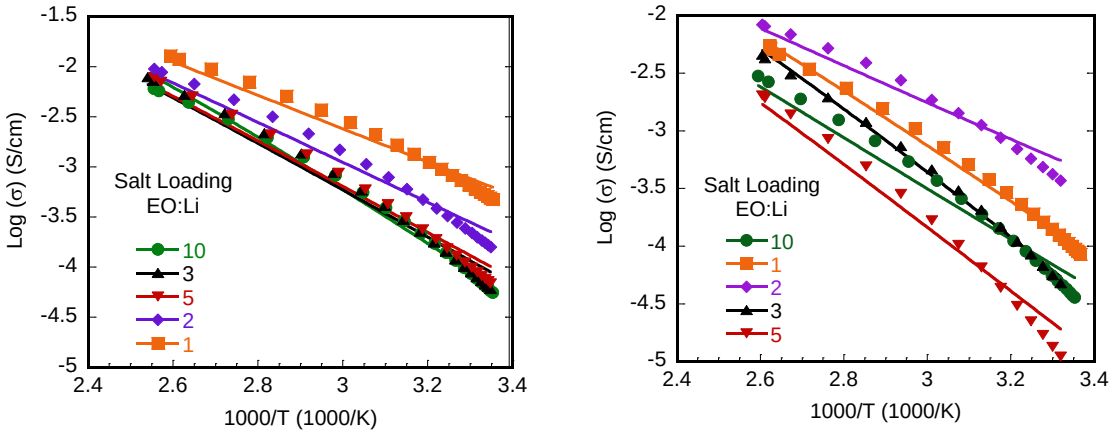

Figure 3.3 Arrhenius Fits to Ion Conductivity for PEG (left) and PEG-PDMS Networks (right).

The activation energy (E_a) from each of the Arrhenius fits is given in Table 1. Samples with a higher ion conductivity tend to have a lower activation energy. However, this may be obvious since the activation energy was calculated using ion conductivity values.

Table 3.2 Activation Energy from Arrhenius Fits to PEG and PEG-PDMS Networks.

EO:Li	PEG E_a (J/mol)	PEG-PDMS E_a (J/mol)
10	60.3 ± 1.5	46.2 ± 2.4
5	52.4 ± 2.5	52.5 ± 2.9
3	53.1 ± 2.4	60.7 ± 1.0
2	55.4 ± 2.4	42.4 ± 2.8
1	46.6 ± 2.3	56.0 ± 0.71

In contrast, the VTF equation describes ion motion that is coupled to polymer chain relaxation and is fit to the sets of PEG and PEG-PDMS networks as shown in Figure 3.4. Similar to the Arrhenius fits, the fit line does not pass through the data points exactly; however, the R-squared values are > 0.96 for all samples.

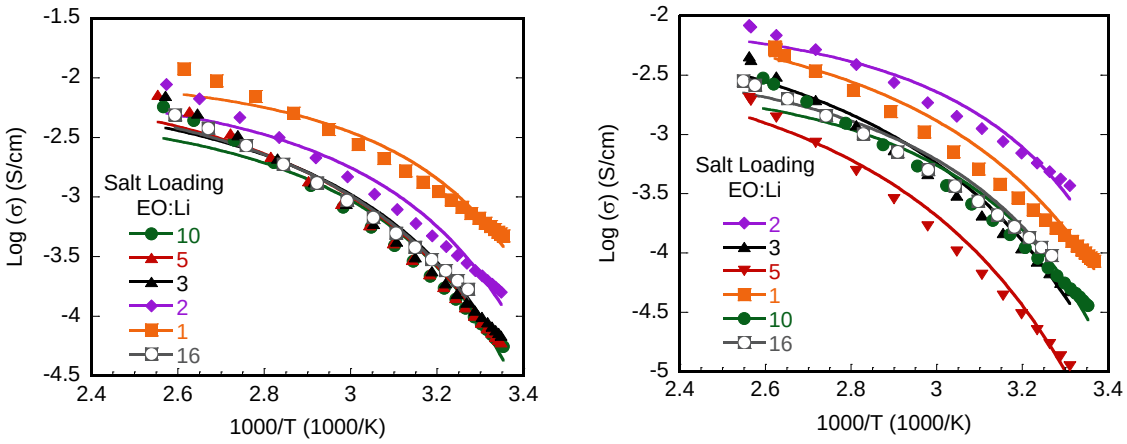

Figure 3.4 VTF Fits to PEG (left) and PEG-PDMS Networks (right).

Several parameters can be abstracted from the VTF fit. A is a pre factor, thought to be related to the number of charge carriers. E_a is similar to the activation energy in the Arrhenius equation. $T_{0,}$ also known as the Vogel temperature,[147] is defined as the temperature at which there is no free volume, usually defined as approximately 50 °C below T_g.[148,149] Greater values of A and lesser values of E_a and T_0 should lead to increased ion conductivity; however as shown in Figure 3.5, none of these values closely relate to high or low ion conductivity. The error bars for each value, taken from the error reported in the fitting parameters, is quite large and makes it difficult to discuss how these quantities relate to ion conductivity.

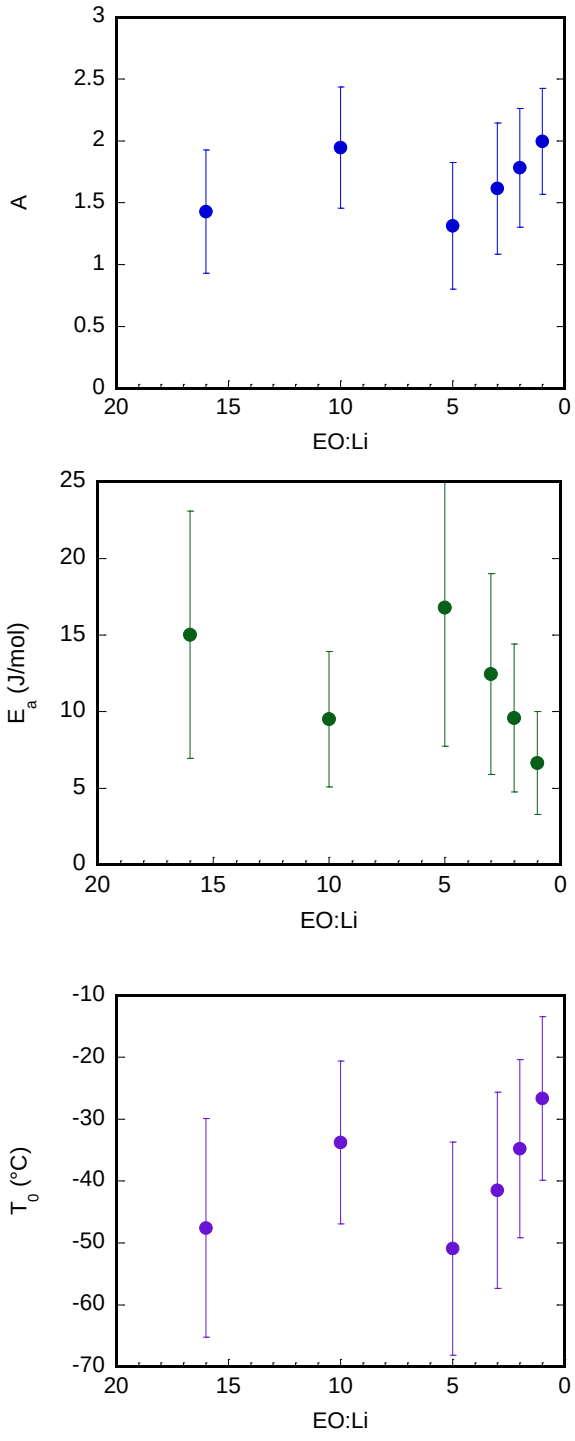

Figure 3.5 Parameters from fitting VTF Equation to PEG Networks

Similarly, the PEG-PDMS networks have fitting parameters that are unconstructive, as shown in Figure 3.6. The values do not correlate with the trends in ion conductivity and have large error bars making the values for each sample difficult to differentiate.

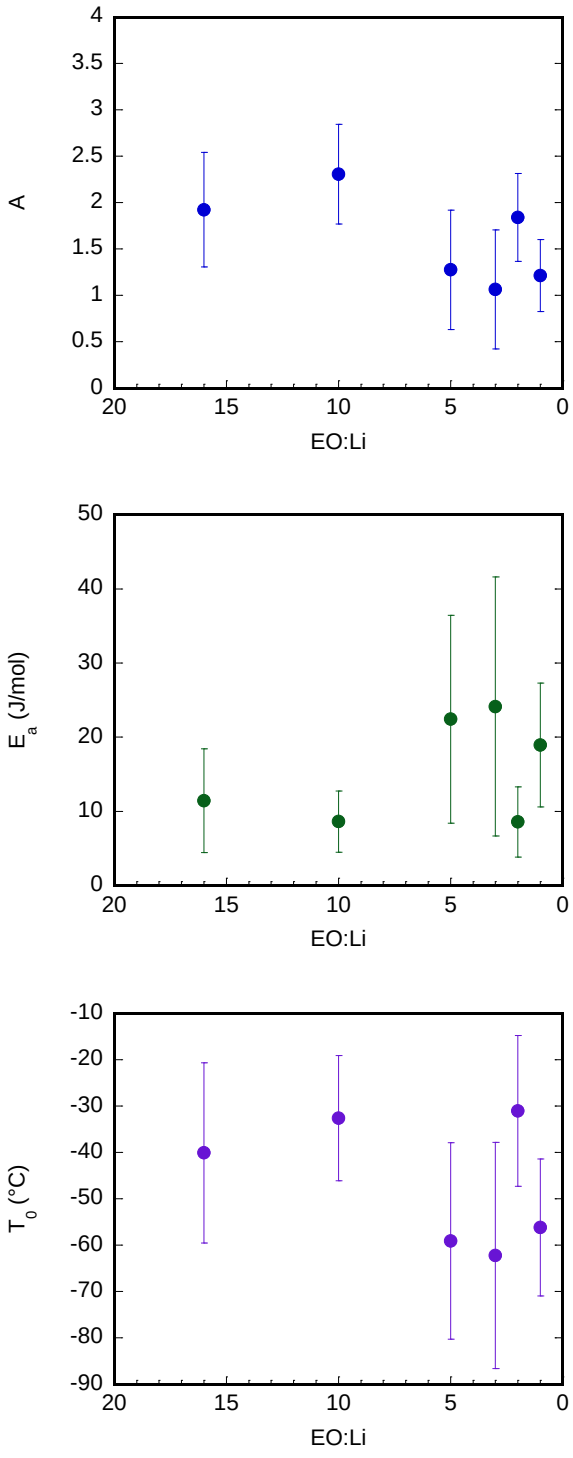

Figure 3.6 Parameters from Fitting VTF Equation to PEG-PDMS Networks.

For this system, Arrhenius and VTF equations describe the temperature dependence of the ion conductivity equally well. The VTF model is best suited to describe the properties of a system near its T_g.[121] The PEG T_gs are between -65 and -20 °C in these systems, as discussed in the next section. The ion conductivity data is taken from approximately 25 °C to 120 °C, which could explain why it appears to be a poor fit. Additional data points from a wider temperature range, especially going below room temperature, may help to clarify which model more accurately describes the temperature dependence.

3.4 Thermal Properties

In order to corroborate the effectiveness of the baking process, thermogravimetric analysis (TGA) measurements were performed. As shown in Figure 3.7, the pure salt, LiTFSI, contains 20% weight moisture which is removed upon heating to 90 °C demonstrating that LiTFSI deliquescence is reversible on heating. Only a slight change is observed (<5 wt%) between 90 °C and the decomposition temperature of 400 °C showing this salt has excellent thermal stability.

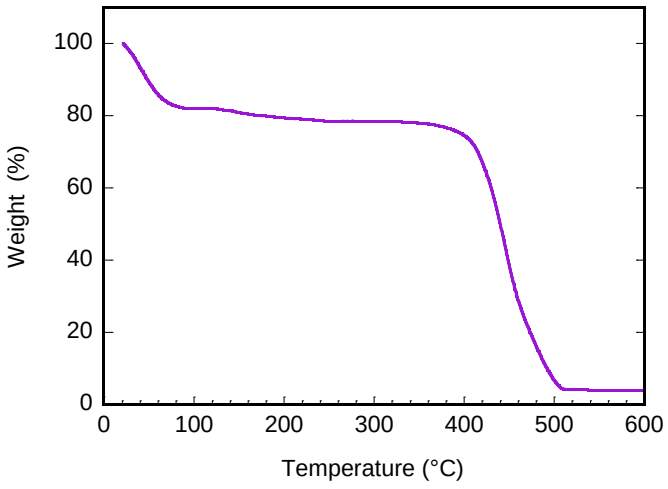

Figure 3.7 TGA of LiTFSI with a heating rate of 10 °C/min.

Plots of weight loss as a function of temperature for the salt-loaded networks (Figure 3.8) show that the samples are quite stable up to 320 °C which allows for a wide range of operating temperatures. This data also confirms that the "baking" process eliminates the majority of the moisture observed in the TGA curve for the pure salt with less than 5 wt % loss for any sample up to 320 °C (Figure 3.8 insets). The sample with the greatest weight loss (5%) below 320 °C, PEG-PDMS EO:Li = 10:1, shows conductivity similar to all the other samples indicating that the weight loss, possibly related to moisture, above 180 °C does not enhance conductivity compared to the other networks.

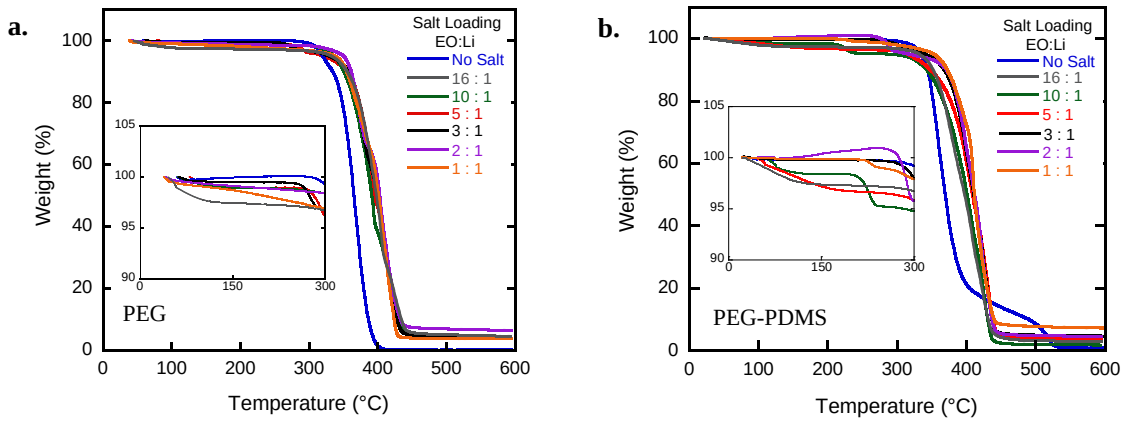

Figure 3.8 TGA of (a) PEG networks and (b) PEG-PDMS networks with a heating rate of 10 °C/min. Figure insets show only slight weight loss due to solvent or moisture.

LiTFSI is known for its ability to disrupt crystallinity due to the irregular shape of the TFSI anion, making this salt a popular choice for PEG-based ion conducting materials.[77] Differential scanning calorimetry (DSC) measurements (Figure 3.9) indicate that any salt loading greater than EO:Li = 10:1 completely disrupts the crystallinity of the PEG chains for both sets of networks, within the DSC detection limits. The crystallinity in both the PEG and PEG-PDMS networks for EO:Li = 16:1 is much less than the crystallinity in the control networks that do not contain salt. However, none of the salt-containing samples show a crystallization-related decrease

in conductivity in the temperature range investigated (Figure 3.1). PDMS T_gs are not shown in Figure 3.9 b because the low PDMS composition (~30 % wt) makes them difficult to reliably detect.

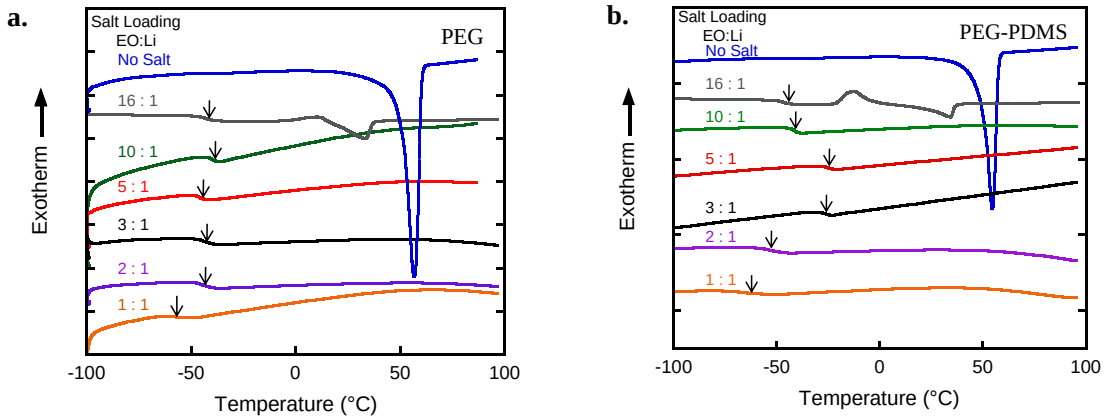

Figure 3.9 DSC traces of (a) PEG and (b) PEG-PDMS networks. All traces are taken from the 2nd heating scan, with a scanning rate of 10 °C/min. Data are offset on the Y-axis for clarity. T_g of PEG is marked with arrows.

All of the salt-loaded networks show a T_g for the PEG component between -65 °C and -20 °C. In the PEG-PDMS networks, T_g goes through a maximum at EO:Li = 5:1 then decreases as salt loading continues to increase. The sample with the highest T_g value also had the lowest conductivity values. Although it is less pronounced, the T_g drops at the highest salt loading in the PEG networks. To illustrate this trend more clearly, T_g vs. salt loading is plotted in Figure 3.10. This trend indicates that the range of salt loading includes both the salt-in-polymer and the polymer-in-salt regimes. At low salt loading, the T_g increases as salt loading increases possibly because the lithium cations serve as additional physical cross-links between chains, decreasing the molecular mobility of the polymer chains.[142] However, once the salt is the major component in the system, the T_g decreases similar to previous observations.[97,144] This regime change occurs when the PEG chains are saturated and cannot complex any additional cations.[144]

3.5 Influence of T_g on Ion Conductivity

Loading salt into the polymer network can have a great effect on the T_g of PEG. As shown in Figure 3.10 the T_g reaches a maximum of approximately -40 °C at EO:Li = 10 for the PEG system and -25 °C at EO:Li = 5 for the PEG-PDMS system, after which it decreases on further salt loading. These observations confirm that this study investigated both the salt-in-polymer and polymer-in-salt regimes.

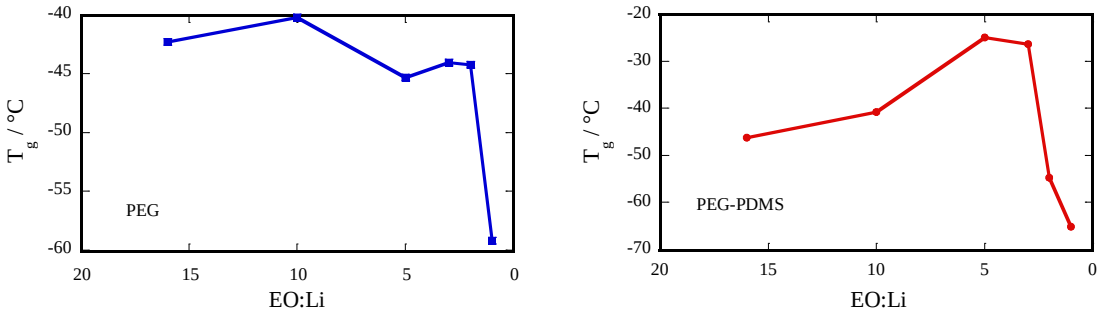

Figure 3.10 Effect of salt loading on PEG T_g.

Similarly, looking at ion conductivity across the range of salt loading, generally, samples with a low T_g show high ion conductivity, as shown in Figure 3.11, such as PEG EO:Li = 1 which has a T_g of -59 °C and an ion conductivity of $10^{-3.2}$ S/cm at 30 °C. This is especially true for the PEG networks. In PEG-PDMS networks, the same trend is observed; for example, the PEG-PDMS EO:Li = 5 has the highest T_g at -25 °C and the lowest ion conductivity at 10^{-5} S/cm. The trend is not observed at the highest salt loadings. PEG-PDMS EO:Li = 2 has a greater ion conductivity than PEG-PDMS EO:Li = 1 despite T_g that is almost 10 °C higher. This could be due to interactions between the PDMS and salt as discussed later.

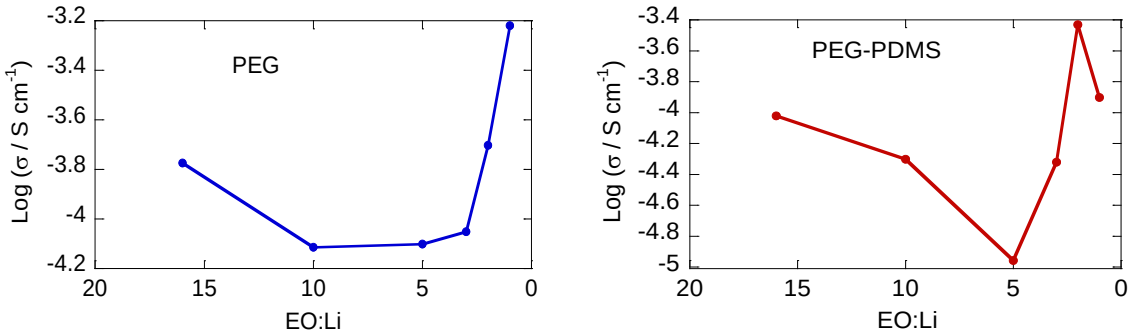

Figure 3.11 Effect of Salt-Loading on Ion Conductivity at 30 °C.

The Vogel temperature (T_0) is compared to the PEG T_gs measured by DSC. Often, it is reported that T_0 is 50 °C lower than T_g. However, the values found here do not have such a simple relationship to T_g, as shown in Figure 3.12. For the PEG networks, the T_g is close to T_0 for most samples, though in some samples the T_g is lower than T_0. However, the T_g for EO:Li = 1 is much lower, even outside the wide error bars, compared to the calculated T_0. The low T_g is consistent with the high conductivity of this sample. In the PEG-PDMS networks, more of the T_gs fall outside the wide error bars of T_0. This could be because the VTF equation is based on polymer chain motion and relaxations. Measuring the T_g with a mechanical measurement such as the local maximum of tan(δ) from DMA may give a more appropriate comparison to T_0 as determined by EIS.

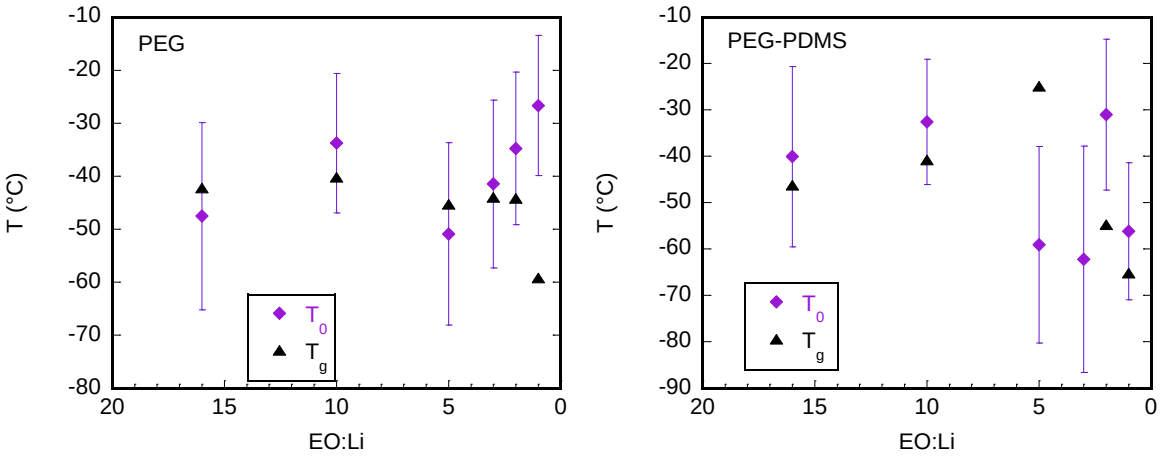

Figure 3.12 Comparison of T_0 and T_g for PEG and PEG-PDMS Networks.

Another way to demonstrate the relationship between conductivity and T_g is to plot the ion conductivity vs. T_g/T. Because the amount and type of salt affect the T_g this scale allows one to compare samples that should have relatively similar local mechanical environments.[150] In the PEG networks, the data collapses rather well, as shown in Figure 3.13. However, the ion conductivity and T_g values were quite similar to each other to begin with.

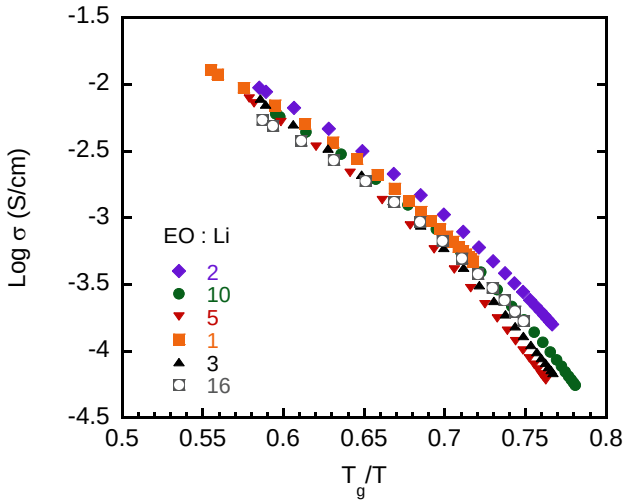

Figure 3.13 Ion conductivity vs. T_g/T for PEG networks.

The PEG-PDMS networks have a comparatively greater distribution of ion conductivity and T_gs. Scaling these ion conductivity values by the T_g for each sample gives very different results, as shown in Figure 3.14. The ion conductivity rankings change significantly after scaling by T_g. The sample EO:Li = 3 has the highest ion conductivity, where it had comparatively low to average ion conductivity in the Arrhenius plot (Figure 3.1). The sample with EO:Li = 5 is now in the middle where it had the lowest ion conductivity in Figure 3.1. The sample with the lowest ion conductivity when scaled by T_g was EO:Li = 1 which had the second highest ion conductivity on the inverse temperature scale. Only the sample with EO:Li = 2, the sample with the highest ion conductivity on the inverse temperature scale remains close to its original rank, showing the second highest ion conductivity in the plot scaled by T_g. The range of ion conductivies in the PEG-PDMS series at a single T_g/T value is comparable to the range at a single inverse temperature value, about 1.5 orders of magnitude. Clearly, there is something more than the local mechanics of the PEG phase affecting the ion conductivity in these PEG-PDMS networks.

What is likely missing from this picture is the PDMS T_g. If the ions are interacting with the PDMS backbone this could explain why scaling by the PEG T_g does not cause the data to collapse onto a single curve. From the DSC measurements, a PDMS T_g was not easily determined. The relatively low amount of PDMS, less than 30 % volume relative to PEG and salt, gave too weak a signal.

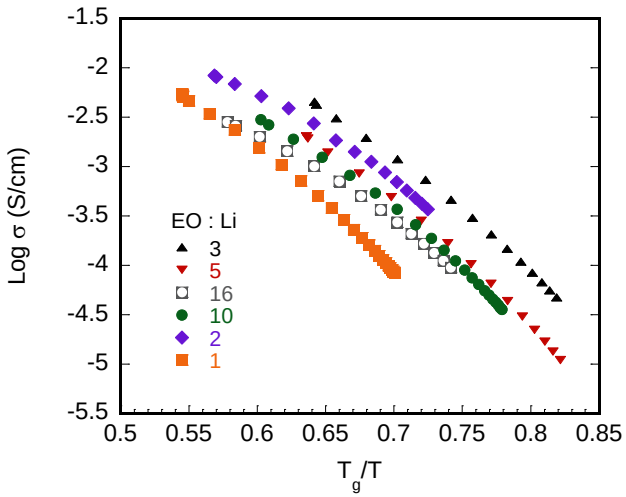

Figure 3.14 Ion conductivity vs. T_g/T for PEG-PDMS networks.

3.6 Comparison to PS

Because PDMS is slightly ionic in character, it is possible that it interacts with the salt as well. This is has potential to improve conductivity. To test this, PEG-PS networks were synthesized and loaded with salt in the same way as the PEG-PDMS networks. Figure 3.15 shows these two networks each with two different salt loadings. In both cases the PEG-PDMS networks have slightly higher ion conductivity than the PEG-PS networks. The difference is small; however, both sets of networks are approximately 70 % PEG. Using more PS and PDMS could widen this difference.

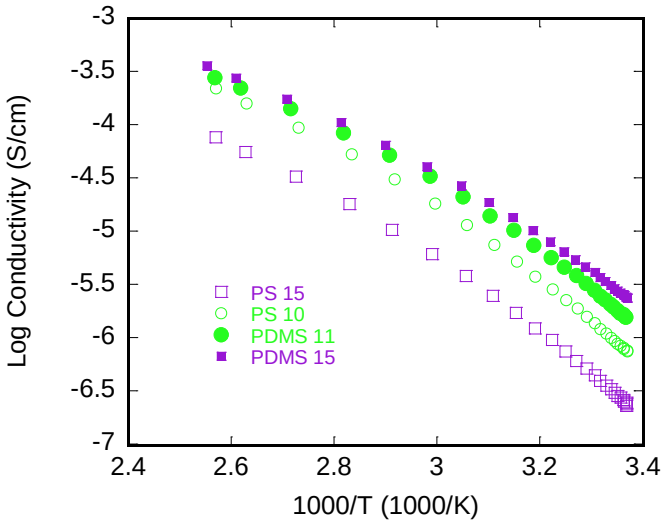

Figure 3.15 Ion conductivity of PEG-PDMS (solid symbols) and PEG-PS (open symbols) networks at two different salt loadings, given in the legend, EO:Li = 15 (purple) and EO:Li ≈ 10 (green).

3.7 Mechanical Properties

Dynamic mechanical analysis (Figure 3.16) shows that both PEG and PEG-PDMS salt-loaded networks have stable mechanical properties in the temperature range probed. As expected, both salt-free control samples show a large drop in storage modulus and a slight increase in tan(δ) as the PEG crystals melt at approximately 60 °C. Even with PEG in the crystalline state, the effect of the soft PDMS chains can be seen as the storage modulus of the control PEG-PDMS network (50 MPa) is lower than that of the PEG control network (150 MPa). The salt-loaded networks do not show this transition because they are predominately amorphous, corroborating the DSC results. Instead, they maintain a relatively constant modulus over the temperature range investigated, 40 kPa for PEG and 200 kPa for PEG-PDMS. As with conductivity, these materials have comparable mechanical properties (approximately 1 MPa) to other materials in this field.[88,93,94,95,145] Even at high salt loading, both the PEG and PEG-PDMS

networks remain elastic, maintaining a rubbery-like modulus and tan(δ) values much less than unity.

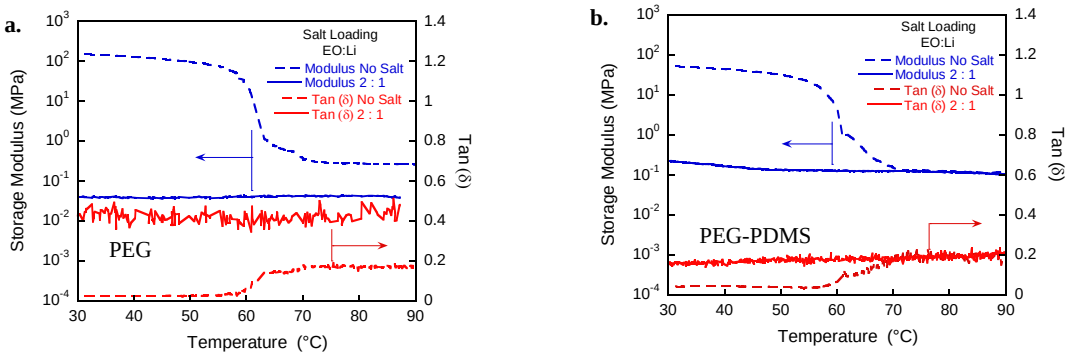

Figure 3.16 Storage modulus and tan (δ) of (a) PEG networks and (b) PEG-PDMS networks measured at 1Hz as a function of temperature. The data for the control sample in both network is given by dashed lines while the EO:Li = 2 are solid. The modulus values are shown in blue while the tan(δ) values are shown in red.

3.8 Conclusions

Here, we presented a chemical platform by which the mechanical properties and ion conductivity can be tuned to produce more effective materials. The mechanical properties can be modified by the incorporation of a non-ion conducting component without greatly reducing the ion conductivity. As previously demonstrated in block-copolymer systems, the ion conductivity of the material is dependent on the volume fraction of PEG. We envisage that using the same chemical platform, the mechanical properties can be further improved by substituting PDMS with a stiffer non-ion conducting component while, maintaining the same ion conducting properties demonstrated in the PEG-PDMS networks. The ion conduction and mechanical properties could also be tuned by changing the molecular weight of the precursor polymers or the volume fraction of the network components.

Furthermore, this system allowed for an investigation into the relationship between the ion conductivity and thermal properties. Both of these characteristics are strongly dependent on salt loading. This chemical platform allowed for a wide array of EO:Li ratios. DSC

measurements confirmed that this investigation spanned both the salt-in-polymer and polymer-in-salt composition regimes. In PEG networks, the ion conductivity is much more closely related to the T_g, because the ion conductivity values when normalized by T_g collapse. This shows ion conductivity is accomplished through polymer backbone relaxations. In the PDMS networks, however, normalizing the ion conductivity by T_g does not cause the curves to collapse, rather the ion conductivity ranking among the samples changes order. This shows that this system is more complex and likely the effects of ions interacting with the PDMS backbone need to be accounted for.

CHAPTER 4

PEG-PS MOLECULAR WEIGHT SERIES

4.1 Introduction

Co-network morphology is an active area of research that is poorly understood. Random cross-linking techniques currently used for co-network synthesis are not well controlled[37,38,41,42] and therefore do not provide a suitable platform for studying variables such as molecular weight between cross-links (M_C). Additionally, the lack of long-range order makes limits the utility of simple techniques, such as SAXS, for rigorous morphological characterization. However, the numerous benefits of materials with a bicontinuous morphology highlights the importance of fundamental understanding of these materials and their properties. In this chapter, co-networks of PEG and PS were cross-linked using the previously described Mitsunobu/thiol-ene platform. Three different precursor polymers were used to give networks with three different M_Cs. Following this systematic synthesis, the relationships between network morphology, thermal and mechanical properties and ion conductivity were investigated. To support the morphology characterization from SAXS and TEM, ion conductivity and storage modulus were used as probes to assess the continuity of their respective phases.

4.2 Design

This co-network approach provides a direct and relatively efficient method to explore the design prospects that generate the bicontinuous morphology. The cross-linking chemistry is performed in a good solvent for both chains which is assumed to provide random precursor polymer chain connections at the network junctions. Previously, this strategy has been used to

give well-defined, cross-linked networks as demonstrated by their resilience at high strain and uniform neutron scattering in the swollen state.[104,105,106]

PEG and PS were chosen for several reasons. Many studies on traditional block copolymers have been reported, thus their phase diagram is well known.[151] Also, PEG is a key polymeric involved in lithium ion conductivity studies[74] and impedance spectroscopy is used here as a probe to demonstrate continuity of the PEG phase. As discussed in Chapter 3, PEG and PDMS were used to generate conducting membranes; however they were soft (~0.1 MPa) due to the rubbery PDMS domains. As a result PS was employed for this study to increase stiffness and provide another orthogonal measure of percolation.

Three precursor polymers with three different molecular weights (M_n = 4.8, 12 and 37 kg/mol) were chosen to investigate the effect of cross-link density on bicontinuous morphology. The variation of M_n and narrow polydispersity of the precursor polymers is demonstrated in Figure 4.1. The predicted boundary of phase separation for block copolymers is $\chi N = 10.5$. The 4.8 kg/mol network was chosen to fall near this critical point. The upper end of the molecular weight range was chosen because the end functionalization and thiol-ene chemistry become difficult as molecular weight increases. Above 37 kg/mol, it is difficult to obtain high-quality (high gel fraction) networks. For example 50 kg/mol PDMS networks have been synthesized by this technique; however the gel fraction of 0.4 was quite poor.[152]

For these studies, the volume fraction of PEG (ϕ_{PEG}) was held constant at approximately 0.55. This is calculated from masses of each polymer used to prepare the network and the density of 100% salt-loaded PEG and PS networks determined using a pycnometer in hexane. Lithium bis(trifluoromethanesulfonylimide) (LiTFSI) was dissolved in the cross-linking solution at a mole ratio of ten PEG repeat units to one lithium ion (EO:Li = 10) for all samples. After curing, the gels were thoroughly dried to give solid, salt-loaded, co-network samples. Removal of the

common solvent induced phase separation. The compositions and properties of the networks in the M_n series are given in

Table 4.1.

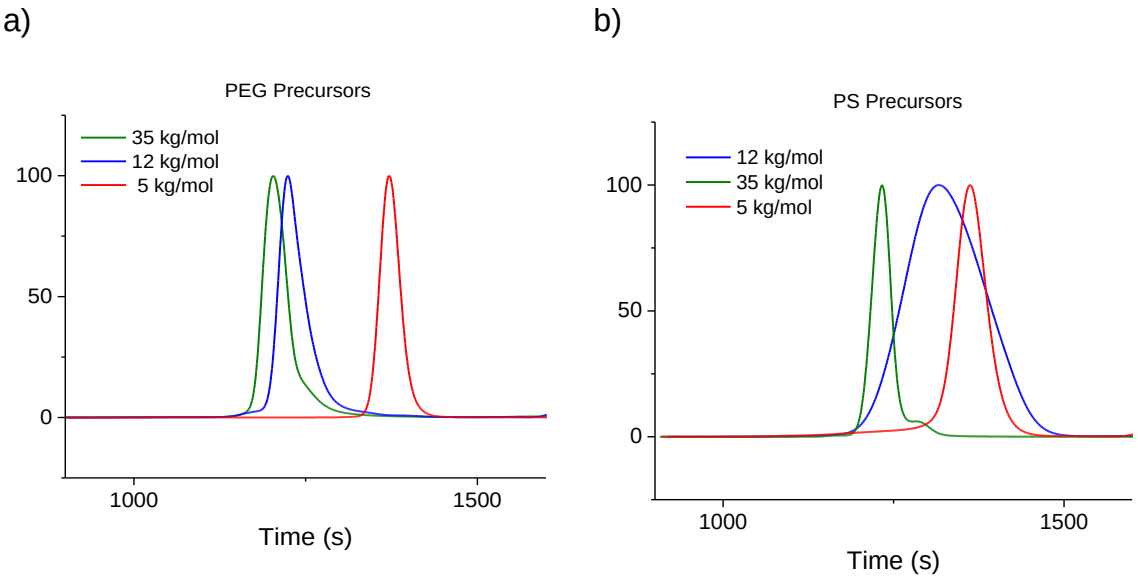

Figure 4.1 GPC traces for a) PEG and b) PS precursor polymers.

Table 4.1 Precursor polymer and network properties. [a] As indicated by supplier. Throughout the text, network samples are identified by the PS molecular weight. [b] Domain spacing was calculated from primary SAXS peak. [c] Fraction of crystalline PEG as measured by DSC, compared to theoretical heat of fusion for PEG.

***M*$_n$ PS Precursor (kg/mol)** [a]	***M*$_n$ PEG Precursor (kg/mol)** [a]	**ϕ_{PEG}**	***d*-spacing (nm)** [b]	**PEG Crystalline Fraction** [c]
4.8	4.6	0.55	22 ± 2	~0
12	12	0.55	31 ± 1	0.07
37	35	0.55	55 ± 2	0.25

4.3 Morphology

The morphology of the network samples was investigated using SAXS, and TEM. SAXS has the capability to give three dimensional orientation for highly ordered morphologies. TEM gives only a two dimensional image of the sample. However, these limitations are overcome by supplementing SAXS and TEM observations with property measurements.

4.3.1 SAXS

Figure 4.2, shows that the position of the primary scattering peak (q*) decreases with M_n. This corresponds to an increase in domain spacing (*d.)* Well-ordered morphologies, typically observed in annealed block copolymer samples, are not expected here because network connectivity limits long-range order. Nonetheless, a secondary reflection, at approximately *3q** is observed for each sample. This feature can be seen more clearly in the Kratky plot in Figure 4.3. Similar scattering features have been observed in other bicontinuous disordered systems such as amphiphilic co-networks,[37] morphologies obtained by spinodal decomposition,[153] kinetically trapped phases,[30] and polydisperse triblocks.[15,17] It has been proposed that the presence of the 3q* peak and absence of the 2q* peak arises from morphologies with weakly ordered lamellar phases, where the length scale of ordered morphology is only a few times greater than the *d*-spacing.[37] In samples with nearly symmetric compositions, it is common that the evenly ordered peaks (2q*, 4q*…) are suppressed.[154]

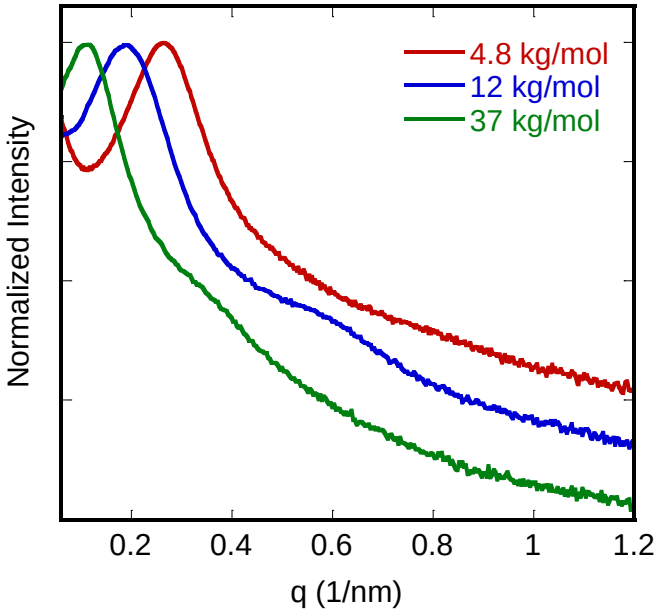

Figure 4.2 SAXS curves for the molecular weight series. Data was normalized to the q*peak intensity.

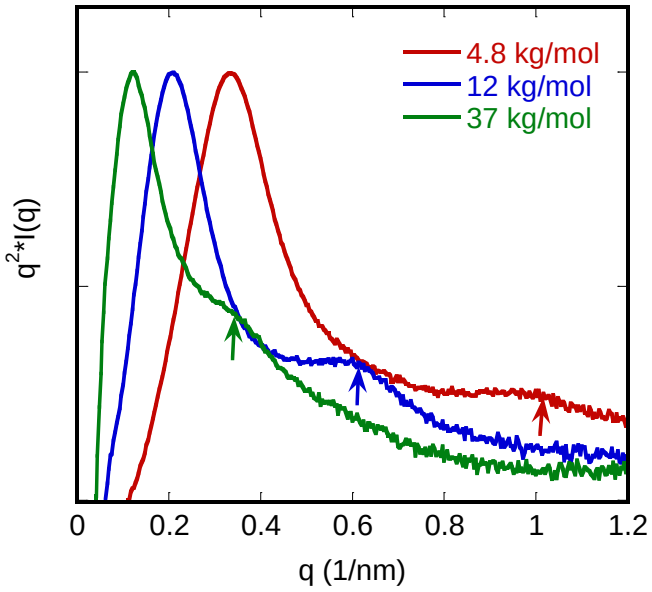

Figure 4.3 Kratky plot of SAXS data. Kratky plot. Higher order reflections, marked with arrows correspond to approximately *3q**.

As shown in Figure 4.4, the domain spacing ($d = 2\pi/q^*$) increases with M_n, in a manner consistent with de Gennes's prediction of $d \sim M_c^{0.5}$ for a cross-linked blend.[39] This trend has been observed in other disordered, bicontinuous phase-separated systems.[155]

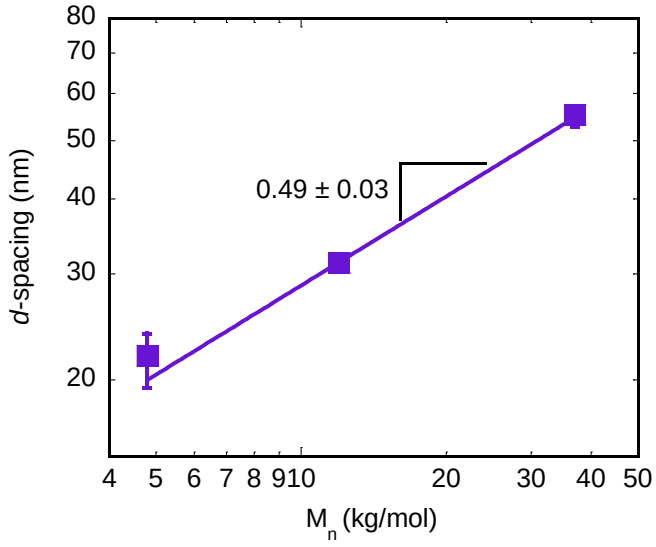

Figure 4.4 Scaling relationship between M_n and d-spacing closely follows the relationship predicted by de Gennes of $d \sim M_c^{0.5}$. The fit line is a power law expression with an exponent of 0.49 ± 0.03. Error bars represent the maximum and minimum of three independent measurements, or the distribution of measurements is smaller than the symbol.

By fitting the primary scattering peak with a Gaussian equation, the full width at half of the maximum (FWHM) can be obtained. This gives information on the length scale of the ordered domains or grain size (g) in the system by Scherrer's equation, $g = 2\pi/\text{FWHM}$. Well-ordered systems have sharp peaks which gives a small FWHM and therefore long range order. Systems with short-range or local order have broader peaks and smaller grain sizes. Figure 4.5 gives a representative Gaussian fit to the primary scattering peak from the 12 kg/mol network. The scattering peak is well described by the Gaussian fit with R = 0.99. Representative values for FWHM obtained for all three networks are given in Table 4.2 along with the grain size given by

Scherrer's equation. The grain size does not seem to trend with M_n. The 12 kg/mol network has a smaller grain size than the 4.8 kg/mol network, 61.6 nm and 68.1 nm respectively. However it does make sense that the 37 kg/mol network has the largest grain size as it also has the largest d-spacing. Each network has only a few, ~3 or less, domains per grain.

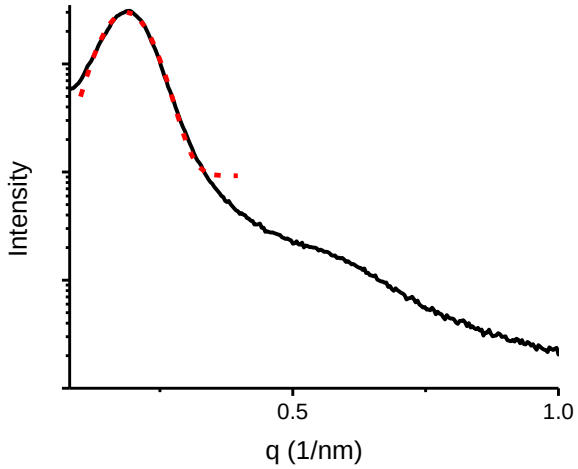

Figure 4.5 Representative Gaussian fit (red dash) to primary scattering peak (black solid) of 12 kg/mol network.

Table 4.2 Full width at half max (FWHM) and grain size obtained from Gaussian fits to SAXS data.

Network (kg/mol)	FWHM (1/nm)	Grain Size (nm)	Domains/Grain
4.8	0.0923	68.1	3.1
12	0.102	61.6	2.0
37	0.0791	79.5	1.4

4.3.2 TEM

This bicontinuous morphology is further supported by the representative TEM image of the 12 kg/mol system shown in Figure 4.6. The domain spacing of 30 nm is consistent with the

SAXS result from this sample. The irregularly shaped domains show areas with slight lamellar characteristics and are consistent with highly connected, disordered structures which are similar to other materials with this type of morphology.[15,17,30,37,153]

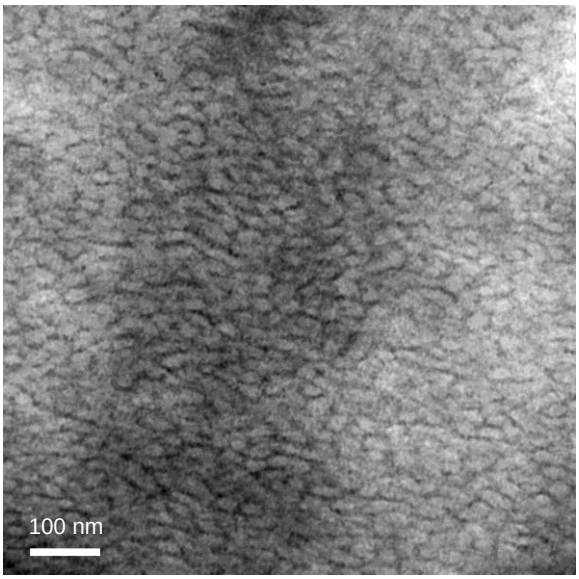

Figure 4.6 TEM image of the 12 kg/mol network. The PEG domains, stained with RuO_4, appear dark. The disordered domains are consistent with the SAXS pattern.

From the TEM, there appears to be some slight order, or bias in the direction of the domains. To see if this was an artifact of how the samples were dried, three SAXS measurements were taken, through each axis of the material. From Figure 4.7, the three directions cannot be differentiated based on their *d* values. Any directional bias in the TEM could be an artifact of microtoming or random sample variation.

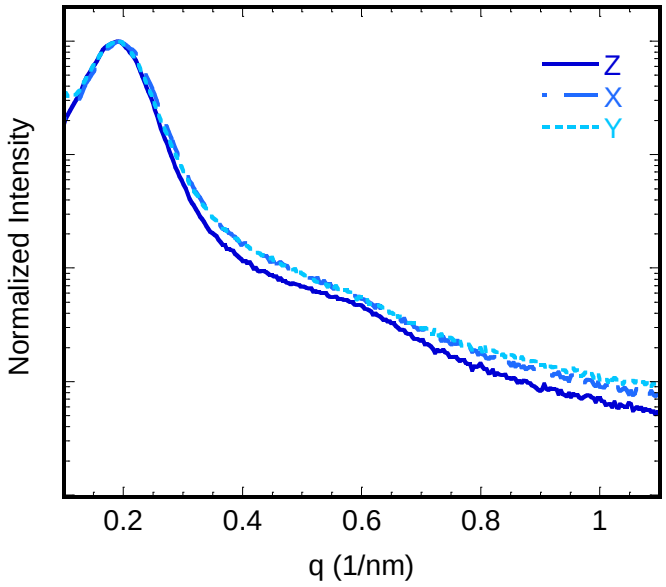

Figure 4.7 scattering in different directions, Z 32.6 nm, Y 32.6 nm, X 33.1 nm. Z is the direction of drying.

4.3.3 Phase Separation

With respect to phase separation of these networks, it is important to consider the molecular weight and χ value for PEG-PS (< 0.1).[156] In the simplest case of a traditional block copolymer,[13] the 4.8 kg/mol network should be near the limit of weak segregation predicted by mean field theory to fall at $\chi N = 10.5$. Randomly cross-linked networks and multiblock copolymer require a higher value of χN for phase separation compared to diblock copolymers.[40,55] However, this network was clearly phase-separated at room temperature as demonstrated by SAXS and up to 100 °C as demonstrated by differential scanning calorimetry (DSC) and dynamic mechanical analysis (DMA), shown later. This is likely due to the presence of LiTFSI within the PEG domains, which increases the effective χ value for the system,[70,71,157,158] allowing this relatively low molecular weight sample to micro-phase separate.

To further probe this idea, the morphology of a PEG-PS 4.8 kg/mol network without salt was studied by SAXS and is shown in Figure 4.8. At room temperature, there is a relatively strong scattering signal, likely due to the contrast in density as the PEG domains are crystalline. This will be discussed further in Section 4.4. For a wide range of temperatures above the PEG melting temperature, (60 to 120 °C), a weak shoulder is still visible. These networks show some phase separation, yet it is greatly weakened. At 200 °C, these networks do not scatter X-rays showing that the two phases are mixed. If further studies on these systems require thermal annealing, this would be a good temperature to use.

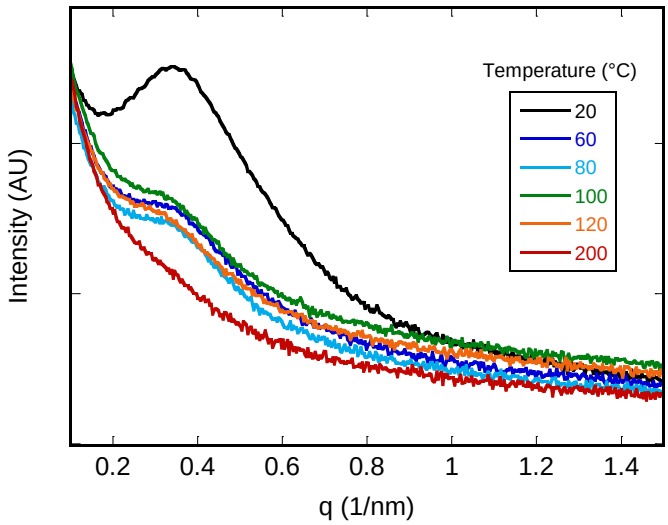

Figure 4.8 SAXS of 4.8 kg/mol network, without salt at various temperatures.

4.4 Thermal Properties

All of the salt-loaded PEG-PS networks are thermally stable up to 350 °C according to thermal gravimetric analysis, shown in Figure 4.9. This allows this system to withstand measurements or thermal processing at a wide range of temperatures.

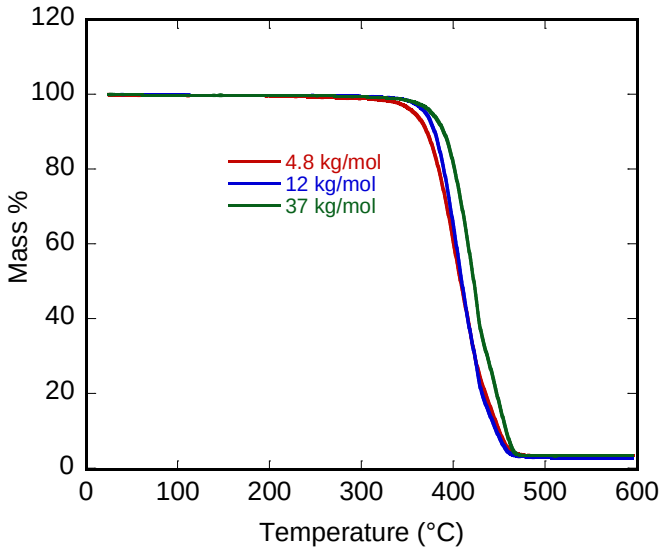

Figure 4.9 TGA of PEG-PS salt-loaded networks.

DSC measurements, shown in Figure 4.10, demonstrate that the salt-loaded networks have limited crystallinity compared to the theoretical maximum heat of fusion for PEG. In the 4.8 kg/mol network, there was no crystallinity within the detection limit of this technique. The 12 and 37 kg/mol networks have approximately 7 and 28% crystalline PEG phases, respectively, despite the 10:1 EO:Li salt concentration. The melting temperature also increases slightly with M_n; the 12 kg/mol network melts at 36 °C while the 37 kg/mol network melts at 39 °C. Additionally, no endothermic peak was observed at the reported melting temperature of the LiTFSI salt, approximately 230 °C, demonstrating that the salt is highly dissociated within the PEG phase.

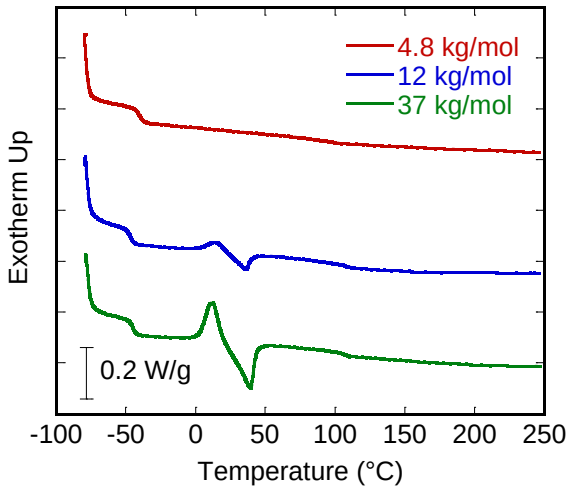

Figure 4.10 DSC measurements show that the LiTFSI loading effectively reduces crystallinity in the PEG phase. All data were taken from the second heating scan at a rate of 10 °C/min. Curves are offset for clarity.

To separate the effects of cross-linking, phase separation, and salt loading on crystallinity, PEG precursor polymers, 100% PEG networks and PEG-PS networks without salt were also analyzed by DSC. The crystallinity of these samples is compared to the PEG-PS salt-loaded networks in Figure 4.11. The three PEG precursor polymers had similar amounts of crystallinity, (Figure 4.12 a) indicating that molecular weight the linear polymer has a minimal effect on crystalline fraction in these samples. However, the melting point showed a slight temperature dependence; the 4.8 kg/mol polymer melted at 51 °C, while the 12 kg/mol polymer melted at 57 °C and the 35 kg/mol polymer melted at 60 °C. Next, (Figure 4.12 b) the 100% PEG networks show a slight M_n dependence in both crystalline fraction and melting temperature. In this series, networks show a crystalline fraction between 0.47 and 0.61 that increases with M_n. The bulk of the cross-link junction and the network connectivity reduce crystallinity compared to the linear precursor polymers. The melting points show a similar trend to the linear polymers. Introducing the polystyrene phase into the network (Figure 4.12 c) has little effect on the PEG crystallinity in the 12 and 35 kg/mol networks. However, in the 4.8 kg/mol network, crystallinity

decreases slightly due to more pronounced edge effects as this sample has the smallest domain spacing. The glassy PS domains act as anchors, restricting the motion of the PEG chains, making it more difficult for them to form crystals.[159] Finally, returning to the salt-loaded PEG-PS networks, it can be seen that the LiTFSI greatly reduces PEG crystallinity, yet these networks still show a similar dependence on M_n to PEG-PS networks or PEG networks without salt.

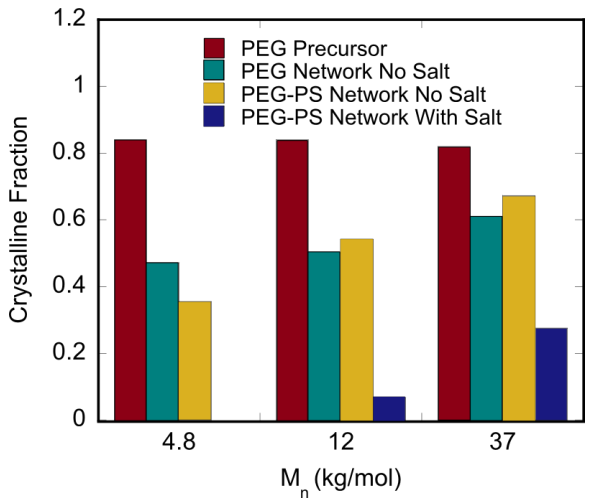

Figure 4.11 Crystalline fraction of PEG precursors, PEG networks without salt, PEG-PS networks without salt and PEG-PS networks with salt.

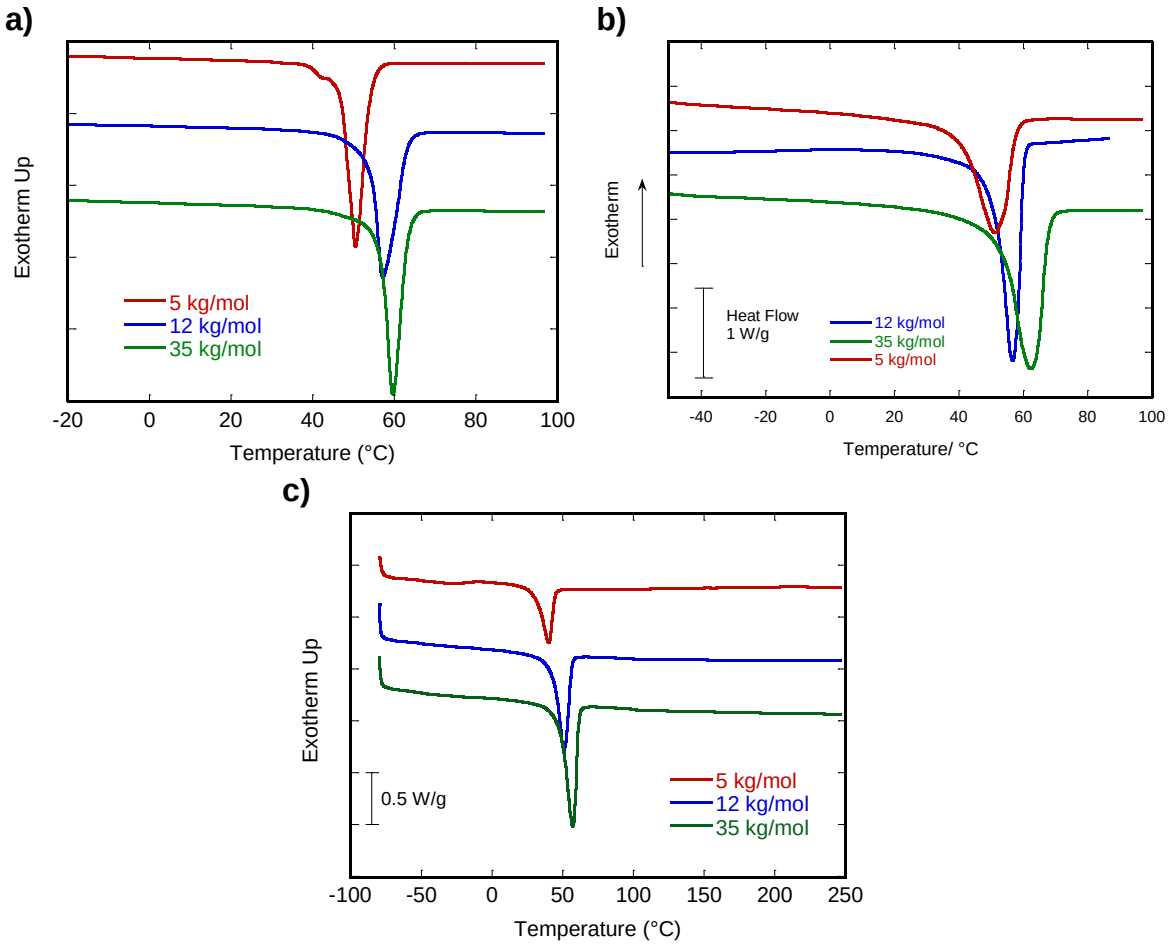

Figure 4.12 DSC traces for a) norbornene-terminated PEG precursors, b) PEG networks and c) PEG-PS networks without salt.

4.5 Mechanical Properties

Mechanical properties were evaluated using DMA under tension of rectangularly shaped samples. The plots of storage moduli (*E'*) and the loss tangents (*Tan(δ)*) (Figure 4.13) show that each sample displays two glass transition temperatures (T_gs) as indicated by the temperature at which *Tan(δ)* displays a local maximum. The PEG T_gs in each sample are between -20 °C and -10 °C. The 4.8 kg/mol network has a slightly higher T_g due to glassy PS hindering the motion of

the PEG chains near the interface.[159] The PS T_gs are between 107 °C and 112 °C. The low T_g and amorphous nature of the PEG phase allows for high ion conductivity, while the high T_g of the PS phase imparts mechanical rigidity. Between the two T_gs, *E'* is fairly stable with values of 50 to 90 MPa for the three networks, values much higher than those reported for other PEG-based ion conducting materials,[93,95] and on par with some of the highest reported to date.[29,70] These values also show favorable comparison to commercial separators made of polytetrafluoroethylene or a composite of silica, alumina and poly(ethylene terephthalate) that each showed a Young's modulus of approximately 60 MPa by nanoindentation.[160]

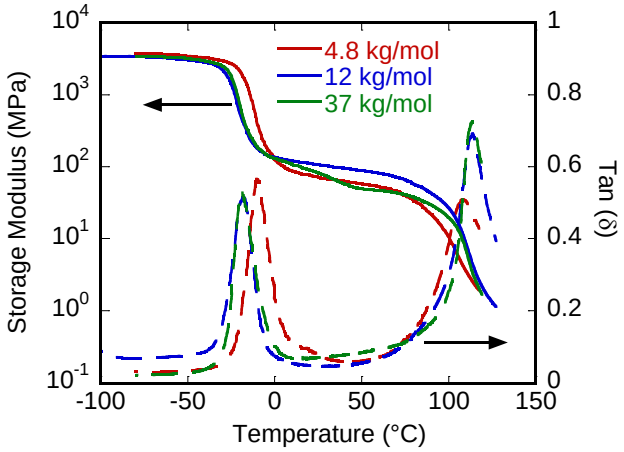

Figure 4.13 Dynamic Mechanical Analysis (DMA) measurements of storage modulus (left axis, solid lines) and *Tan(δ)* (right axis, dashed lines) show each sample has two glass transitions. (T_gs).

4.6 Ion Conductivity

Ion-conducting materials are of interest for solid electrolyte applications. Electrochemical Impedance Spectroscopy (EIS) was used here to measure ion conductivity (σ), as a probe to demonstrate that the salt and PEG phase percolates throughout the sample. Figure

4.14 shows ion conductivities for networks of all three molecular weights to be approximately 10^{-5} to $10^{-4.5}$ S/cm at 60 °C, similar to other PEG-based materials.[78,79,93] Specifically, LiTFSI-loaded PEG-PS block copolymers with similar *d*-spacing, volume fraction, and salt loading (70 nm, ϕ_{PEG} = 0.54, and EO:Li = 12, respectively) have an ion conductivity of approximately 10^{-4} at 80 °C.[96] In the temperature range investigated, there was minimal evidence of crystallinity interfering with the ion conductivity. Only the 37 kg/mol network shows a slight drop in σ at ~25 °C (3.35 1000/K), which was consistent with the DSC measurements. The networks with the higher M_n, 12 and 37 kg/mol, have slightly higher conductivities compared to the 4.8 kg/mol network especially below 60 °C. This could be due to the larger *d*-spacing in these networks, giving them fewer domains per grain and more grain boundaries than the 4.8 kg/mol network. The increase in grain boundaries leads to a greater chance that the grains have adjacent PEG phases increasing the ion conductivity.[36,96] This could be confirmed by calculating the tortuosity of each co-network which would require ion conductivity measurements of 100% PEG networks at each molecular weight.

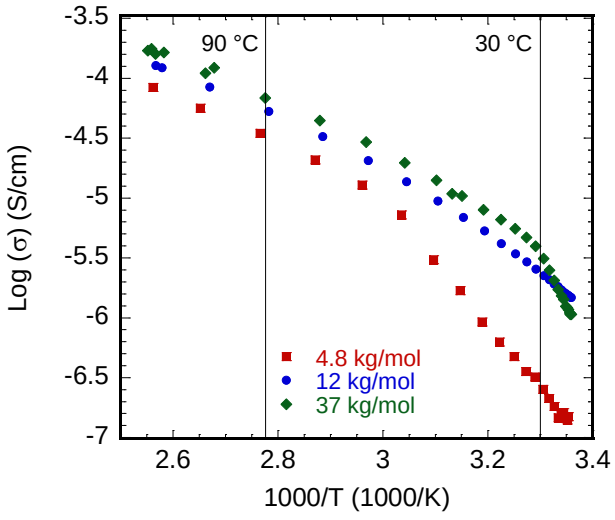

Figure 4.14 Impedance spectroscopy measurements show that the three networks have similar conductivity values above 60 °C. 90 °C and 30 °C are marked for reference.

The temperature dependence of the ion conductivity in polymer electrolytes is often described by one of two relationships. As explained in Chapter 1, the Williams-Landel-Ferry or Vogel-Tammen-Fulcher (VTF) relationship describes ion motion coupled to polymer chain relaxation, while the Arrhenius relationship describes an ion hopping mechanism. As shown in Figure 4.15, this fit appears to describe the data better at lower temperatures, especially in the 4.8 and 37 kg/mol network. This is possibly due to the fact that the VTF relationship was developed for measurements made near the T_g. Despite their appearance, all fits have R value of > 0.96.

As demonstrated in the previous chapter, one of the VTF parameters is T_0 is thought to be related to the PEG T_g. In this series of networks, the T_g determined by DMA as wells as DSC. The T_g values from DSC are approximately -45 °C, shown in bright green in Figure 4.16, while the T_g values from DMA are between -20 °C and -10 °C, Figure 4.16 in purple. The T_0 values, shown in black in Figure 4.16, are much closer to the T_g values from DMA. For the 4.8 network, the T_0 value is approximately 10 °C lower than the T_g, while the T_0 and T_g values for the 12 and 37 kg/mol networks are much closer together. The relationship between T_0 and T_g still does not appear to follow the 50 °C difference as described in the literature by either measurement. However, using PEG-PS networks and DMA seems to give a closer and more consistent relationship between T_0 and T_g compared to the PEG or PEG-PDMS networks measured by DSC. This is possibly due to ionic interactions between the salt and the PDMS backbone and DMA probing chain relaxations, as discussed in Chapter 3.

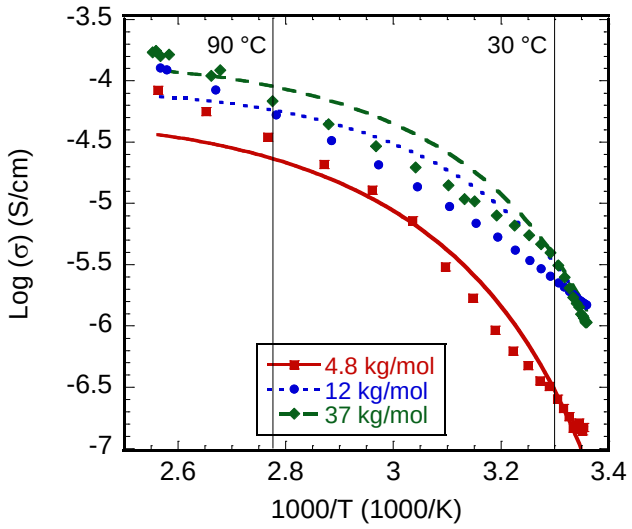

Figure 4.15 VTF fits to Ion Conductivity vs. Temperature.

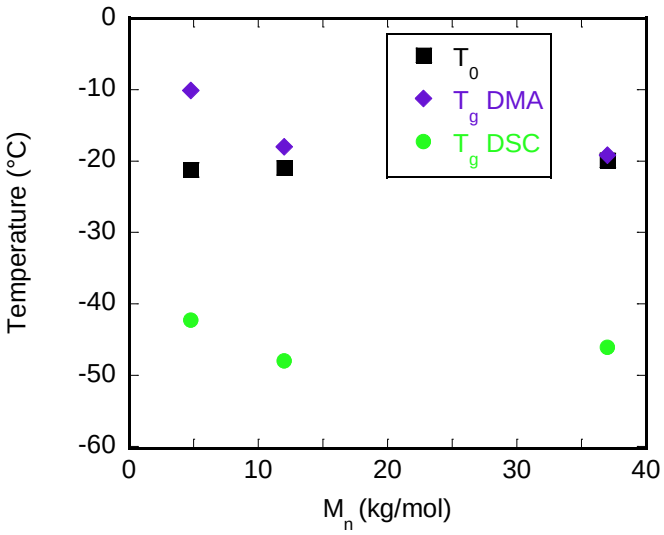

Figure 4.16 T_0 values extracted from VTF parameter and T_g values as measured by DMA and DSC.

The Arrhenius fits are shown in Figure 4.17. For the 37 kg/mol network, the fit does not capture the additional decrease in ion conductivity due to crystallinity, though an Arrhenius fit is

not expected to describe this behavior. For the 4.8 and 12 kg/mol networks, the behavior is non-Arrhenius with the fit overestimating ion conductivity at the highest and lowest temperatures and underestimating ion conductivity in the mid-range. However, the R values are again < 0.96. To demonstrate if the 4.8 kg/mol network has some kind of transition at ~60 °C, two separate Arrhenius fits are shown in Figure 4.18. The slopes differ by almost a factor of two, which corresponds to an increased activation energy at low temperatures. More investigations are needed to determine why this could be the case. With the given data set it is difficult to distinguish whether the VTF or Arrhenius fit describes the data more accurately. It is possible that a more detailed model is needed to accurately describe the ion conductivity temperature dependence shown in Figure 4.14.

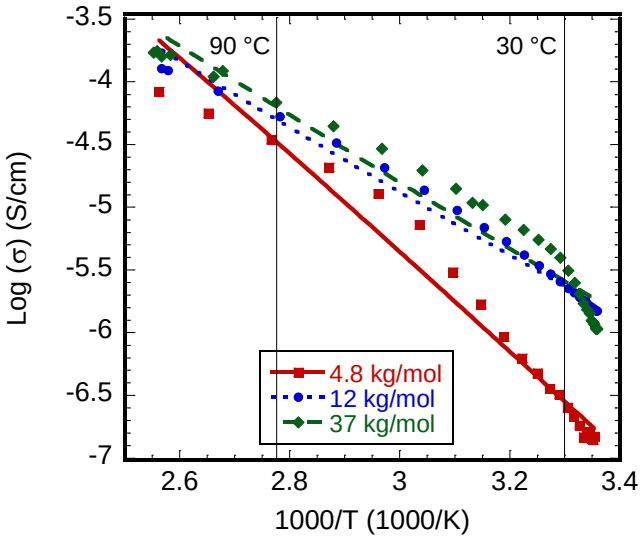

Figure 4.17Arrhenius Fits to Ion Conductivity vs. Temperature.

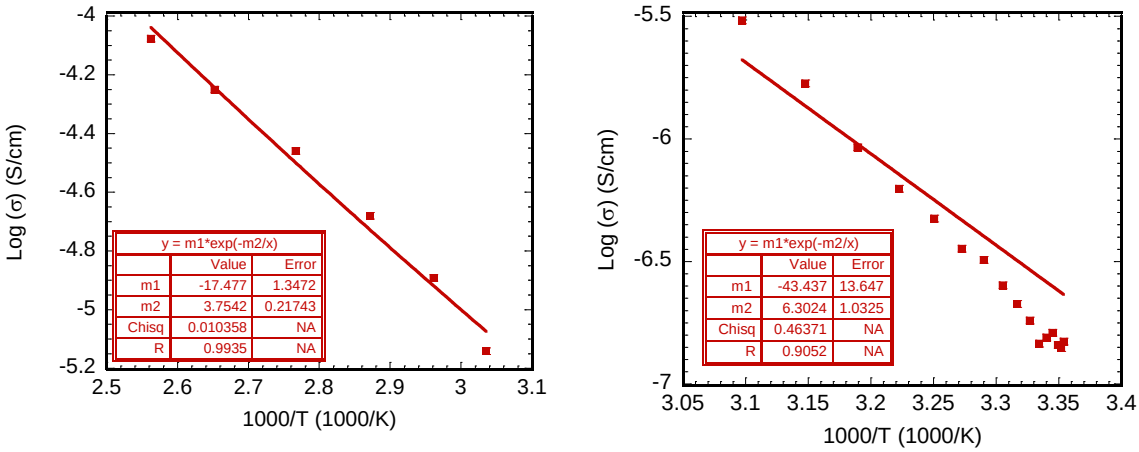

Figure 4.18 Arrhenius fits to 4.8 kg/mol at high and low temperatures.

4.7 Conclusions

Here, we systematically investigated a bicontinuous morphology on a variety of length scales and volume fractions via a clean and efficient thiol-ene platform. Changing the molecular weight between the precursor polymers allowed for control over the size of the phase-separated domains. The phase separation allowed us to synthesize networks with a high storage modulus and high ion conductivity. These bulk properties were consistent across the length scales probed, further demonstrating this as a versatile platform; one that will allow this co-network strategy and thiol-ene chemistry to be used for a variety of applications where bicontinuous morphologies are desirable. Given the general utility of the Mitsunobu and thiol-ene reactions, we envision this strategy to be applicable to many combinations of polymers and will generate materials with broad applicability even beyond the high-modulus, ion-conducting materials discussed here.

CHAPTER 5

PEG-PS VOLUME FRACTION SERIES

5.1 Introduction

A composite system with a high degree connectivity between the two components, such as a co-network should show a large compositional range of bicontinuous structures. To assess the breadth of the bicontinuous phase window, a series of samples with varied weight ratio of PEG to PS were synthesized using the 12 kg/mol precursor polymers. This system follows the same design principals as the M_C series from the previous chapter. The samples were synthesized by varying the weight fraction of the two components. This was converted to volume fraction using the density of 100% salt-loaded PEG or 100% PS networks as measured by a pycnometer. The volume and density of the PEG phase included the LiTFSI. The LiTFSI loading was kept constant relative to the amount of PEG in each network at EO:Li = 10. Ion conductivity and storage modulus at 30 °C were compared across a wide range of volume fractions to assess whether both phases percolated through the sample.

5.2 Morphology

The morphology of the PEG-PS volume fraction series of networks was investigated by SAXS. Each sample shows a broad q* peak indicative of a disordered system, as shown in Figure 5.1. The full width at half max (FWHM) of each peak is between approximately 0.10 nm^{-1} and 0.15 nm^{-1}, as shown in Figure 5.2. Using Scherrer's equation,[161] this gives a grain size of ~40 to 64 nm. Given the d-spacings are between 25 and 32 nm (Figure 5.5), this means only 2-3 domains are aligned per grain. For comparison, the primary peak from ordered block copolymer phases generally shows a FWHM of less than 0.02 nm^{-1} giving grain sizes of over 300 nm.[4]

Despite this disorder, each sample shows a higher order shoulder at approximately 3q*. This feature can be seen more clearly, in the Kratky plot, Figure 5.3, which highlights higher q values. Across the range of volume fractions, this higher order peak consistently appears at 3q*, as shown in Figure 5.4. It has been suggested that this feature is due to weakly ordered lamellar phases, where the 2q* peak is suppressed due to the high symmetry of the phases.[154] However, upon expanding the volume fraction series to highly asymmetric samples, a 2q* peak is still not present. An alternate explanation for this type scattering pattern from disordered systems is that the 3q* peak is related to the curvature of the interfaces. This could explain the absence of the 2q* peak from the asymmetric samples.

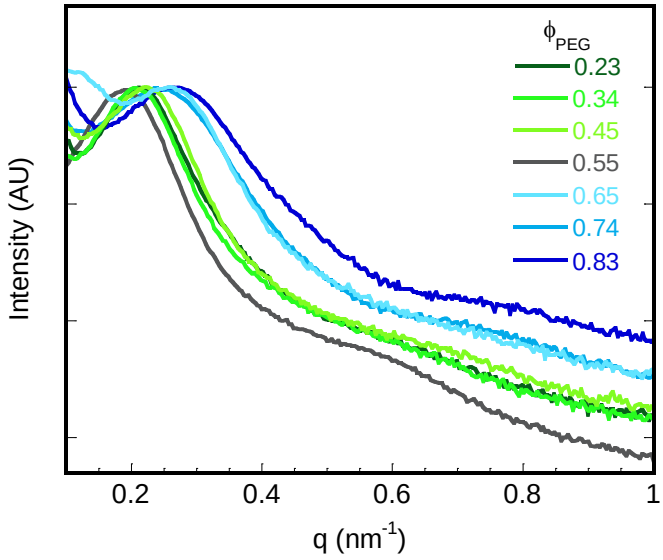

Figure 5.1 Representative SAXS curves for the volume fraction series showing a broad q* peak in each sample.

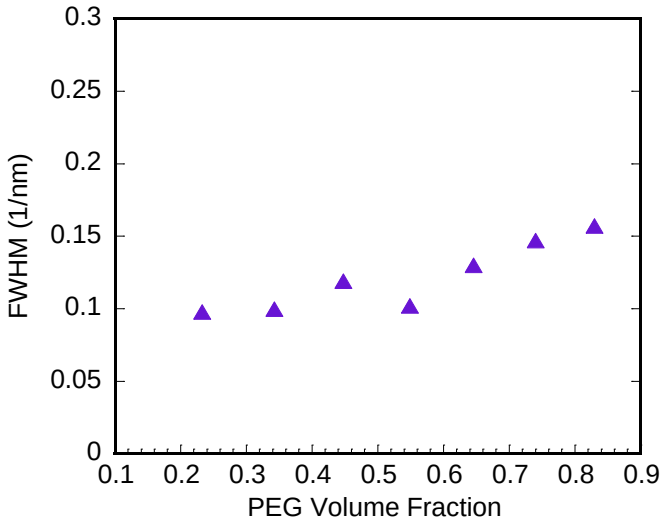

Figure 5.2 Representative FWHM of the q* peak vs. PEG volume fraction.

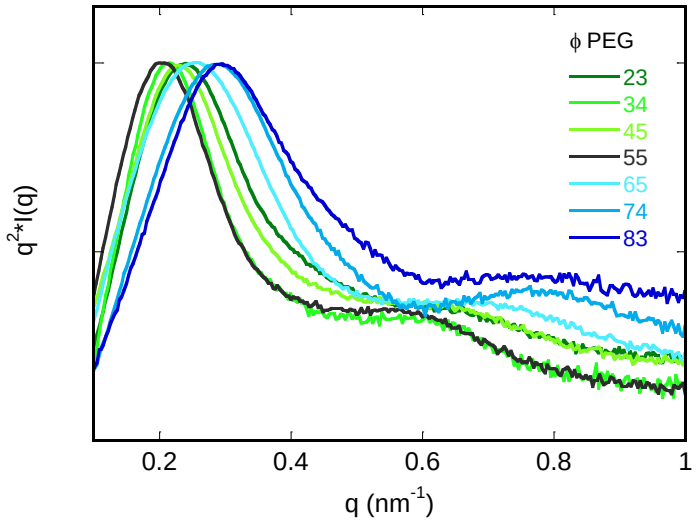

Figure 5.3 Kratky plot of representative SAXS curves for the PEG-PS volume fraction series. Curves are labeled as % volume of PEG.

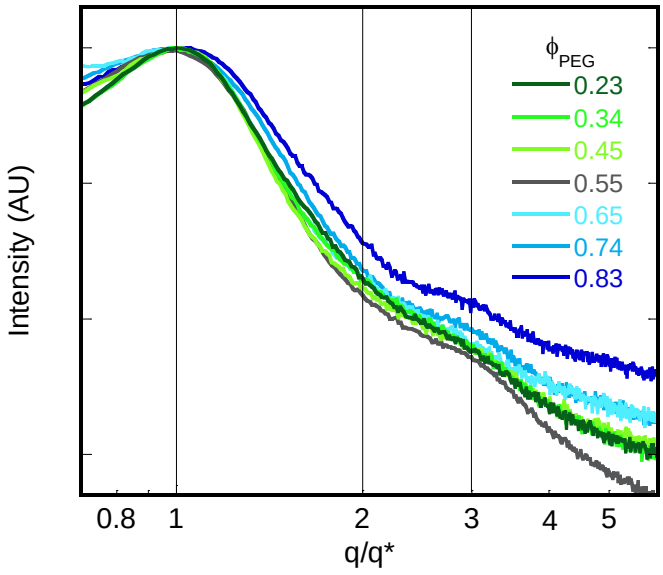

Figure 5.4 SAXS curves scaled by q*. Lines highlight positions of q*, 2q* and 3q*.

The volume fraction has only a slight effect on the domain spacing (*d*) of the overall system. The values were calculated from the relationship $d = 2\pi/q^*$. Overall, the slightly decreasing trend is explained by the difference in density of each phase. Cross-linked networks of PS and LiTFSI-loaded PEG synthesized so that the density could be measured by a pycnometer in hexanes. The PEG/LiTFSI sample has a much greater density, 1.57 g/cm^3, than the PS sample, 1.17 g/cm^3.

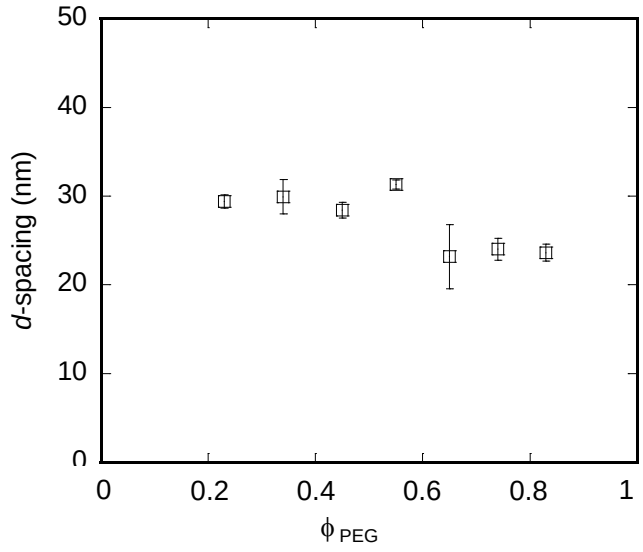

Figure 5.5 Domain spacing vs. PEG volume fraction. Error bars represent the standard deviation of three measurements.

5.3 Ion Conductivity

Most ion conductivity samples, Figure 5.7, show similar temperature dependence to each other. This non-Arrhenius type of behavior is consistent with what was seen in the M_C series. The outlier from this group is the $\phi_{PEG} = 0.23$ sample, as it shows almost no temperature dependence. This measurement also displays a high amount of noise because it is near the detection limit of the instrument. This response, however minimal, is due to the nature of the impedance measurement.

Electrochemical impedance spectroscopy (EIS) uses alternating current (AC) conductivity and measure the current response to an applied voltage. The applied voltage switches directions, or alternates, over a wide range of frequencies. Even in isolated domains, the likely case for $\phi_{PEG} = 0.23$, ions can move within the conducting phase, shown in blue in Figure 5.6 a. The distance the ions move is dictated by their diffusion coefficient which is on the order of 10^{-12} m^2/s for random motion of LiTFSI in PEG.[162] At long times, or low frequencies, lithium

ions will accumulate one end of the domain. Once a number of charges have reached the barrier, or edge of the domain, it causes a local a charge imbalance. Consequently, the internal electric field is reduced, which in turn decreases the ion transport. At the end of the frequency period, the voltage switches and the ions begin moving in the other direction, once again, generating a current response. At higher frequencies, the current and ions change direction more frequently. As a result, fewer ions reach the edge of the conducting domain and the degree of connectivity cannot be discerned. In other words, at high frequencies, the ions are only probing the system locally. At lower frequencies, they are probing the system at greater distances. Fortunately, the ion conductance is determined by the response in the low frequency regime, approximately 10^3 Hz for this series. At this frequency, lithium ions are expected to randomly diffuse 100 nm which is greater than the *d* values observed using SAXS. This estimate represents a lower-bound as it was calculated assuming random diffusion,[162] when in fact the diffusion is not random due to the applied voltage. The fact that the ions are expected to diffuse much farther than *d*-spacing, enables EIS to differentiate between highly connected, Figure 5.6 b, (larger than diffusion length) and isolated (smaller than diffusion length) sized domains. This indirect measurement of connectivity allows us to use EIS as a three dimensional probe rather than making difficult, yet more direct, morphology measurements.

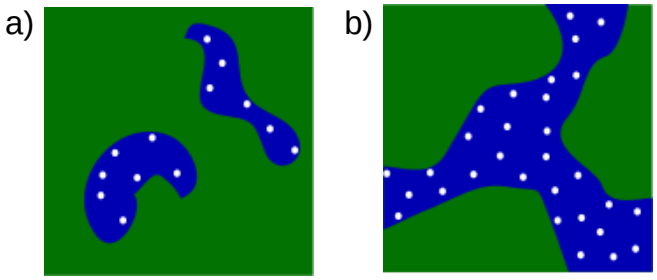

Figure 5.6 Illustrations of a) isolated and b) percolated domains where PEG is represented by blue, PS is represented by green and lithium ions are depicted as white circles.

In contrast, direct current (DC) resistance measurements require at least one physically connected path--from one side of the sample to the other--to exhibit conductivity. If the conductive domains are isolated in any way, the measured DC resistance becomes infinite.

Looking at a single temperature, 30 °C or 70 °C, both shown in Figure 5.8 a and b, the ion conductivity undergoes a large step change of almost three orders of magnitude between ϕ_{PEG} = 0.23 and 0.32. In this region, even small changes in volume fractions, from ϕ_{PEG} = 0.23 to 0. 27 cause large differences in ion conductivity, as more domains become connected. Above ϕ_{PEG} = 0.32, ion conductivity increases more gradually due to the increasing volume of PEG. The area shaded in blue represents the range of volume fractions of suspected PEG percolation. Between Figure 5.7 and Figure 5.8, it can be demonstrated that, for the temperature range tested, temperature has a minimal effect on domain connectivity. Each sample in Figure 5.7 has a similar temperature dependence, aside from ϕ_{PEG} = 0.23, as discussed previously. Figure 5.8 a and b have similar trends, aside from the overall magnitude of the ion conductivity, which is temperature dependent.

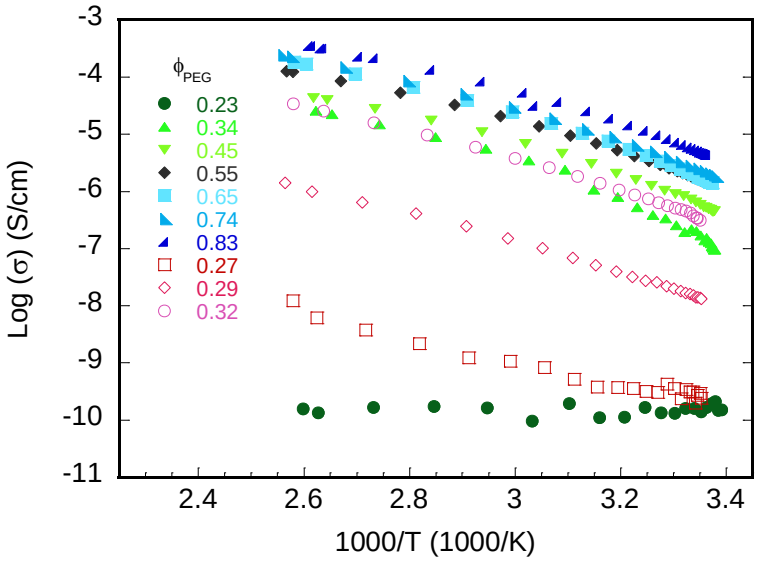

Figure 5.7 Ion conductivity of representative samples from the volume fraction series at the full temperature range measured.

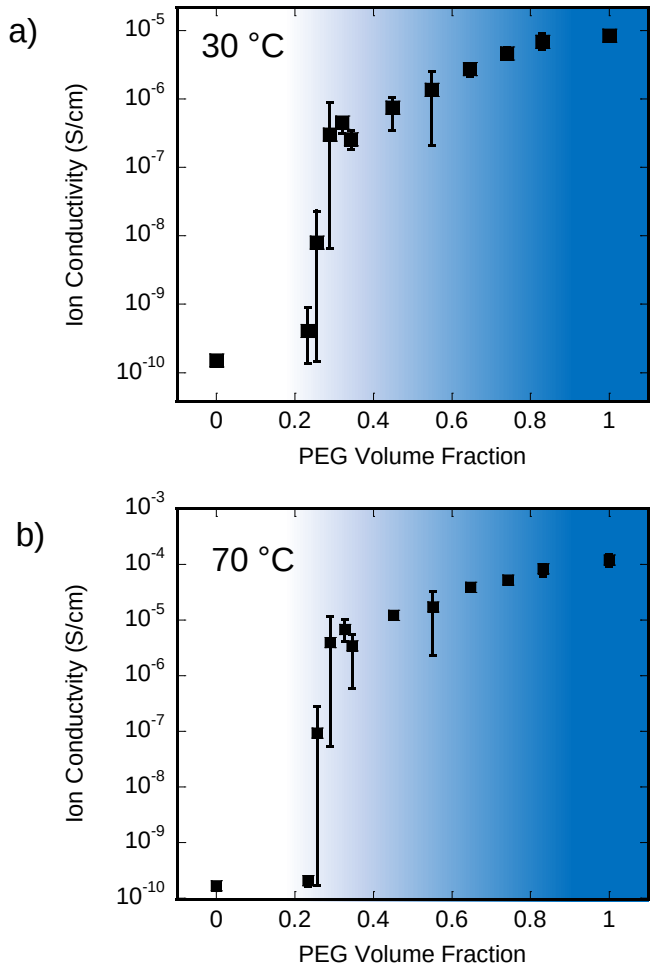

Figure 5.8 Ion conductivity at a) 30 °C and b) 70 °C vs. volume fraction. Areas of suspected PEG percolation are shaded in blue. Error bars represent the maximum and minimum of three measurements.

The Voigt and Reuss bounds, also called the "rule of mixtures" gives upper and lower bounds, respectively, for a variety of composite properties based on the volume fraction of the components and their assumed orientation.[163] These bounds give reasonable maximum and minimum ion conductivity values for the measured composites, as shown in Figure 5.9. Only some of the wider error bars are outside the predicted bounds. The Voigt-Reuss-Hill prediction gives the average of the Voigt and Reuss bounds. Only at the high ϕ_{PEG} is the ion conductivity

above this average. While the Voigt and Reuss models give reasonable predictions for the limits of ion conductivity values, this model is not useful for determining domain connectivity.

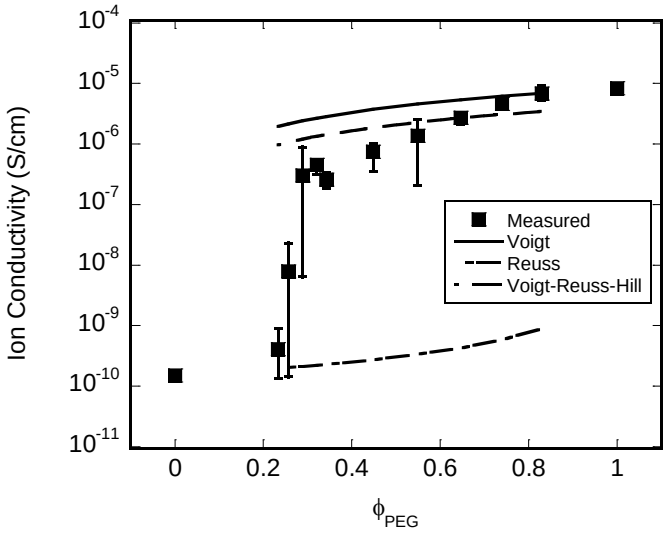

Figure 5.9 Rule of mixtures applied to ion conductivity measurements.

When considering the ion conductivity of composite materials, it is important to consider the tortuosity of the ion conducting pathways. As the fraction of impeding material decreases, connectivity of the conducting phase should increase. This will lead to more direct pathways for ion conduction. At high ϕ_{PS} (low ϕ_{PEG}) the ions will have to move around large PS barriers. This deviation from the most direct pathway is called tortuosity. Tortuosity can be easily examined by equation 5.1, where τ is the tortuosity factor, σ_{PEG} is the ion conductivity of a 100% PEG network, σ_{meas} is the ion conductivity of the composite sample and ϕ_{PEG} is the volume fraction of PEG.

$$\tau = \frac{\phi_{PEG} * \sigma_{PEG}}{\sigma_{meas}} \qquad \text{Equation 5.1}$$

The tortuosity values found using this method are given in Table 5.1. Bicontinuous materials usually have τ values between 1.5 and 3. Using that guideline, only the 65 % PEG sample is bicontinuous. However, this method only takes into account the ion conductivity and does not consider the mechanical properties.

.

Table 5.1 Tortuosity of ion conducting pathways at 30 °C in PEG-PS networks.

ϕ_{PEG}	τ
0.23	4800
0.34	11.2
0.45	5.04
0.55	3.38
0.65	1.99
0.74	1.33
0.83	1.02

In order to get a more precise value of the PEG percolation threshold, percolation theory, as explained in the introduction was applied to the data in Figure 5.8. Equation 5.2 is percolation theory with variables specific to this application: σ is the ion conductivity measured for each composite sample, σ_0 is the ion conductivity of a PS network, A is a fitting parameter, ϕ is the volume fraction of the composite, ϕ_C is the critical volume fraction and P is the scaling exponent.

$$\sigma = \sigma_0 + A(\phi - \phi_C)^P \qquad (5.2)$$

In order to more easily fit the data, σ_0 was subtracted from σ and the log was taken of both sides of the equation. Various estimated values of ϕ_C were tested in the resulting expression, equation 5.3, until a linear plot of data was obtained, thereby identifying the best fit value of ϕ_C.

$$Log(\sigma - \sigma_0) = LogA + PLog(\phi - \phi_C) \qquad (5.3)$$

Any volume fractions below the chosen ϕ_C were eliminated from the plot as they gave undefined values. The value of ϕ_C = 0.225 gave points that when fit with a linear curve gave an R value of 0.97, as shown in Figure 5.10. From this fit the value of P, the scaling exponent is 2.16 ± 0.18. For conductivity, it is predicted that the critical scaling exponent has a value of 2 for three dimensional systems. This was obtained using the average conductivity data at 30 °C.

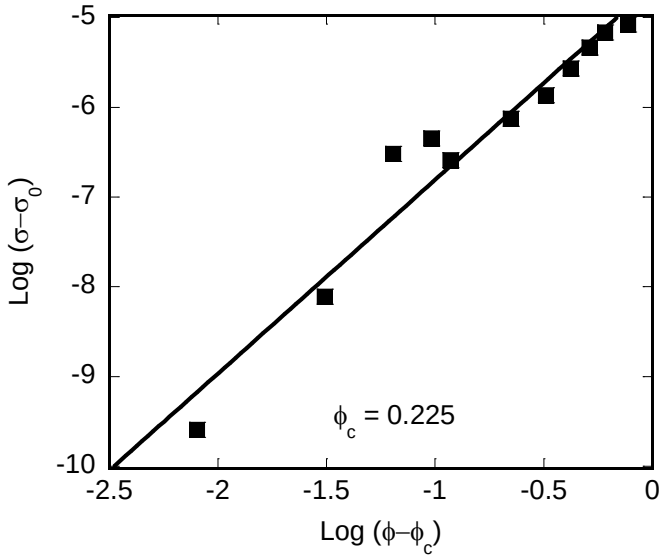

Figure 5.10 Percolation theory fitting to ion conductivity values at 30 °C with $\phi_C = 0.225$.

In order to check the value of $\phi_C = 0.225$ is valid, other ϕ_C values were fit in the same manner. Values below 0.225 give data points that are too concave down to be fit by a linear curve, as shown in Figure 5.11a where $\phi_C = 0.20$. Similarly, values above 0.225 give data points that would be better described by a concave up fit, rather than linear, as shown in Figure 5.11b where $\phi_C = 0.275$. Also the values of P given by linear fits to these plots give 3.75±0.78 and 0.86±0.16, respectively. These values are much farther away from the prediction of P = 2.

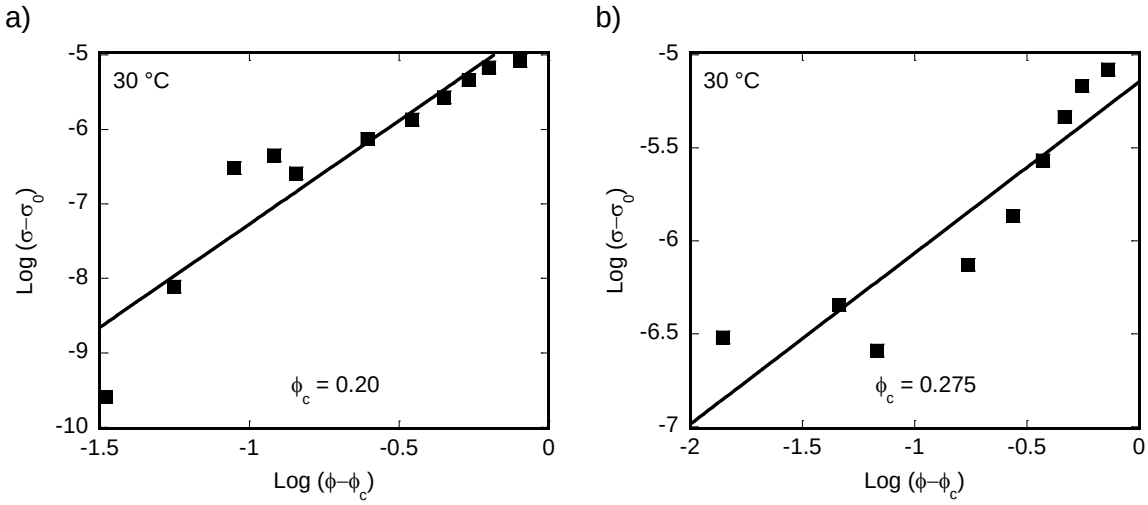

Figure 5.11 ϕ_C predictions that are a) too low at 30 °C, b) too high at 30 °C.

Several iterations of this fitting method were attempted with various ϕ_C. The results are summarized in Table 5.2. As ϕ_C increases, the value for the critical exponent (P) decreases. Also, the R value increases until it reaches a maximum of 0.97 at $\phi_C = 0.225$. This also happens to correspond with a value of P that most closely matches the Monte Carlo prediction.[58] In this system, the percolation of PEG domains has a critical threshold of approximately 0.225.

Table 5.2 ϕ_C values and their resulting critical exponent and R-value when fit to σ measurements.

ϕ_C	P	R
0.10	5.6±1.6	0.78
0.15	4.7±1.2	0.81
0.20	3.75±0.78	0.86
0.225	2.16±0.18	0.97
0.2375	1.66±0.16	0.96
0.25	1.38±0.12	0.97
0.275	0.86±0.16	0.91
0.30	0.91	0.92

.

To further confirm this ϕ_C value, the data was fit with the percolation theory equation with the critical exponent held fixed at 2. The data was weighted by 10% of the value during the fit. A value of $\phi_C = 0.237\pm0.0002$ was obtained with R = 0.92. The R value could be better; however, the ϕ_C values are in good agreement with the fitting from the log-log plots.

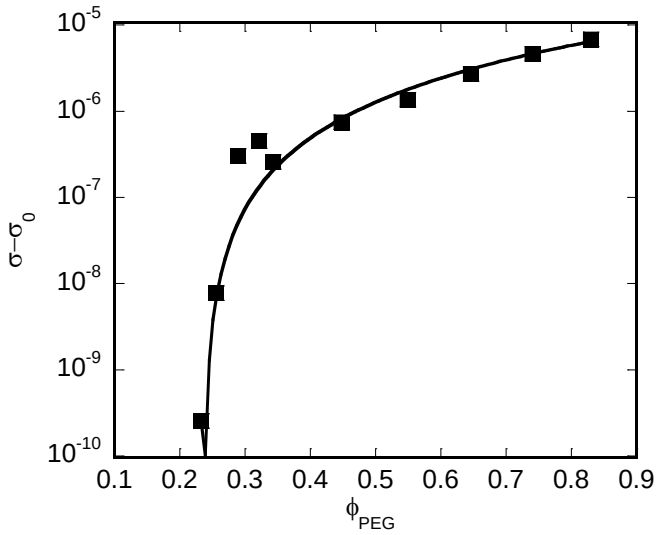

Figure 5.12 Percolation theory fitting with P =2.

5.4 Mechanical Properties

From Figure 5.13, it can be seen that most samples demonstrate two glass transitions (T_gs). For the sample that does not obviously show both transitions, ϕ_{PEG} = 0.83, it is likely due to the fact that the amount of PS is too low to produce a strong signal. Observing both T_gs corroborates the SAXS data that these co-networks are phase-separated up to at least 125 °C. Across the range of compositions, the T_gs are reasonably consistent for each phase. The PEG T_gs fall between -30 °C and -16 °C while the PS T_gs fall between 112 °C and 122 °C. The PEG T_gs are high because multiple polymer chains can coordinate to the same lithium ion providing physical cross-links in addition to the chemical co-network.

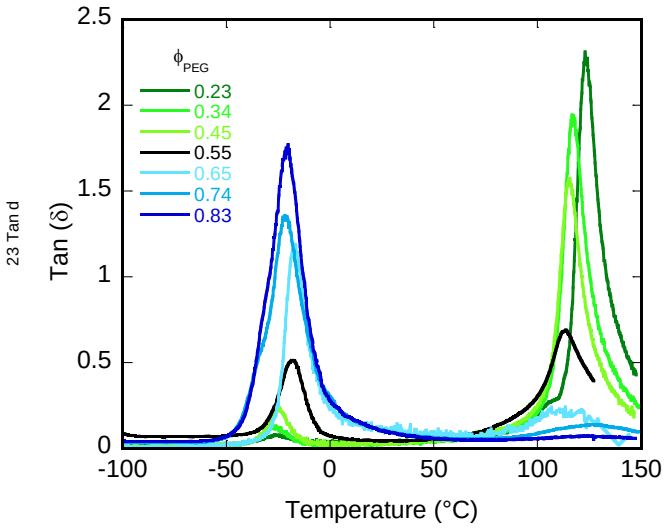

Figure 5.13 Tan(δ) vs. Temperature for the PEG-PS volume fraction series Curves are labeled as % volume of PEG.

Figure 5.14 shows the storage modulus vs. temperature for representative samples in the volume fraction series. All samples show similar E' below approximately -30 °C. All of these values are greater than 1 GPa, which is predicted to suppress dendrite growth.[88] However, at this low temperature, the PEG phase is glassy and ion conductivity is poor. Similarly, at high temperatures, above 120 °C the E' values converge at approximately 0.5 MPa, a value which is quite low for solid electrolytes because this is above the PS T_g. These samples have a wide potential operating range, from -30 °C to 120 °C, where PEG is rubbery and PS is glassy. In this temperature range, the volume fraction of the components has a large effect, approximately three orders of magnitude, on the storage modulus.

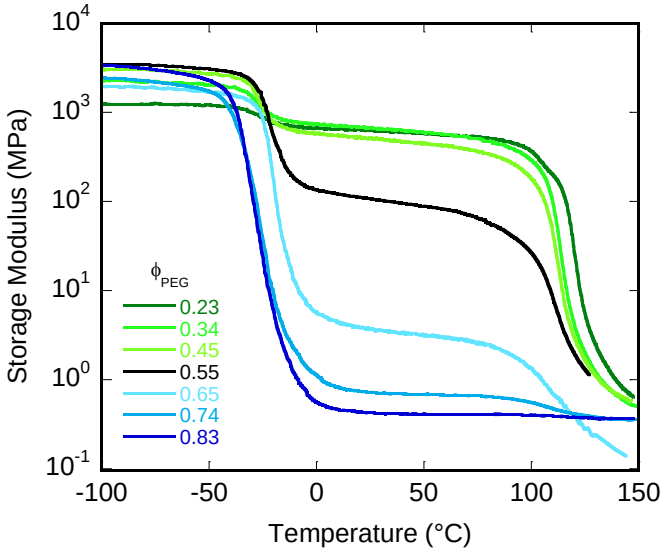

Figure 5.14 Storage Modulus vs. Temperature for of the PEG-PS volume fraction series. Curves are labeled as % volume of PEG.

The difference in mechanical properties over the volume fraction series is evident from handling the samples at room temperature. Samples with ϕ_{PEG} < 0.40 were rigid, brittle, and often fractured during sample preparation. Samples with ϕ_{PEG} > 0.70 volume PEG were rubbery and sticky, also making them challenging to handle and cut to the desired geometry. Intermediate samples with similar amounts of PEG and PS were rigid enough to cut without deforming yet are not so brittle that they fractured. The storage modulus, as measured by DMA at 30 °C, as shown in Figure 5.15, confirmed these qualitative observations. For volume fractions of PEG below 0.45 the samples had a storage modulus above 500 MPa which could be useful in preventing dendrite growth on lithium metal electrodes and is a value rarely demonstrated in solid electrolytes. Even the 0.55 network had a storage modulus of approximately 100 MPa which is on par with values leading the field.[70] Networks with ϕ_{PEG} < 0.65 had a much lower storage modulus of less than one MPa, which is similar to the 0.5 MPa of a 100% PEG network.[107] The area shaded in green represents the range of volume fractions where it is suspected that

PS percolates throughout the sample. The green fades gradually to white to represent that this is an initial estimation.

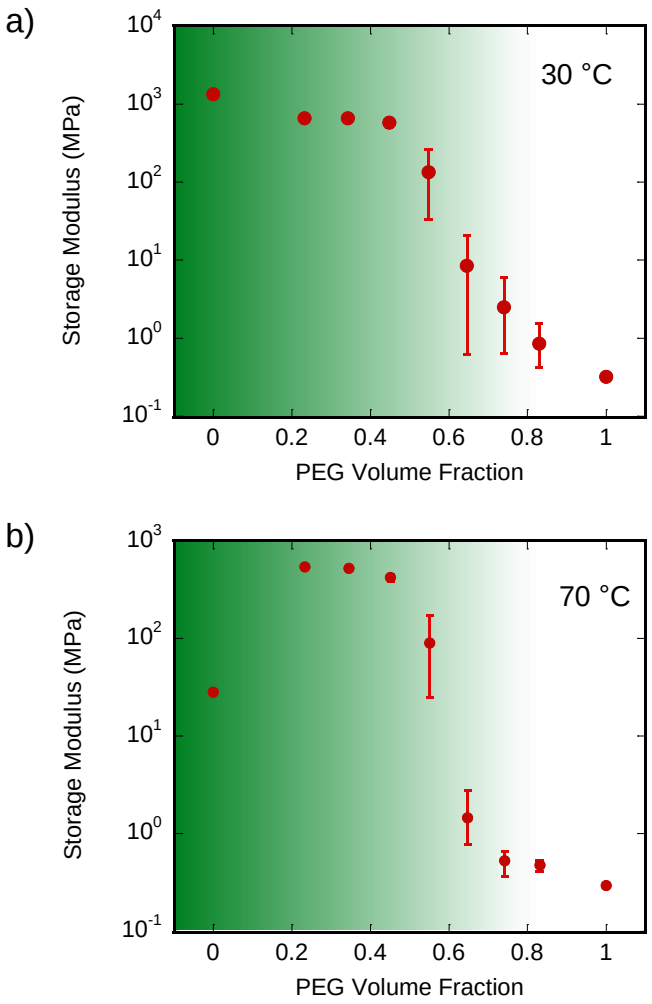

Figure 5.15 Storage Modulus at a) 30 °C and b) 70 °C vs. PEG Volume Fraction. The region of suspected PS continuity is shaded in green. Error bars represent the maximum and minimum of three measurements.

As shown in Figure 5.16, the composites fall between the Voigt and Reuss predictions. Below $\phi_{PEG} = 0.45$, the storage modulus is above the value predicted by the Voigt-Reuss-Hill average. These models gave reasonable boundaries for the storage moduli of the volume fraction series. However, the large difference in PEG and PS storage moduli give a range of values that

spans three orders of magnitude between the Voigt and Reuss predictions. This broad spread makes it difficult to use this model to determine if the PS phase is percolated or not.

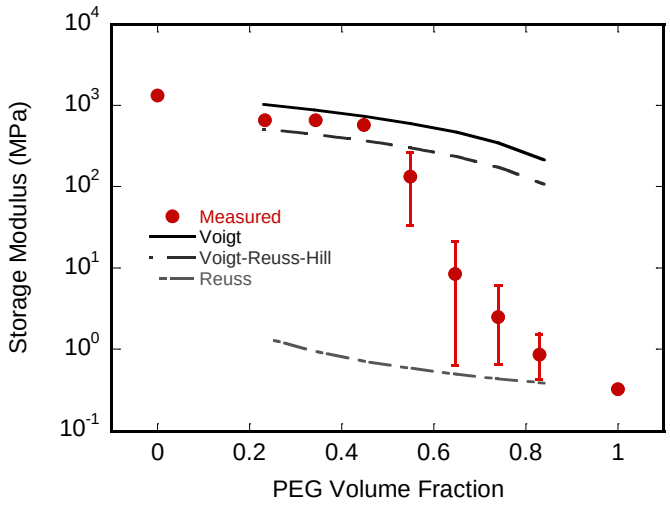

Figure 5.16 Voigt, Reuss and Voigt-Reuss-Hill predictions for PEG-PS volume fraction series at 30 °C. Error bars give the maximum and minimum of three measurements.

Since Voigt and Reuss predictions did not give any insight to the percolation threshold, a similar strategy to ion conductivity (σ) was applied. Equation 2 was modified so that instead of using σ, the storage modulus (E') was used. This equation did not apply to E' as well as σ. However, after several iterations, a good fit was obtained for $\phi_C = 0.325$, as shown in Figure 5.17. Many of the R values for E' are higher than the results for σ. This is likely because fewer E' measurements were made. $\phi_C = 0.325$ was chosen as the percolation threshold because it had a good fit, R = 0.97 and it had a value of P closest to 2. As shown in Table 5.3, $\phi_C = 0.35$ had a higher R value; however, the value for P was much too low. Additional data points near the suspected percolation threshold may improve the outcome of this fit.

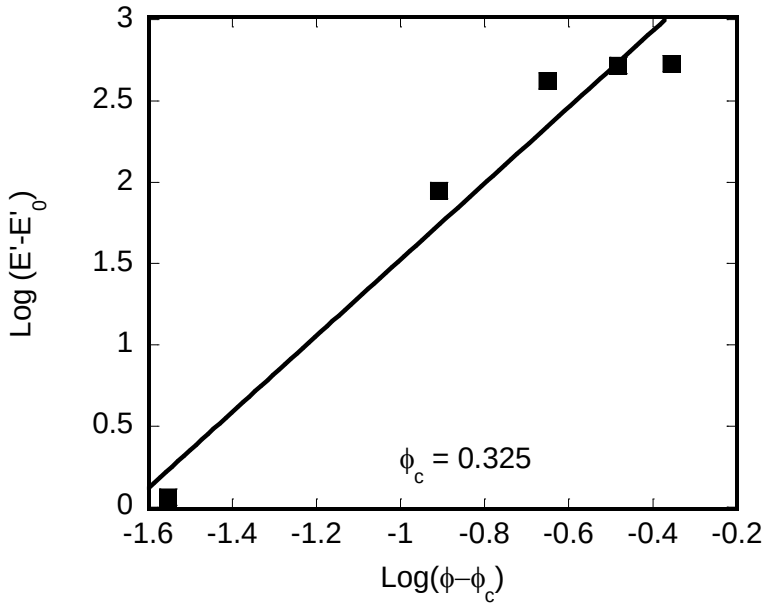

Figure 5.17 Percolation theory fits to storage modulus for a) $\phi_C = 0.255$ and b) $\phi_C = 0.260$ at 70 °C.

Table 5.3 ϕ_C values and their resulting critical exponent and R-value when fit to E' measurements.

ϕ_C	P	R
0.15	2.65±0.69	0.86
0.2	3.91±0.61	0.96
0.25	2.05±0.45	0.91
0.255	1.62±0.41	0.89
0.2583	3.72	0.94
0.26	3.69±0.77	0.94
0.265	3.60±0.74	0.94
0.275	3.42±0.67	0.94
0.3	2.93±0.50	0.96
0.325	2.34±0.30	0.97
0.35	1.30±0.08	0.99

Unfortunately, setting P = 2 and fitting the E' data did not turn out as well as the conductivity data. The value of ϕ_C is 0.105±0.006, which is much lower than the log-log fitting predicts. As seen in Figure 5.18, the fit is quite poor, with R = 0.68. Data points were weighted by 10% of their value and data points above $\phi_{PS} = 0.6$ were omitted.

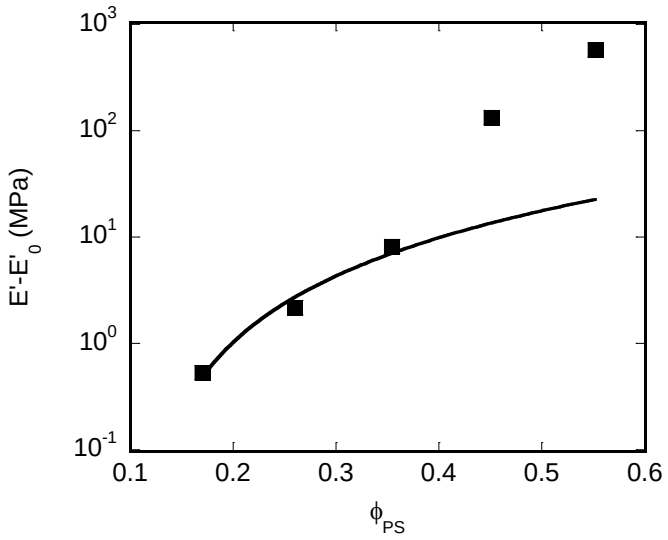

Figure 5.18 Percolation theory fitting with P =2.

5.5 The Bicontinuous Window

Examining both measurements provides an estimate of what volume fractions the system is bicontinuous. The region of high ion conductivity has been shaded in blue, see Figure 5.19, to highlight the volume fraction window for PEG percolation. Similarly, the area shaded in green highlights the volume fraction over which PS is continuous as evidenced by the high storage modulus. Samples between the bounds found using percolation theory ϕ_{PEG} = 0.225 to 0.675 show PEG-like ion conductivies and PS-like storage moduli. They are shaded in yellow to show the overlap of the PEG percolation and PS percolation. While this is an indirect measurement of the morphology, these results are an encouraging glimpse of the possible range of volume fractions that could be bicontinuous. Further property and morphology studies are underway to offer a more well-defined measure of this bicontinuous window.

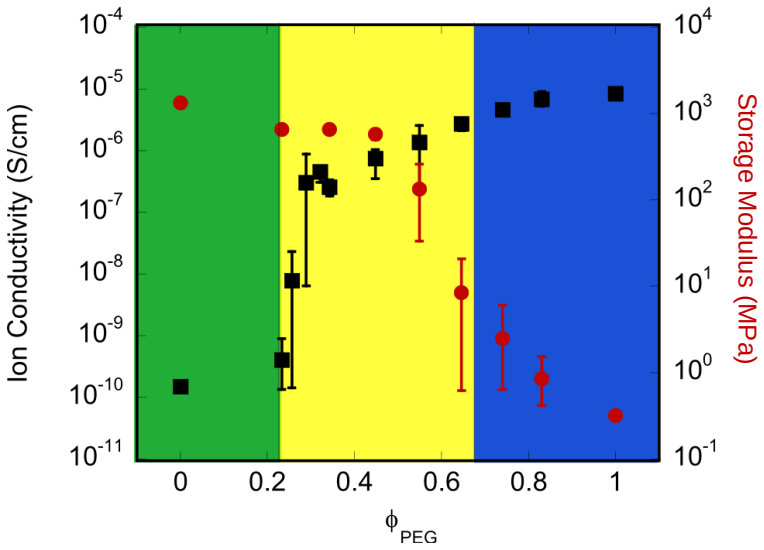

Figure 5.19 Ion conductivity and storage modulus versus PEG volume fraction series using 12 kg/mol precursor polymers at 30°C. Green regions highlight where only PS is continuous, blue regions depict where only PEG is continuous and yellow regions depict where both phases are continuous. Boundaries between the phases were chosen using percolation theory fits to log-log plots for both sets of data. The bicontinuous window is $0.225 < \phi_{PEG} < 0.675$.

5.6 Conclusions

A series of co-networks with a wide range of compositions was synthesized using a versatile Mitsunobu/thiol-ene platform. Across this series, the samples showed similar *d*-spacing and SAXS patterns. However, for the extremely asymmetric compositions ($\phi_{PEG} < 0.225$ or > 0.675) the morphology is quite different from the symmetric or moderately asymmetric compositions. This was determined using ion conductivity and storage modulus measurements as probes for PEG and PS percolation, respectively. From initial evaluation, it is obvious that there is a wide range of compositions that yield materials with PEG-like ion conductivity and PS-like storage moduli. Appling percolation theory to this data, demonstrates that the critical percolation threshold for PEG is 0.225 and 0.325 for PS. This gives a bicontinuous phase compositional window from $\phi_{PEG} = 0.225$ to 0.675. A system with this breadth had not previously been demonstrated in dry, solid materials.

Combining the results from the M_C series in Chapter 4 with the ϕ series gives a phase diagram for this system, shown in Figure 5.20. N is the average number of repeat units in the PEG and PS precursor polymers used for that network and χ is assumed to be 0.2.[157] Nearly all of the networks investigated in the previous two chapters are bicontinuous based on their properties fit with percolation theory. These preliminary results suggest that bicontinuous morphology is accessible over a wide variety of compositions and length scales.

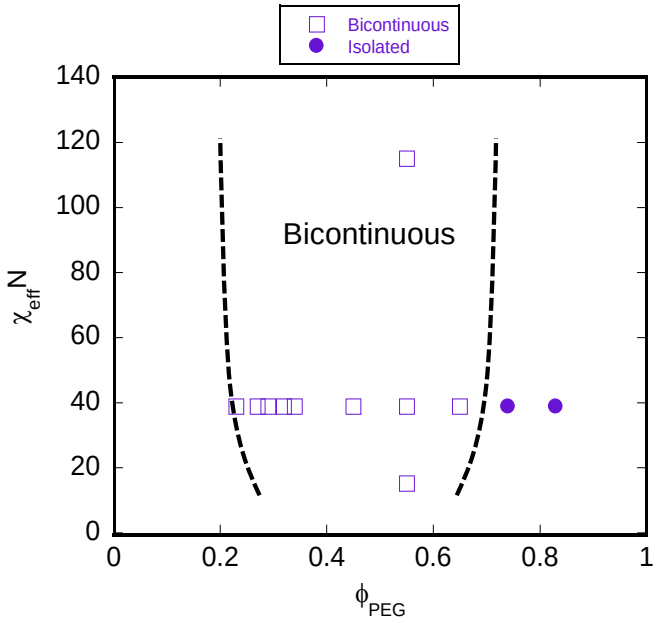

Figure 5.20 Phase diagram for salt-loaded PEG-PS co-networks. Open squares represent bicontinuous structures while filled circles represent isolated structures. Dashed lines represent possible boundaries for the bicontinuous phase.

CHAPTER 6

MULTIBLOCK COPOLYMERS

6.1 Introduction

Multiblock copolymers (MBCs) offer similar advantages to co-networks in that the ends of the blocks are somewhat restrained. This increased connectivity offers improved mechanical properties and unique morphologies compared to traditional diblock copolymers.[122] Disordered bicontinuous phases from multiblock copolymers have demonstrated improved mechanical properties including higher stress and strain at break compared to analogous triblock copolymers.[53,56] This is due to one multiblock copolymer chain spanning several microdomains.[132] Unlike co-network materials which are thermosets, MBCs are thermoplastics.[55,132] This would allow for easier thermal processing of the final material. Here, the thermal properties and morphology of MBCs synthesized by the end-linking method described in Chapter 2, are presented.

6.2 Thermal Properties

Thermal gravimetric analysis of **R2** and **A2** demonstrated thermal stability at temperatures up to 340 °C, similar to reported values of both PS[164] and PEO[165] macromonomers (Figure 6.1). This would allow for thermal annealing experiments in the future. Comparatively, **R3** shows decreased thermal stability. This is likely due to the PDMS domain which decomposes at 250 °C to give the cyclic D_3 monomer.[166]

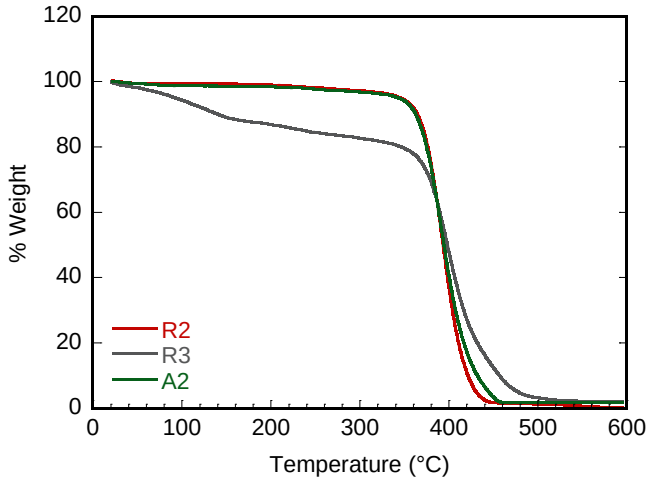

Figure 6.1 TGA of multiblock copolymers. **R2** and **A2.**

Analysis by DSC of **R2** and **R3** yielded two and three different T_g values, respectively, one for each block chemistries, as shown in

Figure 6.2, Column 2. In **R2** the PEG T_g is -54 °C and the PS T_g is 73 °C. **R3** shows T_gs at -141 °C for PDMS, -54 °C for PEG and 86 °C for PS. This demonstrates these MBCs are phase separated.[167] If the blocks were significantly mixed, one intermediate T_g between the T_g values of the macromonomers would have been observed. The absence of such an intermediate T_g indicates that microphase separation is present within these samples. Additionally, prominent endotherms were observed corresponding to the crystalline domain of PEO melting are shown in Figure 6.2, Column 1. These peaks gave 31 % crystalline PEG phase for **R2** and 23 % crystalline PEG phase in **R3** compared to the heat of fusion for theoretically 100 % crystalline PEG.[168] While **A2** behaved similarly to the random MBCs in that it maintained two T_g values, the T_g of the PS was lowered 20-30 °C further than that of the other two MBCs. Moreover, PEO crystallinity was strongly disturbed, with an endotherm of 3.41 J/g, corresponding to only 2 % crystallinity in the **A2** sample. Additionally the T_m was lowered to 26 °C. These combined factors suggest that while microphase separation was still present, more mixing occurred in **A2**

than in **R2**. The random MBC architecture would allow for multiple PEG macromonomers to be chained together, potentially increasing the PEG domain size, and consequently the degree of crystallinity and phase separation. The dithiol PEG macromonomer is slightly smaller than the dinorbornene PEG macromonomer. This would decrease χN, causing a greater degree of mixing in this sample.

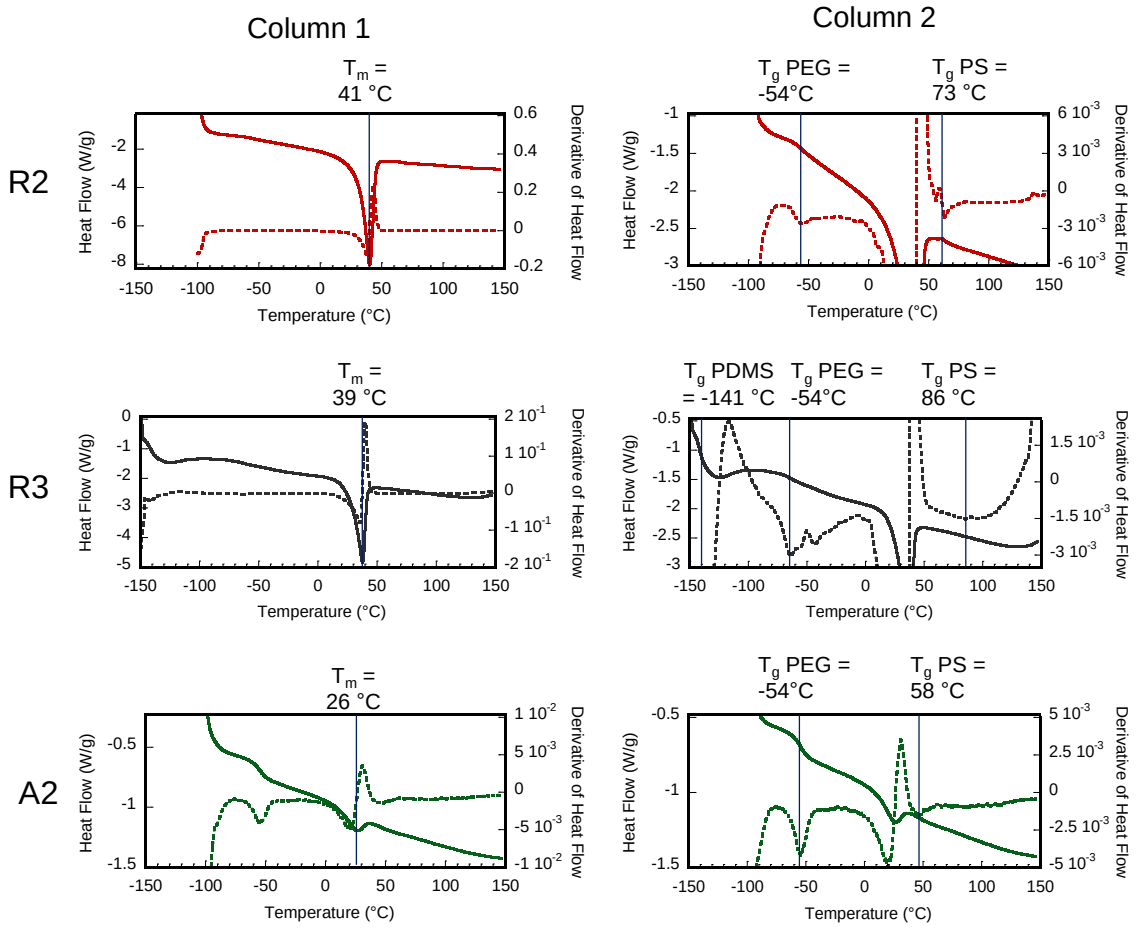

Figure 6.2 DSC traces for each of the multiblock copolymers. Heat flow is given by solid lines while the derivative of heat flow is given by dashed lines. Column 1 shows the temperature full scale and the PEG melting temperature (T_m) is marked with a vertical line. Column 2 expands the Y-axis for clarity, and marks and T_g values with a vertical line.

6.3 Morphology

Further corroborating microphase separation, a broad peak was observed in the SAXS pattern of **R2** with a q value corresponding to a domain spacing of 24 nm which was calculated from $d = 2\pi/q^*$ (Figure 6.3) . The breadth of the peak and lack of higher order reflections support the presence of disordered microphase separation in this MBC.[37] Due to the large χ parameter (~0.1) for PS/PEO, weak to moderate segregation ($\chi N = 10.5$), was still easily achieved at the molecular weights reported here.[13,156]

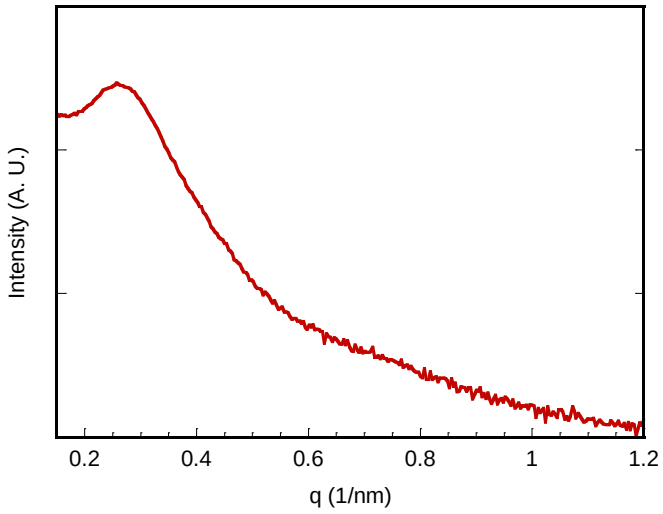

Figure 6.3 Small angle x-ray scattering from multiblock **R2**.

Disordered phase separation is also observed in phase AFM images of **A2** (Figure 6.4). Sample preparation, annealing times and temperatures had strong effects on the observed domain sizes, as expected.[167,169] After annealing for one day at 150 °C, domain sizes of 20-25 nm were observed, in contrast to the sample annealed for three days at 130 °C, which formed larger domains (>70 nm). The 130 °C annealing temperature was chosen because that temperature was more than 50 °C above the highest measured T_g. The longer annealing time was likely the main contributing factor to the increase in domain size,[167,169] as it gave the multiblocks more time to

rearrange and form longer range, potentially "lamellar-like" sheets.[38] From a top-down view, these sheets, if lying flat, could look much larger than the maximum domain size dictated by the end-to-end distance of the individual blocks.

The disordered morphology observed by the SAXS and AFM has been observed previously and is expected because reorganization of MBCs is more difficult than traditional di- or triblock copolymers. Theory predicts MBCs face higher kinetic and thermodynamic barriers to reorganization than their shorter analogues because MBCs bridge several domains.[52,53,170] This barrier increases with the number of blocks in the MBC.[55] These preliminary studies have not included optimization of annealing conditions. However, given the thermal stability, these studies and future applications requiring thermal processing would be feasible.

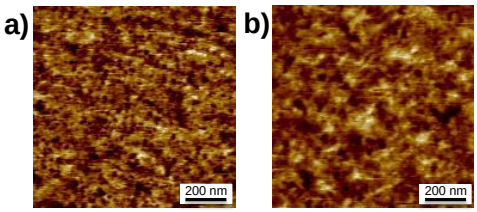

Figure 6.4 AFM phase images of **A2** annealed for a) one day at 150 °C and b) three days at 130 °C.

6.4 Conclusions

Multiblock copolymers represent a rich and underdeveloped field that has, in the past, been difficult to study. The synthesis described in Chapter 2 offers a simple, effective route to these fascinating materials. These MBCs were shown to microphase separate in a disordered manner and demonstrated high thermal stability. Encouraging preliminary conclusions show disordered phase separation, consistent with the bicontinuous phases shown in the co-network materials. However, more detailed studies are necessary to investigate the relationship between the composition of the multiblocks, phase separation behavior, and mechanical properties.

CHAPTER 7

PERSPECTIVE AND FUTURE DIRECTIONS

This thesis addresses two interesting and important problems, ion conductivity in solid, polymer electrolytes and bicontinuous morphology. In the area of ion conductivity, majority of research has been done on PEG-based materials, as used in this thesis. This represents a significant constraint to this field in that the ion conductivity, tied to the motion of the PEG backbone, is limited to the inherent flexibility of PEG. In order to surpass this limit, new chemistries should be explored. One interesting area is single ion conductors. In these materials, the anion is anchored to the polymer chain so any conductivity is due only to the movement of cations. These materials have a high transference number, or the amount of proportion of charge transport due to the lithium ions is near unity. This gives these materials the advantage of being more efficient, they may be able to achieve the same cation transport with lower overall ion conductivity.[171] While it was not investigated, it is likely that the transference number of the materials presented in this thesis is noticeably lower than one.

Another option to improve ion conductivity using chemistry is to incorporate thioethers into the conducting material. Because sulfur is larger, it will bind less tightly to the lithium ion, making these ionic bonds more labile, which will result in faster ion motion. Thiol-ene chemistry can be used to make polymers with thio-ether functionality. Using vinyl-ethers as the ene group allows regular oxygen ethers to be incorporated into the polymer as well. Some oxygen ether functionality could be beneficial so that the polymer bonds tightly enough to dissociate the lithium from its counter ion. Tuning the density and ratio of ethers and thio-ethers, allows the effect of cation coordination on ion conductivity to be studied. Further, multifunctional monomers can be used to cross-link these materials, creating an opportunity to study their mechanical properties.

Exploring other functionalities besides ether could be beneficial. For liquid electrolytes, ethylene carbonate is often used as the solvent, because its cyclic structure increases its polarity, and thus its ability to dissociate the lithium ions from their counter ions. Ethylene carbonate side groups have been attached to a poly(methyl methacrylate) backbone; however, this polymer did not demonstrate high ion conductivity after loading with a lithium salt.[172] This is probably due to the rigidity of the PMMA backbone. The backbone's high T_g leaves the side chains almost solely responsible for ion transport. Taking the same functionality and attaching it to a more flexible backbone such as poly(butadiene) or PDMS could improve the outcome of this strategy.

Other efforts use creative chemistry to attach PEG side-chains to flexible backbones such as PDMS. This choice is motivated by the low glass transition temperature (T_g) of these materials. These materials have improved ion conductivity; however, they are very soft.[78] This agrees with the findings here, that the PEG-PDMS materials are more conductive than the PEG-PS networks and the inverse relation between Tg and ion conductivity. However, it is this type of strategy for improving ion conductivity leads the often discussed trade-off between ion conductivity and mechanical properties.

As previously discussed, phase separation is a promising strategy for decoupling ion conductivity and mechanical properties. In particular bicontinuous morphologies offer extra advantages of isotropic properties through percolated pathways. The co-network strategy presented here shows the great promise of generating bicontinuous morphology over a wide compositional range. Further questions that could be explored using this system are: how do different combinations of molecular weights or polydisperse precursor polymers affect this phase separation? This strategy increased the compositional phase window for triblock copolymers,[16] perhaps it would be beneficial in co-network systems as well. How does the behavior of χ differ between block copolymers and co-networks? It was suggested by deGennes,[39] then Brieber and Bauer[40] that a co-network would require a higher value of χN to phase separate than a block

copolymer material with the same composition. The system presented here has high thermal stability and with sufficient heating, the scattering peak can be eliminated. These features could be used to study the mixed vs. separated transition temperatures at a variety of polymer compositions or salt loading. This could lead to an understanding of what values of χN (or χ_{eff}) are needed to induce phase separation and how the value of χN affects the connectivity of the domains.

Expanding beyond the PEG-PS system, what effect does the choice of probe have on the support for bicontinuous structures. Ion conductivity and storage modulus require very different types of domains. Perhaps in a system in which each phase transports a different gas, for example, it would be easier to compare the continuity of the two phases. Of course the increasing accessibility of three-dimensional imaging techniques such as tomography will simplify the direct study of these complex polymer morphologies.

CHAPTER 8

MATERIALS AND METHODS

8.1 Reagents

Three molecular weights of dihydroxyl-terminated poly(ethylene glycol) (PEG) [(Mn = 4.6 kDa, Đ = 1.03), (12) (35)], three molecular weights of dihydroxyl-terminated polystyrene (PS) (Mn = 4.8 kDa, Đ = 1.14) (12) (37)], dihydroxyl-terminated polydimethylsiloxane (PDMS) (M_n = 4.5 kDa, PDI = 1.72), dihydroxyl-terminated polybutadiene (PB) (M_n = 3.3 kDa, PDI = 1.10) 5-norbornene-2-carboxylic acid (99% *exo*), triphenyl phosphine (PPh_3), diisopropyl azodicarboxylate (DIAD), pentaerythritol tetrakis(3-mercaptopropionate) (4SH), 2-hydroxy-4'-(2-hydroxyethoxy)-2-methylpropiophenone (PI), lithium bis(trifluoromethanesulfonyl imide) (LiTFSI), tetrahydrofuran (THF), dichloromethane (DCM), and methanol (MeOH) were purchased from Alfa Aesar, Sigma Aldrich, Acros Organics or Gelest and used without further purification.

8.2 Instrumentation

1H NMR spectra were recorded at 300 MHz, using a Bruker DPX-300 NMR spectrometer. Chemical shifts (δ) are reported in ppm and coupling constants (J) in Hz.

Gel permeation chromatography (GPC) was performed using Agilent 1260 series system with a PL gel 5 μm guard column, two 5 μm analytical Mixed C columns and a 5 μm analytical Mixed D column (Agilent), incubated to 40 °C. THF was used as the eluent at a flow rate of 1.0 mL/min. Polystyrene standards were used for the calibration and toluene was used for the flow marker.

Impedance measurements were performed using a Solatron 1260 impedance/gain phase analyzer in a Cascade TEK TVO-2 vacuum oven.

Thermogravimetric analysis (TGA) measurements were taken using a TA Instruments TGA Q500 with a heating rate of 10 °C/min up to 600 °C under nitrogen.

Differential Scanning Calorimetry (DSC) measurements were taken using a TA Instruments DSC Q200. Samples were analyzed using a heating rate of 10 °C/min from -100 °C to 100 °C under a flow of nitrogen (50 mL/min).

Mechanical properties were tested using dynamic mechanical analysis (DMA) with a TA Instruments DMA Q800. For PEG and PEG-PDMS networks, a pre-load force of 8.0 mN was applied. Samples were stretched to 0.8 % strain at a constant frequency of 1 Hz. Measurements were taken from 30 °C to 90 °C with a heating rate of 2° C/min. For PEG-PS networks, pre-load force of 1.0 mN was applied. Samples were stretched to 0.1 % strain at a constant frequency of 1 Hz. Measurements were taken from -80 °C to 130 °C with a heating rate of 3° C/min.

SAXS patters were obtained from and Cosmic MaxFlux Cu Kα X-ray source with a wavelength of 1.54 Angstroms and a two-dimensional gas-filled wire array detector (both Molecular Metrology, Inc.) at a distance of 1.476 m from the sample. The raw data were calibrated against the peak position of a silver behenate standard which has a scattering vector of q = 1.076 1/nm. Two-dimensional images were reduced to the one-dimensional form using angular integration. Domain spacings were calculated from the principal scattering maxima (q*) were calculated using $d = 2\pi/q^*$.

TEM analysis was conducted on a JOEL 100CX TEM operating at an accelerating voltage of 100 kV.

8.3 Precursor Synthesis

The Mitsunobu chemistry used to functionalize alcohol terminated polymers with norbornene has been previously reported for PEG and PDMS.[105]

8.3.1 PEG Precursors

To prepare the 4.6 kg/mol PEG precursor, 4.0 g (0.833 mmol) α,ω-dihydroxy terminated PEG, 0.345 g (2.5 mmol) NB and 0.656 g (2.5 mmol) PPh_3 were dissolved in 35 mL DCM which had been dried over calcium hydride, and equilibrated in an ice bath and purged with N_2. 0.506 g (2.5 mmol) DIAD was dissolved in 5 mL dry DCM and equilibrated in an ice bath and purged with N_2. The DIAD solution was added drop-wise to the stirring polymer solution under N_2 flow. The N_2 line was removed and the solution was allowed to slowly warm to room temperature as it was stirred overnight. The product was precipitated three times into diethyl ether three times and collected by filtration at 87% yield and 94% conversion. To functionalize the 12 kDa and 35 kDa PEG precursor polymers, a greater excess of norbornene acid and coupling reageants were used, 5 mole eq. and 30 mole eq. respectively.

8.3.2 PDMS Precursors

To prepare the 4.5 kg/mol poly(dimethyl siloxane) precursor, 4.0 g (0.833 mmol) α,ω-dihydroxy terminated PDMS, 0.345 g (2.5 mmol) NB and 0.656 g (2.5 mmol) PPh_3 were dissolved in 35 mL THF which had been dried over calcium hydride, distilled from sodium and benzophenone, and equilibrated in an ice bath and purged with N_2. 0.506 g (2.5 mmol) DIAD was dissolved in 5 mL dry THF and equilibrated in an ice bath and purged with N_2. The DIAD solution was added drop-wise to the stirring polymer solution under N_2 flow. The N_2 line was

removed and the solution was allowed to slowly warm to room temperature as it was stirred overnight. The product was precipitated three times into MeOH and collected by filtration at 80% yield and 98% conversion.

8.3.3 PS Precursors

To prepare the polystyrene 4.8 kg/mol precursor, 4.0 g (0.833 mmol) α,ω-dihydroxy terminated PS, 0.345 g (2.5 mmol) NB and 0.656 g (2.5 mmol) PPh3 were dissolved in 35 mL THF which had been dried over sodium calcium hydride, distilled from sodium and benzophenone, and equilibrated in an ice bath and purged with N_2. 0.506 g (2.5 mmol) DIAD was dissolved in 5 mL dry THF and equilibrated in an ice bath and purged with N_2. The DIAD solution was added drop-wise to the stirring polymer solution under N_2 flow. The N_2 line was removed and the solution was allowed to slowly warm to room temperature as it was stirred overnight. The product was precipitated three times into MeOH and collected by filtration at 87% yield. To functionalize the 12 kDa and 35 kDa precursor polymers, a greater excess of norbornene acid and coupling reageants were used, 5 mole eq. and 30 mole eq. respectively.

8.3.4 Polybutadiene Precursors

To end-functionalize PB with norbornene, 2.0 g (0.666 mmol) of α,ω-dihydroxy terminated PB was dissolved in dry THF. 0.276 g norbornene acid (2.00 mmol) and 0.525 g PPh_3 (2.00 mmol) were dissolved in dry THF and added to the PB solution. A solution of DIAD was prepared using 0.404 g (2.00 mmol) in dry THF. Both solutions were equilibrated for several minutes in and ice bath and purged with N_2. The DIAD solution was added drop-wise and the yellow color persisted for several minutes. The solutions were prepared so that the final concentration of the reaction was 100 mg/mL of PB. The reaction was allowed to stir and

gradually warm to room temperature overnight. The PB was precipitated three times in methanol. The liquid product was collected at 85 % yield.

8.3.5 Perfluoropolyether Functionalization

To end-functionalize perfluoropolyether (PFPE) 1.0 g PFPE (0.244 mmol) was dissolved in 1,1,2-trichloro-1,2,2-trifluoroethane (TCTFE). 3 molar equivalents of norbornene acid and PPh_3 were added to this solution. A solution of DIAD was prepared in 2.0 mL of TCTFE. This solution and the PFPE solution were cooled in an ice bath and purged with N_2. The DIAD solution was added drop-wise using a syringe. The N_2 line was removed and reaction was allowed to gradually warm to room temperature while stirring overnight.

8.4 Network Synthesis

8.4.1 Typical PEG Network Synthesis

400 mg *nor-PEG-nor* (32.5 μmol), 7.9 mg 4-SH (16.25 μmol) and 4 mg PI were dissolved in 4.0 ml of THF to give an equimolar ratio between the norbornene end groups and the thiol functional groups. The initial concentration of polymer in all curing solutions was 100 mg/mL. The amount of PI used was 0.5 weight % of the polymer precursor. The PEG chains were dissolved after heating with a heat gun for several seconds. After all the components were thoroughly mixed, 1 mL of curing solution was loaded into a syringe mold of the desired size and cured under ultra-violet (UV) light (λ = 365nm) for 45 minutes. The resulting gels were washed in THF overnight to remove any remaining soluble material. The samples were then dried under nitrogen flow overnight, then further in a vacuum chamber for several hours. Once dry, they were weighed to determine their dry mass without salt. Alternatively, these networks were also

synthesized in DMF with the LiTFSI salt dissolved in the curing solution at a ratio of 10 moles of PEG monomers to 1 mole of LiTFSI. These networks were dried first under nitrogen flow then in a vacuum oven.

8.4.2 Typical PEG-PDMS Network Preparation

294 mg *nor-PEG-nor* (23.8 μmol), 106 mg *nor-PDMS-nor* (23.5 μmol), 11.5 mg 4-SH (23.5 μmol) and 4 mg PI were dissolved in 4.0 mL THF to give an equimolar ratio between the norborene end groups and the thiol functional groups. The PEG-PDMS networks were cured and dried in the same manner as the PEG networks.

8.4.3 Typical PEG-PS Network Preparation

200 mg of each precursor polymer, 4SH to give a 1:1.2 mole ratio of double bonds to thiol groups, 4 mg PI and an amount of LiTIFSI to give EO:Li = 10 were dissolved in 2.86 ml of 90%DMF/10%THF. This gave an initial concentration of polymer in all curing solutions of 140 mg/mL. The amount of PI used was 1 weight % of the polymer precursor. The polymers were dissolved after heating with a heat gun for several seconds. After all the components were thoroughly mixed, the solution was loaded into a teflon mold of the desired size and cured under ultra-violet (UV) light (λ = 365nm), in a nitrogen filled bag for 1 hour. The resulting gels dried under nitrogen flow over two days, then further in a vacuum chamber overnight.

8.5 Double Bond Reactivity

To test the reactivity of the various double bonds in the norbornene end-functionalized PB a series of thiol-ene reactions were prepared such that the ratio of a small-molecule thiol to the moles of polymers varied from 1:1 to 168:1. All vials were loaded with 0.1 g of PB, the

prescribed amount of propane thiol and 1 %wt compared to PB of photo-initiator. THF was added until the final concentration of the reaction was 100 mg/mL of PB. The solutions were exposed to UV-light for 40 minutes. PB was collected by precipitation into methanol.

To compare the cross-linking of PB with and without norbornene groups 0.10 g each norbornene terminated PB and hydroxyl terminated PB were dissolved in THF with 1 %wt photoinitiator and 0.5 mol eq of tetra thiol. Additional reactions of hydroxyl terminated PB with 1.16, and 20 mol eq were also tested. All gels were cured under UV light 45 mins, then washed in THF to remove the sol fraction.

8.6 Multiblock Synthesis

As a general procedure, roughly 150 mg total of the two or three macromonomers, and dithiol linker for the random architecture, in stoichiometric ratios, and 2 wt% PI, Irgacure 2959, were dissolved in THF at a concentration total polymer concentration of 100 mg/mL. The solution was degassed and stirred overnight under 365 nm UV exposure. The newly formed multiblock copolymer was then precipitated into diethyl ether, filtered and dried overnight under vacuum at 80 °C. Samples for ^{1}H NMR and GPC were prepared in d-chloroform and THF, respectively. Thin films for AFM were prepared by spin coating a solution of 12 mg/mL multiblock copolymer in toluene at 2500 r.p.m. for one minute, followed by thermal annealing at 130 °C for 72 hours.

8.7 Sample Preparation

For electrochemical impedance spectroscopy, a small disk (1/8” diameter) was cut from the polymer network sample. This disk was then sliced to approximately 0.3 – 0.5 mm in thickness. Aluminum mounts were sputter coated with gold using a Cressington 108 Sputter

Coater. Spacers were cut from Teflon® tape and a 1/8" hole was punched in the center to create a place for the network sample. The spacer and sample were then sandwiched between two gold-coated electrodes. The electrode assemblies were loaded into a custom system that multiplexes the impedance analyzer to one of eight temperature-calibrated positions within a Cascade TEK TVO-2 vacuum oven. Samples were heated under vacuum and held at approximately 120 °C for several hours in order to remove any residual solvent or moisture, then allowed to cool to ambient temperature. Impedance spectra in the frequency range of 10 MHz to 0.1 Hz were recorded for each sample at repeated time intervals of approximately 30 minutes during the whole temperature schedule. The bulk resistance to ion conduction, R, was extracted by fitting a constant function to the first plateau of the impedance magnitude occurring at high frequencies; then conductivity was computed from the known sample area, A = 0.074 cm^2, and thickness of the spacer tape, d = 0.03 cm, as $\sigma = d/(A*R)$. Arrhenius plots in text were constructed using the ionic conductivities from the cooling portion of this experiment.

For thermal gravemmetric analysis a small piece (approximately 5 mg) of salt-loaded network was placed in a tared platinum pan.

For differential scanning calorimetry approximately 5 mg of salt-loaded network and control network (no salt added) were sealed in an aluminum hermetic pan. An empty pan was used as the reference.

For dynamic mechanical analysis, a rectangular piece was cut from the film with the approximate dimensions of 2 mm x 25 mm x 1 mm.

For small angle X-ray scattering, approximately 1mm thick samples were mounted in the sample chamber using kapton tape.

For transmission electron microscopy, a samples were embedded in epoxy, then cut with a diamond knife using a Leica Ultracut microtome, then stained with RuO_4 vapor.

BIBLIOGRAPHY

(1) Register, R. A.: Materials Science: Continuity through Dipsersity. *Nature (London, U. K.)* **2012**, *483*, 167-168.

(2) Matsen, M. W.; Bates, F. S.: Origins of Complex Self-Assembly in Block Copolymers. *Macromolecules* **1996**, *29*, 7641-7644.

(3) Cochran, E. W.; Garcia-Cervera, C. J.; Fredrickson, G. H.: Stability of the Gyroid Phase in Diblock Copolymers at Strong Segregation. *Macromolecules* **2006**, *39*, 2449-2451.

(4) Wanakule, N. S.; Panday, A.; Mullin, S. A.; Gann, E.; Hexemer, A.; Balsara, N. P.: Ionic Conductivity of Block Copolymer Electrolytes in the Vicinity of Order−Disorder and Order−Order Transitions. *Macromolecules* **2009**, *42*, 5642-5651.

(5) Meyer, W. H.: Polymer Electrolytes for Li Ion Batteries *Adv. Mater.* **1998**, *10*, 439-448.

(6) Hickner, M.: Ion-Containing Polymers: New Enery and Clean Water. *Materials Today* **2010**, *13*, 35-41.

(7) Thompson, B. C.; Fréchet, J. M. J.: Polymer–Fullerene Composite Solar Cells. *Angew. Chem., Int. Ed. Engl.* **2008**, *47*, 58-77.

(8) Dair, B. J.; Honeker, C.; Alward, D. B.; Avgeropoulos, A.; Hadjichristidis, N.; Fetters, L. J.; Capel, M.; Thomas, E. L.: Mechanical Properties and Deformation Behavior of the Double Gyroid Phase in Unoriented Thermoplastic Elastomers. *Macromolecules* **1999**, *32*, 8145-8152.

(9) Dair, B. J.; Avgeropoulos, A.; Hadjichristidis, N.; Thomas, E. L.: Mechanical Properties of the Double Gyroid Phase in Oriented Thermpolastic Elastomers. *J. Mater. Sci.* **2000**, *35*, 5207-5213.

(10) Matsen, M. W.: The Standard Gaussian Model for Block Copolymer Melts. *J. Phys.; Condens. Matter* **2002**, *14*, R21.

(11) Bates, F. S.; Fredrickson, G. H.: Block Copolymer Thermodynamics: Theory and Experiment. *Annu. Rev. Phys. Chem.* **1990**, *41*, 525.

(12) Bates, F. S.; Fredrickson, G. H.: Block Copolymers—Designer Soft Materials. *Physics Today* **1999**, *52*, 32.

(13) Bates, F. S.; Fredrickson, G. H.: Block Copolymer Thermodynamics: Theory and Experiment. *Annu. Rev. Phys. Chem.* **1990**, *41*, 525-557.

(14) Brown, J. R.; Sides, S. W.; Hall, L. M.: Phase Behavior of Tapered Diblock Copolymers from Self-Consistent Field Theory. *ACS Macro Lett.* **2013**, *2*, 1105-1109.

(15) Widin, J. M.; Schmitt, A. K.; Schmitt, A. L.; Im, K.; Mahanthappa, M. K.: Unexpected Consequences of Block Polydispersity on the Self-Assembly of Aba Triblock Copolymers. *J Am Chem Soc* **2012**, *134*, 3834-3844.

(16) Widin, J. M.; Schmitt, A. K.; Im, K.; Schmitt, A. L.; Mahanthappa, M. K.: Polydispersity-Induced Stabilization of a Disordered Bicontinuous Morphology in Aba Triblock Copolymers. *Macromolecules* **2010**, *43*, 7913-7915.

(17) Schmitt, A. L.; Mahanthappa, M. K.: Polydispersity-Driven Shift in the Lamellar Mesophase Composition Window of Peo-Pb-Peo Triblock Copolymers. *Soft Matter* **2012**, *8*, 2294.

(18) Schmitt, A. K.; Mahanthappa, M. K.: Characteristics of Lamellar Mesophases in Strongly Segregated Broad Dispersity Aba Triblock Copolymers. *Macromolecules* **2014**, 10.1021/ma5006233.

(19) Jiang, G.; Wu, H.; Guo, S.: Reinforcement of Adhesion and Development of Morphology at Polymer-Polymer Interface Via Reactive Compatibilization: A Review. *Polymer Engineering & Science* **2010**, *50*, 2273-2286.

(20) Pernot, H.; Baumert, M.; Court, F.; Leibler, L.: Design and Properties of Co-Continuous Nanostructured Polymers by Reactive Blending. *Nat Mater* **2002**, *1*, 54-58.

(21) Hodrokoukes, P.; Floudas, G.; Pispas, S.; Hadjichristidis, N.: Microphase Separation in Normal and Inverse Tapered Block Copolymers of Polystyrene and Polyisoprene. 1. Phase State. *Macromolecules* **2001**, *34*, 650-657.

(22) Laurer, J. H.; Smith, S. D.; Samseth, J.; Mortensen, K.; Spontak, R. J.: Interfacial Modification as a Route to Novel Bilayered Morphologies in Binary Block Copolymer/Homopolymer Blends. *Macromolecules* **1998**, *31*, 4975-4985.

(23) Löwen, H.: Solvent-Induced Phase Separation in Colloidal Fluids. *Physical Review Letters* **1995**, *74*, 1028-1031.

(24) Li, L.; Shen, X.; Hong, S. W.; Hayward, R. C.; Russell, T. P.: Fabrication of Co-Continuous Nanostructured and Porous Polymer Membranes: Spinodal Decomposition of Homopolymer and Random Copolymer Blends. *Angew Chem Int Ed Engl* **2012**, *51*, 4089-4094.

(25) Ozaki, T.; Koto, T.; Nguyen, T. V.; Nakanishi, H.; Norisuye, T.; Tran-Cong-Miyata, Q.: The Roles of the Trommsdorff–Norrish Effect in Phase Separation of Binary Polymer Mixtures Induced by Photopolymerization. *Polymer* **2014**, *55*, 1809-1816.

(26) Shukutani, T.; Myojo, T.; Nakanishi, H.; Norisuye, T.; Tran-Cong-Miyata, Q.: Tricontinuous Morphology of Ternary Polymer Blends Driven by Photopolymerization: Reaction and Phase Separation Kinetics. *Macromolecules* **2014**, *47*, 4380-4386.

(27) Hayward, R. C.; Pochan, D. J.: Tailored Assemblies of Block Copolymers in Solution: It Is All About the Process. *Macromolecules* **2010**, *43*, 3577-3584.

(28) Nam, Y. S.; Park, T. G.: Porous Biodegradable Polymeric Scaffolds Prepared by Thermally Induced Phase Separation. *Journal of Biomedical Materials Research* **1999**, *47*, 8-17.

(29) Schulze, M. W.; McIntosh, L. D.; Hillmyer, M. A.; Lodge, T. P.: High-Modulus, High-Conductivity Nanostructured Polymer Electrolyte Membranes Via Polymerization-Induced Phase Separation. *Nano Lett* **2014**, *14*, 122-126.

(30) Price, S. C.; Ren, X.; Jackson, A. C.; Ye, Y.; Elabd, Y. A.; Beyer, F. L.: Bicontinuous Alkaline Fuel Cell Membranes from Strongly Self-Segregating Block Copolymers. *Macromolecules* **2013**, *46*, 7332-7340.

(31) Trinh, X.-A.; Fukuda, J.; Adachi, Y.; Nakanishi, H.; Norisuye, T.; Tran-Cong-Miyata, Q.: Effects of Elastic Deformation on Phase Separation of a Polymer Blend Driven by a Reversible Photo-Cross-Linking Reaction. *Macromolecules* **2007**, *40*, 5566-5574.

(32) Chung, H.-j.; Ohno, K.; Fukuda, T.; Composto, R. J.: Self-Regulated Structures in Nanocomposites by Directed Nanoparticle Assembly. *Nano Lett* **2005**, *5*, 1878-1882.

(33) Seo, M.; Hillmyer, M. A.: Reticulated Nanoporous Polymers by Controlled Polymerization-Induced Microphase Separation. *Science* **2012**, *336*, 1422-1425.

(34) Liu, Y.: Polymerization-Induced Phase Separation and Resulting Thermomechanical Properties of Thermosetting/Reactive Nonlinear Polymer Blends: A Review. *J. Appl. Polym. Sci.* **2013**, *127*, 3279-3292.

(35) Seo, M.; Murphy, C. J.; Hillmyer, M. A.: One-Step Synthesis of Cross-Linked Block Polymer Precursor to a Nanoporous Thermoset. *ACS Macro Lett.* **2013**, *2*, 617-620.

(36) Chintapalli, M.; Chen, X. C.; Thelen, J. L.; Teran, A. A.; Wang, X.; Garetz, B. A.; Balsara, N. P.: Effect of Grain Size on the Ionic Conductivity of a Block Copolymer Electrolyte. *Macromolecules* **2014**, *47*, 5424-5431.

(37) Ivan, B.; Almdal, K.; Mortensen, K.; Johannsen, I.; Kops, J.: Synthesis Characterization and Structural Investigations of Poly(Ethyl Acrylate)-L-Polyisobutylene Bicomponent Conetowork. *Macromolecules* **2001**, *34*, 1579-1585.

(38) Bruns, N.; Scherble, J.; Hartmann, L.; Thomann, R.; Iván, B.; Mülhaupt, R.; Tiller, J. C.: Nanophase Separated Amphiphilic Conetwork Coatings and Membranes. *Macromolecules* **2005**, *38*, 2431-2438.

(39) de Gennes, P. G.: Effect of Cross-Links on a Mixture of Polymers. *Le Journal de Physique - Letters* **1979**, *40*, L-69.

(40) Briber, R. M.; Bauer, J. B.: Effect of Cross-Links on the Phase Separation Behavior of a Miscible Polymer Blend. *Macromolecules* **1988**, *21*, 3296.

(41) Haraszti, M.; Toth, E.; Ivan, B.: Poly(Methacrylic Acid)-L-Polyisobutylene: A Novel Polyelectrolyte Amphiphiclic Conetwork. *Chem. Mater.* **2006**, *18*, 4952-4958.

(42) Fodor, C.; Kali, G.; Iván, B. l.: Poly(N-Vinylimidazole)-L-Poly(Tetrahydrofuran) Amphiphilic Conetworks and Gels: Synthesis, Characterization, Thermal and Swelling Behavior. *Macromolecules* **2011**, *44*, 4496-4502.

(43) Erdodi, G.; Kennedy, J. P.: Amphiphilic Conetworks: Definition, Synthesis, Applications. *Progress in Polymer Science* **2006**, *31*, 1-18.

(44) Hadjiantoniou, N. A.; Patrickios, C. S.; Thomann, Y.; Tiller, J. C.: Amphiphilic Conetworks Based on End-Linked Multiblock Copolymers of Different Numbers of Blocks and Constant Molecular Weight and Composition. *Macromolecular Chemistry and Physics* **2009**, *210*, 942-950.

(45) Kali, G.; Georgiou, T. K.; Ivan, B.; Patrickios, C. S.; Loizou, E.; Thoumann, Y.; Tiller, J. C.: Synthesis and Characterization of Anionic Amphiphilic Model Conetworks of 2-Butyl-1-Octyl-Methacrylate and Methacrylic Acid: Effects of Polymer Composition and Architecture. *Langmuir* **2007**, *23*, 10746-10755.

(46) Rikkou, M. D.; Kolokasi, M.; Matyjaszewski, K.; Patrickios, C. S.: End-Linked Amphiphilic Polymer Conetworks: Synthesis by Sequential Atom Transfer Radical Polymerization and Swelling Characterization. *J. Polym. Sci., Part A: Polym. Chem.* **2010**, *48*, 1878-1886.

(47) Zhou, C.; Qian, S.; Zhang, A.; Xu, L.; Zhu, J.; Cheng, Z.; Kang, E.-T.; Yao, F.; Fu, G. D.: A Well-Defined Amphiphilic Polymer Co-Network from Precise Control of the End-Functional Groups of Linear Raft Polymers. *RSC Advances* **2014**, *4*, 8144.

(48) Li, J.; Liu, T.; Pan, Y.; Xia, S.; Zheng, Z.; Ding, X.; Peng, Y.: A Versatile Polymer Co-Network with Broadened Glass Transition Showing Adjustable Multiple-Shape Memory Effect. *Macromolecular Chemistry and Physics* **2012**, *213*, 2246-2252.

(49) Meskath, S.; Urban, G.; Heinze, J.: A New Optochemical Chlorine Gas Sensor Based on the Application of Amphiphilic Co-Networks as Matrices. *Sensors and Actuators B: Chemical* **2011**, *151*, 327-332.

(50) Mespouille, L.; Coulembier, O.; Paneva, D.; Degée, P.; Rashkov, I.; Dubois, P.: Synthesis of Adaptative and Amphiphilic Polymer Model Conetworks by Versatile Combination of Atrp, Rop, and "Click Chemistry". *J. Polym. Sci., Part A: Polym. Chem.* **2008**, *46*, 4997-5013.

(51) Dech, S.; Wruk, V.; Fik, C. P.; Tiller, J. C.: Amphiphilic Polymer Conetworks Derived from Aqueous Solutions for Biocatalysis in Organic Solvents. *Polymer* **2012**, *53*, 701-707.

(52) Lee, I.; Bates, F. S.: Synthesis, Structure and Properties of Alternating and Random Poly(Styrene-B-Butadiene) Multiblock Copolymers. *Macromolecules* **2013**, *46*, 4529.

(53) Lee, I.; Panthani, T. R.; Bates, F. S.: Sustainable Poly(Lactide-B-Butadiene) Multiblock Copolymers with Enhanced Mechanical Properties. *Macromolecules* **2013**, *46*, 7387-7398.

(54) Krause, S.: Microphase Separation in Block Copolymers. Zeroth Approximation Including Surface Free Energies. *Macromolecules* **1970**, *3*, 84-86.

(55) Wu, L.; Cochran, E. W.; Lodge, T. P.; Bates, F. S.: Consequences of Block Number on the Order−Disorder Transition and Viscoelastic Properties of Linear (Ab)N Multiblock Copolymers. *Macromolecules* **2004**, *37*, 3360-3368.

(56) Lee, I.; Bates, F. S.: Synthesis, Structure, and Properties of Alternating and Random Poly(Styrene-B-Butadiene) Multiblock Copolymers. *Macromolecules* **2013**, *46*, 4529-4539.

(57) Stauffer, D.; Aharony, A.: *Introduction to Percolation Theory*; Taylor and Francis: Philadelphia, 1994.

(58) Pandey, R. B.; Stauffer, D.; Margolina, A.; Zabolitzky, J. G.: Diffusion on Random Systems above, Below, and at Their Percolation Threshold in Two and Three Dimensions. *J Stat Phys* **1984**, *34*, 427-450.

(59) Last, B. J.; Thouless, D. J.: Percolation Theory and Electrical Conductivity. *Physical Review Letters* **1971**, *27*, 1719-1721.

(60) Brigandi, P. J.; Cogen, J. M.; Pearson, R. A.: Electrically Conductive Multiphase Polymer Blend Carbon-Based Composites. *Polymer Engineering & Science* **2014**, *54*, 1-16.

(61) Karpenko-Jereb, L. V.; Berezina, N. P.: Determination of Structural, Selective, Electrokinetic and Percolation Characteristics of Ion-Exchange Membranes from Conductive Data. *Desalination* **2009**, *245*, 587-596.

(62) Hoarfrost, M. L.; Segalman, R. A.: Conductivity Scaling Relationships for Nanostructured Block Copolymer/Ionic Liquid Membranes. *ACS Macro Lett.* **2012**, *1*, 937-943.

(63) Hoyle, C. E.; Lowe, A. B.; Bowman, C. N.: Thiol-Click Chemistry: A Multifaceted Toolbox for Small Molecule and Polymer Synthesis. *Chem. Soc. Rev.* **2010**, *39*, 1355-1387.

(64) Goodenough, J. B.; Kim, Y.: Challenges for Rechargeable Li Batteries†. *Chem. Mater.* **2010**, *22*, 587-603.

(65) Voith, M.: Battery Booster. *Chem. Eng. News* **2010**, *88*, 27-27.

(66) Agrawal, R. C.; Pandey, G. P.: Solid Polymer Electrolytes: Materials Designing and All-Solid-State Battery Applications: An Overview. *J. Phys. D: Appl. Phys.* **2008**, *41*, 223001.

(67) Tarascon, J. M.; Armand, M.: Issues and Challenges Facing Rechargeable Lithium Ion Batteries. *Nature* **2001**, *414*, 359-367.

(68) Quartarone, E.; Mustarelli, P.: Electrolytes for Solid-State Lithium Rechargeable Batteries: Recent Advances and Perspectives. *Chem. Soc. Rev.* **2011**, *40*, 2525.

(69) Gorecki, W.; Jeannin, M.; Belorizky, E.; Armand, M.: Physical Properties of Solid Polymer Electrolyte Peo(Litfisi) Complexes. *J. Phys.: Condens. Matter* **1995**, *7*, 6823-6832.

(70) Singh, M.; Odusanya, O.; Wilmes, G. M.; Eitouni, H. B.; Gomez, E. D.; Patel, A. J.; Chen, V. L.; Park, M. J.; Fragouli, P.; Iatrou, H.; Hadjichristidis, N.; Cookson, D.; Balsara, N. P.: Effect of Molecular Weight on the Mechanical and Electrical Properties of Block Copolymers Electrolytes. *Macromolecules* **2007**, *40*, 4578-4585.

(71) Nakamura, I.; Balsara, N. P.; Wang, Z.-G.: Thermodynamics of Ion-Containing Polymer Blends and Block Copolymers. *Physical Review Letters* **2011**, *107*.

(72) Yuan, R.; Teran, A. A.; Gurevitch, I.; Mullin, S. A.; Wanakule, N. S.; Balsara, N. P.: Ionic Conductivity of Low Molecular Weight Block Copolymer Electrolytes. *Macromolecules* **2013**, *46*, 914-921.

(73) Müller-Plathe, F.; van Gunsteren, W. F.: Computer Simulation of a Polymer Electrolyte: Lithium Iodide in Amorphous Poly(Ethylene Oxide). *J. Chem. Phys.* **1995**, *103*, 4745.

(74) Wright, P. V.: Electrical Conductivity of Ionic Complexes in Peo. *Br. Polym. J.* **1975**, *7*, 319-327.

(75) Hawker, C. J.; Chu, F.; Pomery, P. J.; Hill, D. J. T.: Hyperbranched Poly(Ethylene Glycol)S: A New Class of Ion-Conducting Materials. *Macromolecules* **1996**, *29*, 3831-3838.

(76) Xu, W.; Belieres, J.; Angell, C. A.: Ion Conducctivity and Stabililty of Poly[Oligo(Ethylene Glycol) Oxalate] - Lithium Salt Complexes. *Chem. Mater.* **2001**, *13*, 575-580.

(77) Armand, M.; Gorecki, W.; Andreani: Perfluorosulphonimide Salts as Solute for Polymer Electrolytes. *Int. Symp. Polym. Electrolyets* **1990**, 31-97.

(78) Oh, B.; Vissers, D.; Zhang, Z.; West, R.; Tsukamoto, H.; Amine, K.: New Interpenetrating Network Type Poly(Siloxane-G-Ethylene Oxide) Polymer Electrolyte for Lithium Battery. *J. Power Sources* **2003**, *119-121*, 442-447.

(79) Rossi, N. A. A.; Z., Z.; Schneider, Y.; Morcom, K.; Lyons, L. J.; Wang, Q.; Amine, K.; West, R.: Synthesis and Characterization of Tetra- and Trisiloxane-Containing Oligio(Ethylene Glycol)S - Highly Conducting Electrolytes for Lithium Batteries. *Chem. Mater.* **2006**, *18*, 1289-1295.

(80) Zhang, Z.; Jin, J.; Bautista, F.; Lyons, L.; Shariatzadeh, N.; Sherlock, D.; Amine, K.; West, R.: Ion Conductive Characteristics of Cross-Linked Network Polysiloxane-Based Solid Polymer Electrolytes. *Solid State Ionics* **2004**, *170*, 233-238.

(81) Allcock, H. R.; Austin, P. E.; Neenan, T. X.; Sisko, J. T.; Blonsky, P. M.; Shriver, D. F.: Polyphosphazenes with Etheric Side Groups. *Macromolecules* **1986**, *19*, 1508-1512.

(82) Liu, S.; Wang, H.; Imanishi, N.; Zhang, T.; Hirano, A.; Takeda, Y.; Yamamoto, O.; Yang, J.: Effect of Co-Doping Nano-Silica Filler and N-Methyl-N-Propylpiperidinium Bis(Trifluoromethanesulfonyl)Imide into Polymer Electrolyte on Li Dendrite Formation in Li/Poly(Ethylene Oxide)-Li(Cf3so2)2n/Li. *J. Power Sources* **2011**, *196*, 7681-7686.

(83) Christensen, J.; Newman, J.: Stress Generation and Fracture in Lithium Insertion Materials. *Journal of Solid State Electrochemistry* **2006**, *10*, 293-319.

(84) Armand, M.; Tarascon, J. M.: Building Better Batteries. *Nature (London, United Kingdom)* **2008**, *451*, 652-657.

(85) Peabody, C.; Arnold, C. B.: The Role of Mechanically Induced Separator Creep in Lithium-Ion Battery Capacity Fade. *J. Power Sources* **2011**, *196*, 8147-8153.

(86) Richman, E. K.; Kang, C. B.; Brezesinski, T.; Tolbert, S. H.: Ordered Mesoporous Silicon through Magnesium Reduction of Polymer Templated Silica Thin Films. *Nano Lett.* **2008**, *8*, 3075-3079.

(87) Chen, W.; Fan, Z.; Dhanabalan, A.; Chen, C.; Wang, C.: Mesoporous Silicon Anodes Prepared by Magnesiothermic Reduction for Lithium Ion Batteries. *J. Electrochem. Soc* **2011**, *158*, A1055.

(88) Monroe, C.; Newman, J.: The Impact of Elastic Deformation on Deposition Kinetics at Lithium/Polymer Interfaces. *J. Electrochem. Soc* **2005**, *152*, A396.

(89) Kowalczk, I.; Read, J.; Salomon, M.: Li-Air Batteries: A Classic Example of Limitations Owing to Solubilities. *Pure and Applied Chemistry* **2007**, *79*, 851-860.

(90) Kumar, B.; Kumar, J.; Leese, R.; Fellner, J. P.; Rodrigues, S. J.; Abraham, K. M.: A Solid-State, Rechargeable, Long Cycle Life Lithium–Air Battery. *J. Electrochem. Soc* **2010**, *157*, A50.

(91) Teran, A. A.; Balsara, N. P.: Effect of Lithium Polysulfides on the Morphology of Block Copolymer Electrolytes. *Macromolecules* **2011**, *44*, 9267-9275.

(92) Welna, D.; Stone, D.; Allcock, H. R.: Lithium-Ion Conductive Polymers as Prospective Membranes for Lithium-Seawater Batteries. *Chem. Mater.* **2006**, *18*, 4486-4492.

(93) Kono, M.; Hayashi, E.; Watanabe, M.: Network Polymer Electrolytes with Free Chain Ends as Internal Plasticizer. *J. Electrochem. Soc* **1998**, *145*, 1521-1527.

(94) Trapa, P. E.; Won, Y.-Y.; Mui, S. C.; Olivetti, E. A.; Huang, B.; Sadoway, D. R.; Mayes, A. M.; Dallek, S.: Rubbery Graft Copolymer Electrolytes for Solid-State, Thin-Film Lithium Batteries. *J. Electrochem. Soc* **2005**, *152*, A1.

(95) Tigelaar, D. M.; Meador, M. A. B.; Kinder, J. D.; Bennett, W. R.: New Aptes Cross-Linked Polymers from Poly(Ethylene Oxide)S and Cyanuric Chloride for Lithium Batteries. *Macromolecules* **2006**, *39*, 120-127.

(96) Panday, A.; Mullin, S.; Gomez, E. D.; Wanakule, N.; Chen, V. L.; Hexemer, A.; Pople, J.; Balsara, N. P.: Effect of Molecular Weight and Salt Concentration on Conductivity of Block Copolymer Electrolytes. *Macromolecules* **2009**, *42*, 4632-4637.

(97) Angell, C. A.; Liu, C.; Sanchez, E.: Rubbery Solid Electrolytes with Dominant Cationic Transport and High Ambient Conductivity. *Nature* **1993**, *362*, 137-139.

(98) Mitsunobu, O.; Yamada, M.: Preparation of Esters of Carboxylic and Phosphoric Acid <I>Via</I> Quaternary Phosphonium Salts. *Bull. Chem. Soc. Jpn.* **1967**, *40*, 2380-2382.

(99) Pojman, J. A.; Varisli, B.; Perryman, A.; Edwards, C.; Hoyle, C.: Frontal Polymerization with Thiol−Ene Systems. *Macromolecules* **2004**, *37*, 691-693.

(100) Tyson, E. L.; Ament, M. S.; Yoon, T. P.: Transition Metal Photoredox Catalysis of Radical Thiol-Ene Reactions. *J. Org. Chem.* **2013**, *78*, 2046-2050.

(101) Lowe, A. B.: Thiol-Ene Click Reactions and Recent Applications in Polymer and Material Synthesis. *Polym. Chem.* **2010**, *1*, 17-36.

(102) van Hensbergen, J. A.; Burford, R. P.; Lowe, A. B.: Post-Functionalization of a Romp Polymer Backbone Via Radical Thiol-Ene Coupling Chemistry. *J. Polym. Sci., Part A: Polym. Chem.* **2013**, *51*, 487-492.

(103) Lu, D.; Jia, Z.; Monteiro, M. J.: Synthesis of Alkyne Functional Cyclic Polymers by One-Pot Thiol-Ene Cyclization. *Polym. Chem.* **2013**, *4*, 2080-2089.

(104) Cui, J.; Lackey, M. A.; Tew, G. N.; Crosby, A. J.: Mechanical Properties of End-Linked Peg/Pdms Hydrogels. *Macromolecules* **2012**, *45*, 6104-6110.

(105) Cui, J.; Lackey, M. A.; Madkour, A. E.; Saffer, E. M.; Griffin, D. M.; Bhatia, S. R.; Crosby, A. J.; Tew, G. N.: Synthetically Simple, Highly Resilient Hydrogels. *Biomacromolecules* **2012**, *13*, 584-588.

(106) Saffer, E. M.; Lackey, M. A.; Griffin, D. M.; Kishore, S.; Tew, G. N.; Bhatia, S. R.: Sans Study of Highly Resilient Poly(Ethylene Glycol) Hydrogels. *Soft Matter* **2014**, *10*, 1905-1916.

(107) Walker, C. N.; Versek, C.; Touminen, M.; Tew, G. N.: Tunable Networks from Thiolene Chemistry for Lithium Ion Conduction. *ACS Macro Lett.* **2012**, *1*, 737-741.

(108) Cramer, N. B.; Davies, T.; O'Brien, A. K.; Bowman, C. N.: Mechanism and Modeling of a Thiol-Ene Photopolymerization. *Macromolecules* **2003**, *36*, 4631-4636.

(109) Hoyle, C. E.; Bowman, C. N.: Thiol-Ene Click Chemistry. *Angew. Chem.* **2010**, *49*, 1540-1573.

(110) Fairbanks, B. D.; Singh, S. P.; Bowman, C. N.; Anseth, K. S.: Photodegradable, Photoadaptable Hydrogels Via Radical-Mediated Disulfide Fragmentation Reaction. *Macromolecules* **2011**, *44*, 2444-2450.

(111) Koo, S. P. S.; Stamenovic, M. M.; Prasth, A. R.; Inglis, A. J.; Du Prez, F. E.; Barner-Kowollik, C.; Van Camp, W.; Junkers, T.: Limitations of Radical Thiol-Ene Reactions for Polymer-Polymer Conjugation. *J. Polym. Sci., Part A: Polym. Chem.* **2010**, *48*, 1699.

(112) Derboven, P.; D'hooge, D. R.; Stamenovic, M. M.; Espeel, P.; Marin, G. B.; Du Prez, F. E.; Reyniers, M. F.: Kinetic Modeling of Radical Thiol-Ene Chemistry for Macromolecular Design: Importance of Side Reactions and Diffusional Limitiations. *Macromolecules* **2013**, *46*, 1731-1472.

(113) Roper, T. M.; Guymon, C. A.; Jönsson, E. S.; Hoyle, C. E.: Influence of the Alkene Structure on the Mechanism and Kinetics of Thiol-Alkene Photopolymerizations with Real-Time Infrared Spectroscopy. *J. Polym. Sci., Part A: Polym. Chem.* **2004**, *42*, 6283-6298.

(114) Hoyle, C. E.; Lee, T. Y.; Roper, T.: Thiol–Enes: Chemistry of the Past with Promise for the Future. *J. Polym. Sci., Part A: Polym. Chem.* **2004**, *42*, 5301-5338.

(115) Ito, O.; Matsuda, M.: Reactivities of Cycloalkenes toward Phenylthio Radicals. *The Journal of Organic Chemistry* **1984**, *49*, 17-20.

(116) *Radiation Curing in Polymer Science and Technology Iii: Polymerization Mechanisms Chapter 7*; Jacobine, A. F., Ed.; Elsevier: London, 1993, pp 219.

(117) Northrop, B. H.; Coffey, R. N.: Thiol-Ene Click Chemistry: Computational and Kinetic Analysis of the Influence of Alkene Functionality. *J. Am. Chem. Soc.* **2012**, *134*, 13804-13817.

(118) Cramer, N. B.; Reddy, S. K.; Cole, M.; Hoyle, C. E.; Bowman, C. N.: Initiation and Kinetics of Thiol-Ene Photopolymerization without Photoinitiators. *J. Polym. Sci., Part A: Polym. Chem.* **2004**, *42*, 5817-5826.

(119) Morgan, C. R.; Magnotta, F.; Ketley, A. D.: Thiol/Ene Photocuable Polymers. *J. Polym. Sci.: Polym. Chem. Ed.* **1977**, *15*, 627-645.

(120) Wutticharoenwong, K.; Soucek, M. D.: Influence of the Thiol Structure on the Kinetics of Thiol-Ene Photopolymerization with Time-Resolved Infrared Spectroscopy. *Macromol. Mater. Eng.* **2008**, *293*, 45-56.

(121) Young, R. J.; Lovell, P. A.: *Introduction to Polymers*; 2nd ed.; CRC Press: New York, 1991.

(122) Bates, F. S.; Hillmyer, M. A.; Lodge, T. P.; Bates, C. M.; Delaney, K. T.; Fredrickson, G. H.: Multiblock Polymers: Panacea or Pandora's Box? *Science* **2012**, *336*, 434-440.

(123) Zhang, J.; Bates, F. S.: Dodecagonal Quasicrystalline Morphology in a Poly(Styrene-B-Isoprene-B-Styrene-B-Ethylene Oxide) Tetrablock Terpolymer. *J Am Chem Soc* **2012**, *134*, 7636-7639.

(124) Gody, G.; Maschmeyer, T.; Zetterlund, P. B.; Perrier, S.: Rapid and Quantitative One-Pot Synthesis of Sequence-Controlled Polymers by Radical Polymerization. *Nat Commun* **2013**, *4*, 2505.

(125) Touris, A.; Lee, S.; Hillmyer, M. A.; Bates, F. S.: Synthesis of Tri- and Multiblock Polymers with Asymmetric Poly(Ethylene Oxide) End Blocks. *ACS Macro Lett.* **2012**, *1*, 768-771.

(126) Jia, Z.; Xu, X.; Fu, Q.; Huang, J.: Synthesis and Self-Assembly Morphologies of Amphiphilic Multiblock Copolymers [Poly(Ethylene Oxide)-B-Polystyrene]N Via Trithiocarbonate-Embedded Peo Macro-Raft Agent. *J. Polym. Sci., Part A: Polym. Chem.* **2006**, *44*, 6071-6082.

(127) Gemici, H.; Legge, T. M.; Whittaker, M.; Monteiro, M. J.; Perrier, S.: Original Approach to Multiblock Copolymers Via Reversible Addition–Fragmentation Chain Transfer Polymerization. *J. Polym. Sci., Part A: Polym. Chem.* **2007**, *45*, 2334-2340.

(128) Harrison, W. L.; Hickner, M. A.; Kim, Y. S.; McGrath, J. E.: Poly(Arylene Ether Sulfone) Copolymers and Related Systems from Disulfonated Monomer Building Blocks: Synthesis, Characterization, and Performance – a Topical Review. *Fuel Cells* **2005**, *5*, 201-212.

(129) Roy, A.; Yu, X.; Dunn, S.; McGrath, J. E.: Influence of Microstructure and Chemical Composition on Proton Exchange Membrane Properties of Sulfonated–Fluorinated, Hydrophilic–Hydrophobic Multiblock Copolymers. *J. Membr. Sci.* **2009**, *327*, 118-124.

(130) Odian, G. G.: Principles of Polymerization. Wiley: Hoboken, N.J., 2004.

(131) Ryu, C. Y.; Ruokolainen, J.; Fredrickson, G. H.; Kramer, E. J.; Hahn, S. F.: Chain Architecture Effects on Deformation and Fracture of Block Copolymers with Unentangled Matrices. *Macromolecules* **2002**, *35*, 2157-2166.

(132) Hermel, T. J.; Hahn, S. F.; Chaffin, K. A.; Gerberich, W. W.; Bates, F. S.: Role of Molecular Architecture in Mechanical Failure of Glassy/Semicrystalline Block Copolymers: Cec Vs Cecec Lamellae. *Macromolecules* **2003**, *36*, 2190-2193.

(133) Priola, A.; Bongiovanni, R.; Malucelli, G.: Uv-Curable Systems Containing Perfluoropolyether Structures: Synthesis and Characterization. *Macromol. Chem. Phys.* **1997**, *198*, 1893-1907.

(134) Rolland, J. P.; Van Dam, M.; Schorzman, D. A.; Quake, S. R.; DeSimone, J. M.: Solvent-Resistant Photocurable "Liquid Teflon" for Microfluidic Device Fabrication. *J. Am. Chem. Soc.* **2004**, *126*, 2322-2323.

(135) Lackey, M. A.: Novel Peg-Based End-Linked Networks: From Synthesis to Mechanics. Ph. D., University of Massachusetts Amherst, 2013.

(136) Cui, J.: Resilient Polymer Networks Via Thiol-Norbornene Chemistry: Mechanical and Adhesive Properties. Ph. D., Universtiy of Massachusetts Amherst, 2013.

(137) Li, Q.; Zhou, H.; Hoyle, C. E.: The Effect of Thol and Ene Structures on Thiol-Ene Networks: Photopolymerization, Physical, Mechanical and Optical Properties. *Polymer* **2009**, *50*, 2237.

(138) Walker, C. N.; Versek, C.; Touminen, M.; Tew, G. N.: Tunable Networks from Thiolene Chemistry for Lithium Ion Conductinon. *ACS Macro Lett.* **2012**, *1*, 737-741.

(139) Schulz, M.; Tanner, S.; Barqawi, H.; Binder, W. H.: Macrocyclization of Polymers Via Ring-Closing Metathesis and Azide/Alkyne-Click-Reactions: An Approach to Cyclic Polyisobutylenes. *J. Polym. Sci., Part A: Polym. Chem.* **2009**, *48*, 671-680.

(140) Zhang, K.; Lackey, M. A.; Cui, J.; Tew, G. N.: Gels Based on Cyclic Polymers. *J Am Chem Soc* **2011**, *133*, 4140-4148.

(141) Krumpfer, J. W.; McCarthy, T. J.: Rediscovering Silicones: "Unreactive" Silicones React with Inorganic Surfaces. *Langmuir : the ACS journal of surfaces and colloids* **2011**, *27*, 11514-11519.

(142) Kakihana, M.; Schantz, S.; Torell, L. M.: Raman Spectroscopic Study of Ion–Ion Interaction and Its Temperature Dependence in a Poly(Propylene-Oxide)-Based Nacf3so3 – Polymer Electrolyte. *J. Chem. Phys.* **1990**, *92*, 6271.

(143) Mishra, R.; Baskaran, N.; Ramakrishnan, P. A.; Rao, K. J.: Lithium Ion Conduction in Extreme Polymer in Salt Regime. *Solid State Ionics* **1998**, *112*, 261-273.

(144) Fan, J.; Angell, C. A.: The Preparation, Conductivity, Viscosity and Mechanical Properties of Polymer Electroltyes and New Hybrid Ionic Rubber Electrolytes. *Electrochim. Acta* **1995**, *40*, 2397-2400.

(145) Nishimoto, A.; Watanabe, M.; Ikeda, Y.; Kohjiya, S.: High Ionic Conductivity of New Polymer Electrolytes Based on High Molecular Weight Polyether Comb Polymers. *Electrochim. Acta* **1998**, *43*, 1177-1184.

(146) Munshi, M. Z. A.; Owens, B. B.: A Study Inot the Effect of Humidity on (Peo)6licf3so4 Polymer Electrolyte. *Appl. Phys. Comm.* **1987**, *6*, 299-312.

(147) Rubinstein, M.; Colby, R.: *Polymer Physics*; Oxford University Press: New York, 2003.

(148) Angell, C. A.; Imrie, C. T.; Ingram, M. D.: From Simple Electrolyte Solutions Throught Polymer Electrolytes to Superioninc Rubbers: Some Fundamental Considerations. *Polym. Int.* **1998**, *47*, 9-15.

(149) Ratner, M. A.; Nitzan, A.: Conductivity in Polymer Ionics. Dynamic Disorder and Correlation. *Faraday Discussions of the Chemical Society* **1989**, *88*, 19-42.

(150) Tominaga, Y.; Takizawa, N.; Ohno, H.: Effect of Added Salt Species on the Ionic Conductivity of Peg/Sulfonamide Salt Hybrids. *Electrochim. Acta* **2000**, *45*, 1285-1289.

(151) Gervais, M.; Gallot, B.: Phase Diagram and Structural Study of Polystyrene - Poly(Ethylene Oxide) Block Copolymers, 1. *Macromol. Chem. Phys.* **1973**, *171*, 145-178.

(152) Cui, J.: Resilient Polymer Networks Vi Thiol-Norbornene Chemistry: Mechanical and Adhesive Properties. Doctoral Dissertation, University of Massachusetts Amherst, 2013.

(153) Jinnai, H.; Nishikawa, Y.; Koga, T.; Hashimoto, T.: Direct Observation of 3-D Bicontinuous Structure Developed Via Spinodal Decomposition. *macromolecules* **1995**, *28*, 4782-4784.

(154) Bockstaller, M.; Kolb, R.; Thomas, E. L. "Metallodielectric Photonic Crystals Based on Diblock Copolymers," Brookhaven National Lab, 2001.

(155) Panyukov, S.; Rubinstein, M.: Stress-Induced Orderting in Microphase Separated Multicomponent Networks. *Macromolecules* **1996**, *29*, 8220-8230.

(156) Frielinghaus, H.; Mortensen, K.; Almdal, K.: Differences of Interaction Parameter of a Ps/Peo Homopolymer Blend and Diblock Copolymer in Comparison to Other Systems. *Macromolecular Symposia* **2000**, *149*, 63-67.

(157) Wanakule, N. S.; Virgili, J. M.; Teran, A. A.; Wang, Z.-G.; Balsara, N. P.: Thermodynamic Properties of Block Copolymer Electrolytes Containing Imidazolium and Lithium Salts. *Macromolecules* **2010**, *43*, 8282-8289.

(158) Nakamura, I.; Balsara, N. P.; Wang, Z.-G.: First-Order Disordered-to-Lamellar Phase Transition in Lithium Salt-Doped Block Copolymers. *ACS Macro Lett.* **2013**, *2*, 478-481.

(159) Vaia, R. A.; Sauer, B. B.; Tse, O. K.; Giannelis, E. P.: Relaxations of Confined Chains in Polymer Nanocomposites: Glass Transition Properties of Poly(Ethylene Oxide) Intercalated in Montmorillonite. *J. Polym. Sci. Part B: Polym. Phys.* **1997**, *35*, 59-67.

(160) Halalay, I. C.; Lukitsch, M. J.; Balogh, M. P.; Wong, C. A.: Nanoindentation Testing of Separators for Lithium-Ion Batteries. *J. Power Sources* **2013**, *238*, 469-477.

(161) Patterson, A. L.: The Scherrer Formula for X-Ray Particle Size Determination. *Physical Review* **1939**, *56*, 978-982.

(162) Johansson, A.; Gogoll, A.; Tegenfeldt, J.: Diffusion and Ionic Conductivity in Li(Cf3so3)Peg10 and Lin(Cf3so2)2peg10. *Polymer* **1996**, *37*, 1387-1393.

(163) Askeland, D.: *The Science and Engineering of Materials*; 1st ed.; Wadsworth, Inc: Belmont, CA, 1997.

(164) Gianotti, V.; Antonioli, D.; Sparnacci, K.; Laus, M.; Giammaria, T. J.; Ferrarese Lupi, F.; Seguini, G.; Perego, M.: On the Thermal Stability of Ps-B-Pmma Block and P(S-R-Mma) Random Copolymers for Nanopatterning Applications. *Macromolecules* **2013**, *46*, 8224-8234.

(165) Calahorra, E.; Cortazar, M.; Guzman, G. M.: Thermal Decomposition of Poly(Ethylene Oxide), Poly(Methyl Methacrylate), and Their Mixtures by Thermogravimetric Method. *J. Polym. Sci.: Polym. Lett. Ed.* **1985**, *23*, 257-260.

(166) Radhakrishnan, T. S.: Thermal Degredation of Poly(Dimethylsilylene) and Poly(Tetrametyldisilylene-Co-Styrene). *J. Appl. Polym. Sci.* **2006**, *99*, 2679-2686.

(167) Koberstein, J. T.; Russell, T. P.: Simultaneous Saxs-Dsc Study of Multiple Endothermic Behavior in Polyether-Based Polyurethane Block Copolymers. *Macromolecules* **1986**, *19*, 714-720.

(168) Blane, R., L.: Polymer Heats of Fusion. TA Instruments; Vol. 2013.

(169) Segalman, R. A.: Patterning with Block Copolymer Thin Films. *Mater. Sci. Eng., R* **2005**, *48*, 191-226.

(170) Krause, S.: Microphase Separation in Block Copolymers. Zeroth Approximation Including Surface Free Energies. *Macromolecules* **1970**, *3*, 84-86.

(171) Liang, S.; O'Reilly, M. V.; Choi, U. H.; Shiau, H.-S.; Bartels, J.; Chen, Q.; Runt, J.; Winey, K. I.; Colby, R. H.: High Ion Content Siloxane Phosphonium Ionomers with Very Lowtg. *Macromolecules* **2014**, *47*, 4428-4437.

(172) Britz, J.; Meyer, W. H.; Wegner, G.: <Wegner, Macro 07, Pma Diololane Blends.Pdf>. *Macromolecules* **2007**, *40*, 7558-7565.